TRIBOCHEMICAL INVESTIGATION OF MICROELECTRONIC MATERIALS

A Dissertation

by

MILIND SUDHAKAR KULKARNI

Submitted to the Office of Graduate Studies of
Texas A&M University
in partial fulfillment of the requirements for the degree of

DOCTOR OF PHILOSOPHY

August 2006

Major Subject: Materials Science & Engineering

TRIBOCHEMICAL INVESTIGATION OF MICROELECTRONIC MATERIALS

A Dissertation

by

MILIND SUDHAKAR KULKARNI

Submitted to the Office of Graduate Studies of
Texas A&M University
in partial fulfillment of the requirements for the degree of

DOCTOR OF PHILOSOPHY

Approved by:

Chair of Committee,	Hong Liang
Committee Members,	Andreas Holzenburg
	Richard Griffin
	Jun Kameoka
Chair of Faculty of Materials Science and Engineering,	Joseph Ross Jr.

August 2006

Major Subject: Materials Science & Engineering

ABSTRACT

Tribochemical Investigation of Microelectronic Materials.

(August 2006)

Milind Sudhakar Kulkarni, B.E., University of Pune;

M.Tech., Indian Institute of Technology, Mumbai

Chair of Advisory Committee: Dr. Hong Liang

To achieve efficient planarization with reduced device dimensions in integrated circuits, a better understanding of the physics, chemistry, and the complex interplay involved in chemical mechanical planarization (CMP) is needed. The CMP process takes place at the interface of the pad and wafer in the presence of the fluid slurry medium. The hardness of Cu is significantly less than the slurry abrasive particles which are usually alumina or silica. It has been accepted that a surface layer can protect the Cu surface from scratching during CMP. Four competing mechanisms in materials removal have been reported: the chemical dissolution of Cu, the mechanical removal through slurry abrasives, the formation of thin layer of Cu oxide and the sweeping surface material by slurry flow. Despite the previous investigation of Cu removal, the electrochemical properties of Cu surface layer is yet to be understood.

The motivation of this research was to understand the fundamental aspects of removal mechanisms in terms of electrochemical interactions, chemical dissolution, mechanical wear, and factors affecting planarization. Since one of the major requirements in CMP is to have a high surface finish, i.e., low surface roughness, optimization of the surface finish in reference to various parameters was emphasized.

Three approaches were used in this research: in situ measurement of material removal, exploration of the electropotential activation and passivation at the copper surface and

modeling of the synergistic electrochemical-mechanical interactions on the copper surface.

In this research, copper polishing experiments were conducted using a table top tribometer. A potentiostat was coupled with this tribometer. This combination enabled the evaluation of important variables such as applied pressure, polishing speed, slurry chemistry, pH, materials, and applied DC potential. Experiments were designed to understand the combined and individual effect of electrochemical interactions as well as mechanical impact during polishing. Extensive surface characterization was performed with AFM, SEM, TEM and XPS. An innovative method for direct material removal measurement on the nanometer scale was developed and used.

Experimental observations were compared with the theoretically calculated material removal rate values. The synergistic effect of all of the components of the process, which result in a better quality surface finish was quantitatively evaluated for the first time. Impressed potential during CMP proved to be a controlling parameter in the material removal mechanism. Using the experimental results, a model was developed, which provided a practical insight into the CMP process. The research is expected to help with electrochemical material removal in copper planarization with low-k dielectrics.

DEDICATION

To

My parents
Ti. Baba, Ti. Sau. Aai,

My wife
Sau. Manasi,

And my kids
Chi. Ketaki and Chi. Atharva

ACKNOWLEDGMENTS

I would like to thank my committee chair, Dr. Hong Liang, and my committee members, Dr. Andreas Holzenburg, Dr. Richard Griffin, and Dr. Jun Kameoka, for their guidance and support throughout the course of this research. I hereby express my deep gratitude for their encouragement. I would also like to thank the department faculty and staff for providing me a great experience at Texas A&M University.

I also want to extend my gratitude to the funding agencies, the National Science Foundation, the University of Alaska Fairbanks, the Department of Mechanical Engineering at Texas A&M University, and the Texas Engineering and Experiment Station. My sincere thanks to those faculty members who collaborated on my research work, namely, Dr. Hung-Jue Sue, Dr. Jun Zao, Dr. Karl Aufderhide, Dr. Debjyoti Banerjee, and Dr. Alan Palazzolo.

Thanks also to my friends and colleagues in Dr. Liang's research group, namely, Dr. Gun-in Kim, Dr. Bo Ning, Srinivas Guruzu, Rahul Ribeiro, Dedy Ng, Daniel Greisen, Melloy Baker, Hyungoo Lee, Alice Pendleton, Yolanda Jordan, Pranay Asthana, Taekwon Jee, Sharmili Datta and Luohan Peng.

Finally, thanks to my family members, teachers and friends for their encouragement and moral support.

TABLE OF CONTENTS

Page

ABSTRACT.......... iii

DEDICATION.......... v

ACKNOWLEDGMENTS.......... vi

TABLE OF CONTENTS.......... vii

LIST OF FIGURES.......... x

LIST OF TABLES.......... xiii

CHAPTER

I INTRODUCTION 1

1.1 Tribology.......... 1
1.2 Friction.......... 2
1.2.1 Surface Heating.......... 4
1.2.2 Plastic Deformation.......... 4
1.2.3 Phase Changes.......... 5
1.3 Wear.......... 6
1.3.1 Classification 7
1.3.2 Testing.......... 8
1.4 Lubrication.......... 11
1.5 Tribochemistry.......... 12
1.6 Triboelectrochemistry.......... 15
1.7 Surface Characterization for Tribological Surfaces.......... 17
1.7.1 Scanning Electron Microscopy (SEM).......... 17
1.7.2 Transmission Electron Microscopy (TEM).......... 18
1.7.3 Atomic Force Microscopy (AFM).......... 19
1.7.4 X-Ray Photoelectron Spectroscopy (XPS).......... 22

II TECHNOLOGICAL DEVELOPMENT OF CHEMICAL-MECHANICAL POLISHING.......... 26

2.1 History of CMP.......... 26
2.2 Evolution of Integrated Circuit Technology.......... 27
2.3 Role of CMP in IC Manufacturing.......... 29
2.4 Research Areas in CMP.......... 31
2.5 Copper CMP Challenges.......... 32
2.6 Business in CMP.......... 33
2.7 International Roadmap for Semiconductors.......... 33

CHAPTER Page

III INVESTIGATION OF CHEMICAL MECHANICAL PLANARIZATION………………………………………………………… 35

3.1 Motivation ………………………………………………………… 35
3.2 Approach………………………………………………………… 35
3.3 Materials Used in CMP…………………………………….............. 35
3.4 Material Removal Rate………………………………………… 36
3.5 Down Pressure…………………………………………………….. 37
3.6 Speed..…………………………………………………………… 38
3.7 Slurry Abrasives…………………………………………………… 39
3.7.1 Abrasive Types………………………………………….. 39
3.7.2 Particle Size…………………………………………… 40
3.7.3 Abrasive Concentration………………………………….. 40
3.8 Polishing Pad……………………………………………………. 40
3.9 Methods and Materials…………………………………………….. 42
3.9.1 Alumina Abrasives……………………………………… 43
3.9.2 Polymer Additives……………………………………….. 43
3.9.3 Oxidizer……………………………………………….. 44
3.10 Characterization……..…………………………………………… 44
3.10.1 Scanning Electron Microscopy…………………………… 44
3.10.2 Transmission Electron Microscopy……………………… 44
3.10.3 Atomic Force Microscopy……………………………... 45
3.11 Observations…………………………………………………… 46
3.11.1 Friction Coefficient for Slurries…………………………… 46
3.11.2 SEM Analysis of Slurry Particles………………………… 49
3.11.3 TEM Analysis of Slurry Particles………………………… 55
3.11.4 Post CMP Surface Analysis Using SEM………………….. 60
3.11.5 Post CMP Surface Analysis Using AFM……………….... 60
3.12 Discussion……………………………………………………… 62
3.12.1 Oxidizer in Slurry……………………………………….. 62
3.12.2 Polymer Additives in Slurry…………………………….. 62
3.13 Summary….…………………………………………………… 64

IV ELECTROCHEMICAL-MECHANICAL PLANARIZATION MECHANISMS………………………………………………………… 66

4.1 Brief Background……………………………………………..... 66
4.1.1Chemistry in CMP……………………………………….. 66
4.1.2 Electrochemistry and CMP……………………………..... 72
4.2 Motivation for Research……………………………………….... 80
4.3 Approach……………………………………………………….... 81
4.4 Methods and Materials………………………………………..... 81
4.4.1 Static Electrochemistry (Open Circuit Potential Measurement)…………………………………………… 81

CHAPTER Page

4.4.2 Polarization Test………………………………………………. 82
4.4.3 ECMP (Dynamic Test)……………………………………… 82
4.4.4 Atomic Force Microscopic Characterization……………….. 85
4.4.5 Spectroscopic Characterization ……………………………. 88
4.5 Observations………………………………………………………… 88
4.5.1 Open Circuit Potential Measurement……………………..... 88
4.5.2 Potentiodynamic Polarization Test…………………………. 89
4.5.3 In situ Current Measurement……………………………….. 93
4.5.4 AFM Topography: Surface Roughness…………………….. 93
4.5.5 Chemical Analysis Using XPS..…………………………….. 99
4.6 Discussions….……………………………………………………….. 102
4.6.1 Static Electrochemistry…………………………………….. 102
4.6.2 Roughness Measurement…………………………………… 104
4.6.3 Surface Phases and Pourbaix Diagram…………………….... 110
4.6.4 Material Removal Rate…………………………………….. 111
4.7 Summary….………………………………………………………….. 118

V CONCLUSIONS AND FUTURE WORK………………………………… 121

5.1 Conclusions….……………………………………………………… 121
5.2 Future Research…………………………………………………….. 122

REFERENCES... 124

APPENDIX I…………………………………………………………………….. 130

VITA 131

LIST OF FIGURES

FIGURE Page

1.1 Coefficient of friction experiment with inclined surface…………………. 2

1.2 Schematic diagram showing cross section of metal surface after sliding friction………………………………………………………………… 3

1.3 Characteristic of stick slip at slow speed of sliding wear, a plot of μ vs time…………………………………………………………………….. 7

1.4 Conventional Stribeck curve, showing three different regimes: boundary lubrication, transition and hydrodynamic lubrication………… 12

1.5 Operating regions for AFM in the van der Waals force regions………... 20

1.6 Schematic diagram of AFM in contact mode…………………………… 21

1.7 Schematic diagram of AFM in non-contact mode……………………….. 22

1.8 Schematic of photoelectron emission…………………………………….. 23

1.9 Schematic of Auger electron emission…………………………………… 24

2.1 Section of component of a Complementary Metal Oxide Semiconductor (CMOS)………………………………………………………………….. 27

2.2 Section of integrated circuit showing copper damascene pattern……….. 28

2.3 Schematic of the steps in IC manufacturing……………………………… 30

3.1 Experimental setup for slurry tests on Cu coated Si wafer………………. 42

3.2 Friction coefficients as a function of time, for CMP in slurries with different oxidizer content…………………………………………… 47

3.3 Average friction coefficients during CMP with different oxidizer content 47

3.4 Friction coefficients as a function of time, for CMP in slurries with different polymer additives……………………………………………. 48

3.5 Average friction coefficient during CMP with different polymer additives. 48

3.6 Alumina abrasive particles before CMP…………………………………. 50

3.7 Alumina abrasive particles after CMP…………………………………… 51

3.8 EDS data for (a) alumina particle, and (b) copper surface……………….. 52

3.9 Latex particles before CMP………………………………………………. 53

FIGURE Page

3.10 Latex particles after CMP…………………………………………………… 54

3.11 TEM and XRD of abrasive alumina and Teflon slurry particles.………… 56

3.12 TEM micrograph of alumina particles at 400000X magnification………. 58

3.13 Copper surface after CMP using alumina slurry…………………………. 59

3.14 Copper surface after CMP, using abrasive slurry with latex additive……. 59

3.15 Average surface roughness after CMP with slurries containing variation in oxidizer……………………………………………………… 61

3.16 Average surface roughness after CMP with slurries containing variation in polymer additive ……………………………………………. 61

3.17 Schematic showing chemo-mechanical actions in CMP…………………. 64

4.1 Schematic of oxide formation and removal process to achieve planarization in CMP…………………………………………………... 68

4.2 Typical graph for Tafel plot………………………………………………. 75

4.3 Construction of electrochemical cell…………………………………... 76

4.4 Effect of oxidizer and active scratching on the polarization curve………. 77

4.5 Stability (Pourbaix) diagram for water…………………………………… 79

4.6 Pourbaix diagram for copper water system at room temperature………… 80

4.7 Experimental setup for copper CMP electrochemical studies…………… 83

4.8 Experimental setup for Cu coated Si wafer ECMP………………………. 84

4.9 Applied potential cycle during ECMP…………………………………… 85

4.10 Schematic of sample surface……………………………………………… 86

4.11 Open Circuit Potentials (OCP) of copper in CMP slurry as a function of pH…….…………………………………………………………. 88

4.12 Open Circuit Potentials (OCP) of copper in CMP slurry as a function of H_2O_2……………………………………………………….. 89

4.13 Tafel plots for copper in CMP slurry containing different level of oxidizer at (a) pH 3 (b) pH5 (c) pH 7 and (d) pH 9, without active polishing……………………………………………………………….. 90

4.14 Tafel plots for copper in CMP slurry at different pH, containing (a) 0.09 % H_2O_2 (b) 0.15 % H_2O_2 and (c) 0.21 % H_2O_2, without active polishing………………………………………………….. 92

FIGURE Page

4.15 Variation in current density as a function of slurry pH, for various %wt H_2O_2 content and applied potentials during CMP…………………. 94

4.16 AFM topography images showing topography after CMP with current densities of (a) 0.01 A/cm^2 and (b) 0.0005 A/cm^2……………………….. 95

4.17 AFM topography images of copper surface after CMP in slurries with (a) pH 3, (b) neutral pH, and (c) pH 9 …………………………………… 95

4.18 Surface plot for post ECMP copper surface roughness………………….. 96

4.19 AFM scan showing a pit in a topography image………………………… 97

4.20 AFM scans showing topography after ECMP with various conditions… 98

4.21 AFM surface topography of copper surface after ECMP ……………….. 100

4.22 Post ECMP surface roughness for different applied potentials ………… 101

4.23 XPS spectra of Cu 2p3/2 and 2p1/2 for Cu after ECMP………………… 101

4.24 Surface roughness Ra value gradient graph superimposed on Pourbaix diagram for copper water system at room temperature………………….. 107

4.25 Schematic model of material removal mechanisms in ECMP…………… 112

4.26 Chart showing MRR for different applied potentials during ECMP…….. 116

4.27 Chart evaluating calculated and observed MRR…………………………. 117

LIST OF TABLES

TABLE Page

1.1 Typical test geometry for various types of wear tests ………………………. 9

1.2 XPS binding energies (eV) for Cu 2p3/2 for different oxidative states…….. 25

2.1 Interdisciplinary research areas in CMP……………………………………. 31

3.1 Slurry composition………………………………………………………….. 43

4.1 Observed and calculated MRR……………………………………………… 115

CHAPTER I
INTRODUCTION

In order to understand the basics of this research, concepts of tribology and tribochemistry are briefly presented in the first chapter. Industrial needs for this research topic in chemical-mechanical planarization (CMP) are discussed in the chapter II. Chapter III discusses the CMP removal mechanisms, and chapter IV investigates the electro-chemical aspects of CMP. The work finishes with the final conclusions and recommendations in chapter V.

1.1 Tribology

Tribology is the science related to friction. When two bodies slide over each other, it causes friction. Early understanding of friction dates back to the time when human used friction for fire generation. They generated fire using friction between a stone and a piece of wood stick. Friction causes resistance to sliding. Work required to keep the object sliding, is to overcome the friction. Use of water as a lubricant for friction reduction in stone sliding can be found in history of pyramid construction. Later, the use of lubrication became an engineering practice after the industrialization.

Commonly known effects of friction are increased force for moving an object, loss of material by wear, heating of the contact faces, and adhering or welding of two contacted surfaces. Such effects are often encountered as damages that lead to high cost due to failures, replacement, and high maintenance cost. Efforts are made to reduce friction. Examples are, for example, using lubrication or new materials, applying surface modifications and coating techniques, etc. However, the friction has been proved beneficial in many situations such as breaking, power transmission, machining, grinding

---

This dissertation follows the style of the *Journal of the Electrochemical Society*.

and polishing. A simple act of safe walking needs an appropriate amount of friction between the road and the foot.

A tribological system is complex. A tribosystem is dynamic in nature and is influenced greatly be the surface interaction of chemical and electrochemical nature. In this chapter, we will study the basic tribology concerning friction, lubrication and wear, and surface interactions as tribochemistry and triboelectrochemistry.

1.2 Friction

As per the early experiments in 17th century, Amontons, Euler and Coulomb concluded that when two surfaces mate in sliding, there is interlocking of asperities. When a lateral force is applied by pulling action,, the mating surfaces are lifted and again dropped to contact, sliding over the asperities. The force required to pull is $1/3^{rd}$ of the load acting. This ratio of the friction force (F) over the normal force (N) is called the coefficient of friction, μ, as

$$\mu = F / N \qquad [1.1]$$

When the μ is calculated using inclined surface experiment (figure 1.1), the angle required for just sliding of the component, over the inclined surface, on its own weight, is measured. The μ then is

$$\tan\theta = \mu = F / N \qquad [1.2]$$

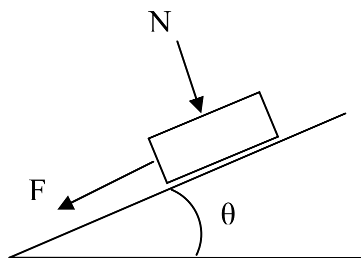

Figure: 1.1 Coefficient of friction experiment with inclined surface

During sliding friction of two surfaces, the contact is not over the entire mating surfaces. Microasperites on the surface are in contact. Hence the load is carried by those asperities. The load (W) is then the product of asperities' area in contact (A) and Pm, the mean pressure.[1]

$$W = A \times Pm \quad [1.3]$$

Bowden and Tabor observed that the deformation occurs only in the asperities to a certain extent, and then the below surface starts to deform.

Friction results tribological wear at the interface between the sliding surfaces according to Shpenkov.[2] During sliding, energy is consumed and forces are transferred to the surface and subsurface region. These energy and forces change the physical and chemical nature. Major effects seen are thermal, deformation, and phase transformation as described below. Magnitudes of the consumed energy and generated stresses are correlated to applied forces, materials properties, and environment present.[3] Schematic representation of the surface and subsurface changes are shown in figure 1.2.

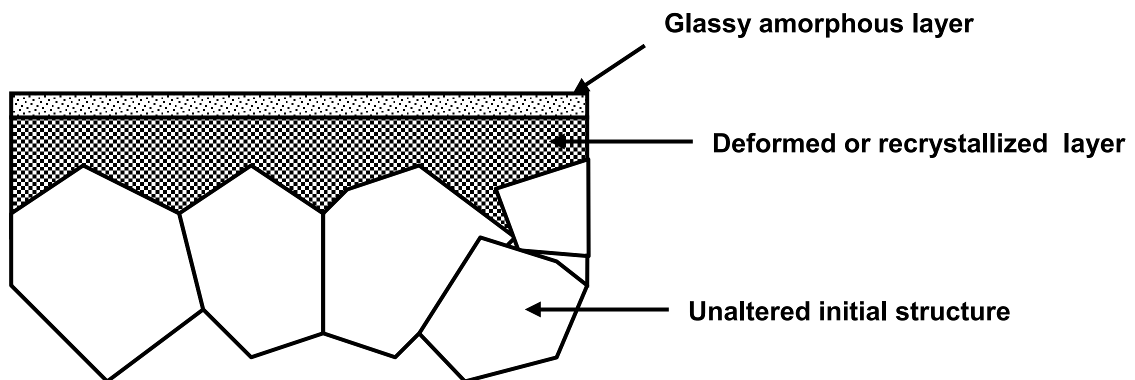

Figure: 1.2 Schematic diagram showing cross section of metal surface after sliding friction

1.2.1 Surface Heating

Is polishing simply fine-scale abrasion or is it more akin to melting? Recent findings suggest that neither of these to old rival hypotheses is entirely correct.

---- *Ernest Rabinowicz (1968)*[4]

Frictional energy during polishing generates heat at the interface.[5,6,7,8] This heat is dissipated slowly in to the surroundings as polishing medium and inside the material being polished. The magnitude of heat generated depends on the interacting materials, applied force, polishing speed, and slurry transport. Especially in dry polishing, a temperature at interface goes above the melting temperature. Often, this leads to melting and liquid flow of the material in surface region, followed by rapid cooling. This phenomenon is termed as burnishing operation and is used for polishing brass or similar metallic components. Rapid cooling of this molten surface layer causes amorphization of the structure. However, with subsequent rise in temperature due to friction, fine crystalline structure can be formed. This leads to the change in mechanical behavior of the material in surface region.

The amount of heat generated Q due to friction can be quantified as given in equation 1.4[3]

$$Q = \mu\, W\, g\, v / J \qquad [1.4]$$

Where μ is coefficient of friction, W is load, G is gravity, v is velocity, and J is mechanical equivalent of heat. The surface temperature increases with the velocity and load. At the point of asperity contact, hot spots are generated.

1.2.2 Plastic Deformation

Friction causes surface flow in ductile metals.[4,7] Deformation can be seen in the cross section. It is also demonstrated that up to 1000Å thick layer on the surface could be more amorphous in nature. Material in the asperities is deformed severely. It forms a thin layer

called smeared layer or Beilby layer.[4,7] This surface film has amorphous structure and is hard.[4, 7]

Surface and subsurface deformation during sliding is well understood in terms of contact mechanics.[3] The high stress generated in the contact area generate dislocation and their movement. This leads to the plastic deformation in the surface region. As explained by Suh,[3] if the sliding is performed for longer time, the repeated loading can cause high stress generation, void formation, and cracking in the subsurface region.

Studies by Hirth and Rigney[9] on plasticity and delamination in wear of Al-Cu alloys have also shown that the deformation does not occur in the near surface region. Instead, the deformation initiates on the surface and the dislocation density increases at grain boundary regions below the surface. This causes the delamination by extreme work hardening.

1.2.3 Phase Changes

Surface and subsurface regions are exposed to a great degree of pressures during polishing.[10] Besides deformation and amorphization, these regions are also susceptible to phase transformations as per the recent studies. Gogotsi and his coworkers have described that pressures in contact loading in polishing can be so high that subsurface phase transformation is induced. Axial compression occurs during the contact point loading condition. Gogotsi has further proved this theory with examples of pressure induced phase transformations in silicon and diamond. Diamond structure changes to graphite like structure under pressure.

Effects of pressure can not be sufficiently studied using conventional cross sectional TEM or XRD of the top surface. These transformations are short order and reported as amorphization in general studies. Nanoindentation studies with Berkovich indenter or nanoscratch experiments; followed by surface characterization with micro Raman is an

effective tool, to understand these nanosized areas of phase transformations. Mössabauer Electron Spectroscopy is also an effective tool for detection of phase transformations in subsurface regions. Molecular dynamics simulation is an effective simulation tool to understand the mechanism involved in pressure induced phase transformations.

Phase transformations just discussed affect the mechanical behavior of the surface layers. It was observed that normally brittle material like silicon behaves like a ductile material when the brittle-to-ductile transition takes place. The increased ductility is in contrast with other mechanisms where the surface amorphization and plastic deformation (work hardening) cause increased brittleness.

1.3 Wear

Wear takes places when two surfaces slid over each other through different mechanisms. Beilby and Rayleigh confirmed that there are plastic deformation and breaking of asperities causing surface wear. The debris particle when trapped in between sliding surfaces typically changes from 2-body wear to a 3-body mode. Surface contamination and oxidation also cause 3-body wear in sliding.

When two elastic bodies slide at low speeds, stick slip phenomena is observed. The stick slip is a non-continuous sliding of two elastic surfaces. Figure 1.3 shows an example of such phenomenon.

In the sliding wear, the wear rate is dependent on the surface roughness, applied load, velocity, and the hardness of the mating surfaces. The wear mechanisms observed are generally abrasion (plowing and scratching, wedge formation and cutting,) adhesion (cold welding). Other common wear modes include corrosion, erosion, tribochemical, among others. Ductile metals like aluminum and copper shows heavy plastic deformation during the sliding friction. The slip lines extend long beyond the wear track.

Surface polishing is one of the important application of sliding friction. Abrasive particles are usually used in forms of either suspended in liquid or glued on paper or disc. Material removal mechanisms during polishing are complex. With higher loads and sliding velocity, material removal rates are expected to be higher. However, with increased load, high stress and speed cause embedding of hard abrasive particles in the soft wafer surface. Slurry chemistry also plays important roles in polishing. Chemical interactions of contacted surfaces affect polishing process drastically. This point will be discussed later.

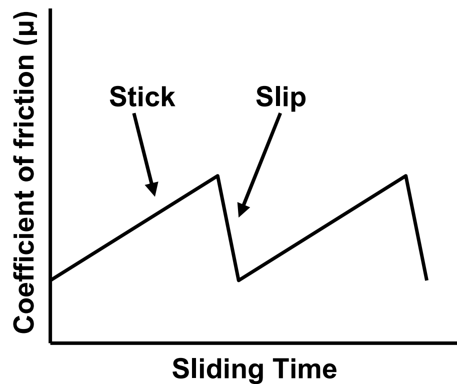

Figure: 1.3 Characteristic of stick slip at slow speed of sliding wear, a plot of µ vs time

1.3.1 Classification

Based on the type of loading conditions, wear forms are classified as abrasive wear, adhesive wear, and fatigue wear. When focused particular to the sliding and polishing wear then it is adhesive and abrasive wear. In presence of a polishing medium, there are chemical wear and erosive wear. Various mechanisms that occur during wear can be explained from the surface and subsurface studies.

Adhesive wear shows the dislodging of material from surface. Abrasive wear introduces grooves on the surface. These grooves are aligned in the direction of sliding. Oxidative wear exhibits mixed surface finish with discoloration. Wear proceeds with formation and removal of oxides on the surface.

Adhesive wear is defined as wear by transferring material from one surface to the other, during relative motion under load due to a process of solid state welding. When adhesive wear is severe, coarse macroscopic metal transfer is seen on the surface. This gross damage on the surface is called galling. In the adhesive wear, terms such as mild and severe wear are often used. Severe wear is characterized by heavy wear track, distortion of grains below the surface, formation of wear debris at surface with large metallic lumps (10 μm to 1 mm size) and high wear rate of 10^{-7} to 10^{-6} mm^3/Nmm. Wear rate is the ratio of wear volume to product of load and distance.

Mild wear is characterized by less distortion, smaller wear track, fine wear debris and low wear rates in the range of 10^{-9} to 10^{-8} mm^3/Nmm. Mild wear is important for polishing.[11]

Erosive wear shows impingement on the surface, as an effect of hitting of particles. Fatigue wear is associated with the crack propagation that often is seen in as the delamination. Tribochemical wear involves removal of surface materials atomically through friction-induced chemical reactions. Erosion is the material removal due to particles impact against wafer surface.

1.3.2 Testing

This research uses basically two configurations, pin-on-disk or disk-on-disk type machines are normally used for wear testing. Reciprocating or rotating motions are used for creating sliding actions between two surfaces. The instruments are equipped with controlled speed, force, time, temperature and environments. Experiments are designed in such a manner that the test conditions simulate the realistic performance conditions of the

components in service. Summary of testing geometry selection for sliding wear is done in table 1.1.

In the tribological experiment, the normal and the tangential force measurements are done to calculate the coefficient of friction (μ) as given in the equation 1.1 above. Piezo-electric crystals or resistance strain gauges can be used for such force measurements. Rapid measurements of the force change is necessary and hence high speed piezo based devices are used instead of mechanical devices. The test setups usually operate on load applications using dead weights or by using electromechanical devices. Dead weight type loading system may show variation in dynamic loading condition during testing. The piezoelectric based electromechanical force application systems are based on feedback system and hence can give a better constant loading condition during testing.

Table 1.1: Typical test geometry for various types of wear tests[12]

Subcategory of sliding wear	Testing geometry
2 body abrasive wear	• Flat pin on rotating drum • Reciprocating pin on abrasive flat • Spiral travel of pin on abrasive disk
3 body abrasive wear	• Dry sand fed between rotating rubber and flat specimen • Reciprocating flat pin on a plate in slurry bath • Block-on-rotating ring in slurry bath
Adhesive wear	• Block on ring • Pin-on-disk
Polishing wear {ibid}	• Flat specimen on vibrating lap • Flat specimen on orbital polishing or lapping machine

In the design of tribological experiment, sample surface preparation is an important step. Film present on the sample surface and surface roughness are dominating factors in wear mechanisms.

In wear tests, surface properties such as roughness along with the normal and frictional forces, and wear are estimated during experiments. For surface roughness measurement, various 2D and 3D topography measuring instrument are used. These instruments can be classified as:

- Stylus profilometry: A 2D/3D technique works on contact movement.
- Optical Profilometry:
    - Focus traveling type
    - Interferometry type
- Scanning Probe Microscopy:
    - Atomic Force Microscope (AFM) and
    - Scanning Tunneling Microscope (STM)

Two dimensional (2D) profilometry is widely accepted in engineering applications. Other precision equipments, such as optical profilometry, or 3D stylus profilometry is used. AFM and STM provide highest resolution but the working area is small. AFM and STM enable precise measurements of the surface topography. These techniques can generate area roughness values rather than a single line roughness values obtained with stylus profilometry.

In regard to the surface integrity, the average surface roughness is one of the most used parameters. In engineering applications, the value Ra is usually less than 5 μm for smooth surfaces, whereas Ra being higher than 10 μm is considered as high roughness surface.[5] In semiconductor application, the requirement is more stringent. Atomically flat surface

finishes are required for achieving better electrical properties. Surface roughness Ra values are of the order of less than a nanometer.

Further to this, for in-depth analysis of the wear test, temperature measurement of surface and bulk, chemistry of surface and wear debris generated, amount of material removed, surface damage occurred, etc., are points of interest. For example, in case of chemical mechanical planarization of integrated circuits, surface roughness after polishing and removal rate are most important factors for obtaining quality surface. To understand this, other parameters are also examined such as slurry chemistry, electrical potential, and surface charges, etc. The objective of wear tests in this research is to understand mechanisms.

1.4 Lubrication

Any third body that separates two sliding surfaces can be called as a lubricant. Lubricant basically to prevent the contact between micro asperities and reduces the wear. With increasing sliding velocity and loads, the lubricant film thickness firstly reduces. Friction coefficient is a function of the viscosity, load, and speed. At higher velocities, a full film is formed. This condition is called the elastohydrodynamic lubrication. Boundary film lubrication is observed at lower velocities, where the surfaces are mainly in physical contact and the friction coefficient μ is high. The diagram below showing these activities is called the Stribeck curve (figure 1.4). It was found by Stribeck in 1902[13] and later on was further modified by McKee in 1929.[14] This curve has been used to describing the behavior of lubricating systems and stood for tests in time.

Mineral oils, often used as lubricants, are usually mixed with additives. These additives are attached to the metal surfaces to assist the formation of the lubricating film. Oils have long chain molecular structure with a polar head that is attached on metal surfaces. In addition, lubricants are used as a coolant to carry heat away, to transfer wear debris, and to protect the surface from corrosion, etc.

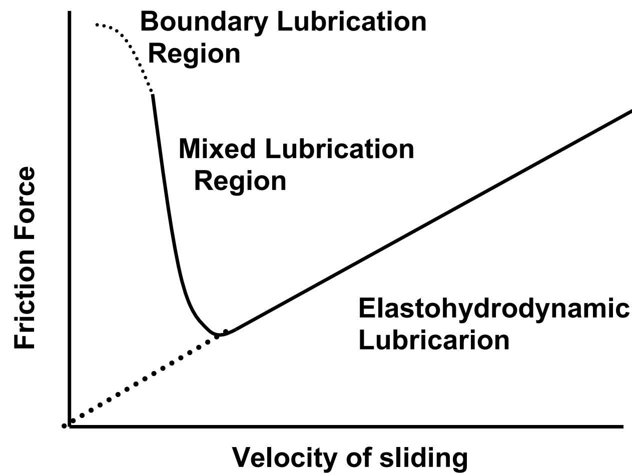

Figure 1.4 Conventional Stribeck curve, showing three different regimes: boundary lubrication, transition and hydrodynamic lubrication[13,14,15]

Recent advances in measuring instruments made it possible to explore wear mechanism to further in depth. The wear occurring due to molecular shear of lubricant at interface can be measured using in situ surface characterization technique[10] and the newly modified Stribeck curves are possible. The molecular structure of lubricants as well as liquid to solid transition of lubricants can be observed. Under high stresses, the transition (liquid to solid) was observed in the boundary lubrication regime associated with higher coefficient of friction. With increased shear resistance, the elastohydrodynamics lubrication presents high coefficient of friction.[14] Further more, it was found by Israelachvili et al. that the lubrication behavior was affected by the adhesive forces between lubricant molecules.

1.5 Tribochemistry

Tribochemistry is dealing with chemical and physicochemical changes of matter due to the influence of mechanical energy.[16,17] During tribochemical wear, synergistic effects between mechanical and chemical phenomena are observed. In the sliding wear contact,

in presence of theoretically inert counter body, the total reaction occurring (J_{tot}) is the sum of anodic wear (J_a) rate and mechanical removal rate (J_m).[8]

$$J_{tot} = J_a + J_m \quad [1.5]$$

This interaction is expected to proceed by various mechanisms as oxidation, removal and ejection of electrons, ions or atoms. The tribochemical reactions are dynamic in nature and follow non-steady state behaviors. In such it is difficult to mathematically model the process of a tribochemical wear.

Under boundary lubrication conditions, at the hot spots of contact, distinct chemical reactions have been observed.[18] These tribochemical reactions differ from thermomechanical ones. The reaction can be considered catalytic. Thermal emission of electrons at hot spot triggers the reaction. According to Kajdas et al.[18] and Heinicke[19] electrons, ions, photons, UV radiation, IR radiation, and acoustic emissions occur during sliding wear. These emissions cause formation of microplasma in the region near the contact area. There is also adsorption and absorption process occurring at the surfaces.

Triboreactions due to friction can be classified as:

- tribochemical reactions only initiated by mechanical friction
- thermochemical reaction (oxidation, polymerization, etc.)
- heat enhanced reactions, and
- catalytic process.

In one of his earlier studies, Fischer et al. conducted experimentation on silicon nitride.[20] With variation of load, temperature, or concentration of medium, linear variation in wear rate was observed. The friction coefficient μ decreases with increasing load which can be correlated with increasing oxidation rate on the surface.

Gases adsorbed on the surface form a layer. The friction is affected by its presence. These molecules when are polar in nature, gets sheared under friction. Molecules are further

adsorbed on the surface. This phenomena causes low wear. However if the load is increased, temperature raises leading to mild oxidation of the surface. The adsorbed molecules onto the oxide film enhances lubrication by maintaining lubricant molecules. These observations are noticed by Sullivan.[21] This is called as oxidational wear boundary lubrication occurred in the steels. It is later further confirmed by Liang in a different tribosystem.[22]

Tribochemical reactions in sliding solids show that friction on surface increases as the oxidation rate increases. This is seen often in steels. This is not necessarily true for other materials. Tribochemical reactions are complex, dynamic, and are not equilibrium. Change in μ can not be used as a parameter to predict the wear in tribochemical interactions. It is difficult to quantify such reactions with mathematical models.[28]
When two body wear of aluminum is considered, transition from mild to severe wear is observed. When aluminum is slid by mild steel in presence of oxygen, it was found that initially the corrosion rate is low, the wear occurs by deformation and delamination mode. In this process a mild wear is observed. At higher sliding velocities, corrosion or oxidation rate increases, causing the formation of an oxide film. The continuous oxide film reduces the friction and mild wear are observed. At high velocities, corrosive wear is high, causing the severe wear.[23] In the tribochemical wear, the corrosive wear rate is the dominating factor for high load and velocity as studied by Cheng et al.[24] This analysis can be used for derivation of wear maps with reference to sliding velocities.

Hogmark et al.[25] and Mishina[26] noticed that the hardness of the counterbody should be considered while predicting the two body or three body abrasive wear of aluminum. Studies were conducted with pure aluminum and aluminum alloys of different hardnesses. It was observed that if the hardness of the counterbody is high, the wear rate is high as more material is removed by plowing of the soft body. However if the wearing material work-hardens, the burr particles are hard enough to wear the counter body as well. In case of high hardness of a counterbody, the wear particles from the hardbody

gets embedded into the soft one and wear is subsequently reduced. In this case the two-body wear becomes a three-body wear. As seen the hardness of the counterbody plays an important role.

In the extensive wear mapping studies, Ashby et al.[27] have reported that at very high loads and velocities during sliding friction, surface metal melts, oxidizes, and severe wear is observed. It is accepted that mild wear provides smooth surface while severe wear leads to a rough one. On the contrary, in an early study by Kerridge,[28] it was estimated that metal transfer, formation of oxide layer, oxide transfer and again metal transfer occurs in cyclic process. This study states the oxidation of transferred metal while the earlier study by Ashby et al.[27] states melting of the transferred metal

Tribochemistry has been studied to a great depth to understand the lubrication behavior. Fishcer[29] has found that at a low sliding speed, tribochemistry is of great importance as the chemistry of the lubricant plays important role. At higher speeds, it is not as complex. When the hydrocarbon lubricant burns at high temperature, in the region of hot spots, peroxides are generated. It causes corrosive wear.

1.6 Triboelectrochemistry

Triboelectrochemistry is defined as the chemical-electro-mechanical process. It consists of material conversion or removal at a surface exposed to sliding or rolling contact immersed in chemically aggressive electrolyte and under action of forced electropotentials. Material conversion means change in chemical forms. For example, metal to metal oxide or oxide to hydroxide are typical ones. Material removal is referred to the physically dislodged from its surface. Burr formation or ionic dissolution is an example of material removal. Individual reactions on the exposed surface are mechanical wear, chemical dissolution, etching or oxidation, and electrolytic or anodic dissolution or cathodic passivation. Friction induced surface reaction may modify the corrosion

sensitivity of the contacting materials and in turn corrosion may modify the friction condition by generating triboreactive surface films. These surface films have unique sliding properties. The resulting interactions however are complex in nature and are of great interests to the researchers in fields of corrosion, lubrication, and polishing. Usually the corrosion or wear rates are observed to be increased as an effect of mixed interactions.[30]

Different materials have been investigated for triboelectrochemical interactions. Mischler et al.[31] investigated TiN in aqueous solutions. Mishler et al.[32] and Ponthiax et al.[30] have investigated 316 stainless steel and nickel Alloy in sulphuric acid solution. Assi et al. in 1999[33] has written on synergy between these interactions. Since synergism is a complex phenomenon and is dynamic in nature, it is often difficult to analytically quantify it. Watson et al.[34] have proposed penetration rate equations for such quantification. Assi et al.[33] in 1999 experimentally measured the triboelectrochemical interaction using a metal probe method.

The combined interactions can be studied with in situ electrochemical measurements during the sliding experiments in presence of corrosive electrolyte. The tests include potentiodynamic, polarization, impedance measurement, and sliding experiments performed at different applied potentials. The other in situ tests include acoustic emission and friction measurement. Ex situ surface characterization techniques are used for understanding the interactions. These include X-ray photoelectron spectroscopy (XPS), Raman laser spectroscopy, X-ray diffraction (XRD), scanning electron, transmission electron, atomic force, scanning tunneling, and optical microscopy.

In situ characterization techniques provide the information about the instantaneous interactions. Since these reactions are dynamic and the data generated is complex. The practical limitations in analysis restrict the collection of useful information.[30] For example, impedance measurement during tests can provide the information about the

oxide films on the metal surface. The test requires positioning of the test probe close to the surface. Since the surface is under sliding condition, it is not accessible to the probe. Furthermore, it should be noted that analysis in electrochemical tests requires an equilibrium state. However, most triboelectrochemical system does not reach a stable state. This exhibits technical challenges for such method. The resultant of the interaction is a race between three different interactions: chemical, electronical, and mechanical. During a tribo-electro-chemical process, the kinetics of three individual and combined interactions are expected to vary with changing conditions. In spite of changing conditions, surface characterization techniques provide useful information that can be correlated to the test parameters.

1.7 Surface Characterization for Tribological Surfaces

Surface characterization is an important technique to reveal surface information such as topography, phases, structure, and composition. This information can then be used for understanding the mechanisms and interaction occurring in the tribological process.

Topography can be obtained by using instruments like optical microscope, Atomic Force Microscope (AFM) and Scanning Electron Microscope (SEM). Chemical, structural and phase information can be received from AFM, SEM, ellipsometry, XRD, XPS or TEM studies. Some of these techniques and their working principles are discussed below.

1.7.1 Scanning Electron Microscopy (SEM)

Electron microscopy takes advantage of the wave nature of rapidly moving electrons. Electrons accelerated to 10 KeV have a wavelength of 0.12 Angstroms. Optical microscopes have their resolution limited by the diffraction of light to about 1000 diameters magnification. Electron microscopes have good resolution up to few nanometer dimension at high magnification. Besides having high magnification, electron microscopy is also useful for structural and chemical characterization. Two of the electron microscopy techniques are discussed here.

The scanning electron microscope generates a beam of electrons in a vacuum. That beam is collimated by electromagnetic condensor lenses, focused by an objective lens, and scanned across the surface of the sample by electromagnetic deflection coils. The primary imaging method is by collecting secondary electrons that are released by the sample. The secondary electrons are detected and amplified by a photomultiplier tube.

By correlating the sample scan position with the resulting signal, an image is formed that provides the three dimensional information of surface topography.

There are other imaging modes available in the SEM. Backscatter electron (BSE) imaging uses high energy electrons that emerge nearly 180 degrees from the illuminating beam direction. The contrast regime in BSE imaging is a function of the atomic number of each point on the sample, and thus can give rise to contrast.

Scanning electron microscopes are often equipped with x-ray analyzers. The energetic electron beam - sample interactions generate x-rays that are characteristic of the elements present in the sample. Many other imaging modes are available that provide specialized information.

In tribology, SEM imaging is done to study the surface morphology, surface chemistry and measurements. These observations are used to study the wear mechanisms and surface interactions in tribosystems. Observations are done for all the components in the system for example polishing pad, slurry particles, surface after sliding friction, etc,.[35]

1.7.2 Transmission Electron Microscopy (TEM)

TEM is a technique of imaging internal structure of solids. It uses a beam of high electrons passing through the samples. TEM can be combined with electron dispersive x-ray spectroscopy and electron energy loss spectroscopy for chemical characterization.

The basic principle of the TEM is that the beam of electrons passes through the sample and thereby generates an image that constitutes a projection. At the back focal plane, electron diffraction pattern is formed that gives the information about the lattice structure and parameters of the sample. In tribology, TEM is used for imaging dislocation in deformed surface layers below the wear track. It is also used for characterization of wear particles and abrasive particles.

The sample preparation for TEM must be done very precisely and may sometimes take a long time. The specimen is thinned to few tens of nanometer thickness. Extreme care is necessary in sample preparation to avoid any alteration in the sample structure.

1.7.3 Atomic Force Microscopy (AFM)

Binnig and Quate[36] invented AFM in 1986. Basic operating principle of AFM is similar to surface profilometer. It uses a sharp tip with a radius less than 10nm on the cantilever of about 100-200 µm length. The tip is moved over the specimen surface using piezo system in raster scan. The displacement of the cantilever is detected by laser reflection from the back of the cantilever. The piezo system moves the cantilever in an up and down direction to maintain the initial position of the cantilever. This is feedback mechanism as utilized by AFM. Various imaging modalities are possible with analysis of signal received in AFM such as friction, phase, magnetism, and topography. Height image is most commonly used mode for observation of topography. To obtain these signals from a surface, various operating modes are implemented. Most common methods of the AFM operation are contact mode and non-contact mode as described below.

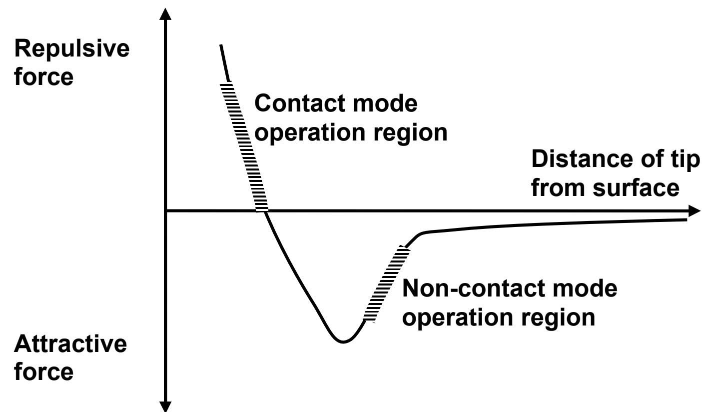

Figure 1.5 Operating regions for AFM in the van der Waals force regions

1.7.3.1 Contact Mode AFM

In this mode of operation, cantilever tip is lowered on the surface of specimen such that according to the van der Walls forces, the tip is in the region of repulsive forces as shown in figure 1.5. As the cantilever tip scans the surface. The cantilever tilts depending on the sliding friction between the tip and the surface. Variation in response due to variation in resistance to sliding can thus be detected to identify different phases on the surface. The height image on the other hand provides the topography image. Basic construction of the AFM and contact mode operation is schematically shown in figure 1.6. Force on the cantilever in contact mode is between 10^{-7} to 10^{-6} N.[37]

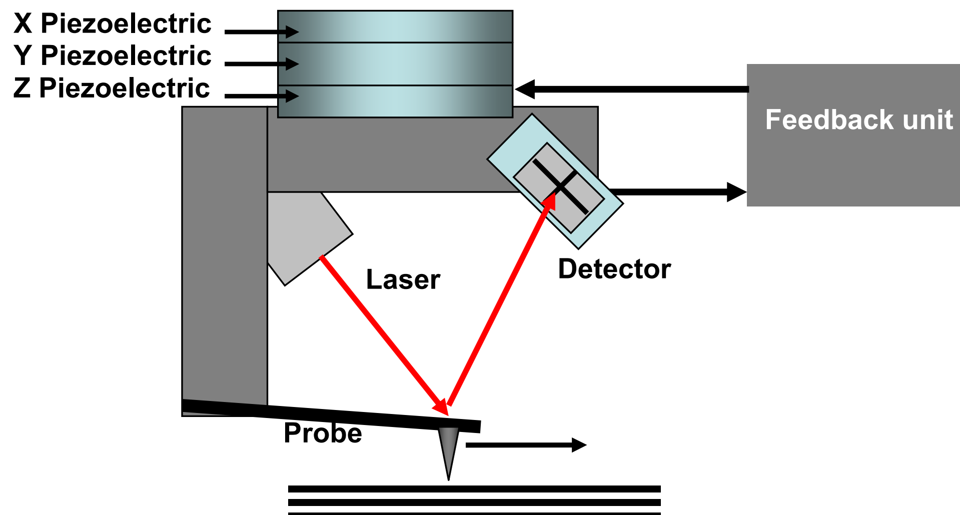

Figure 1.6 Schematic diagram of AFM in contact mode

1.7.3.2 Non-contact Mode AFM

Martin et al. in 1987[38] demonstrated that if the AFM cantilever is vibrated in the attractive force region of surface under study, then high resolution image can be observed. , In non-contact mode, the tip is separated from the surface and synchronizes its vibration in weak attraction region. The cantilever used is having high stiffness than that used in contact mode. AFM cantilever is vibrating with its resonant frequency(200-300kHz) with an amplitude of less than an angstrom as shown in figure 1.7. Attractive van der Waals forces vary with the distance between the tip and the sample and cause the tip's resonant frequency to change. In non-contact mode, a very small force of attraction 10^{-12} is sensed. Use of this mode avoids tip contamination and sample surface is not altered by scratching. Because the probe comes into close contact with the surface upon each oscillation, it is able to sense the materials on a surface.

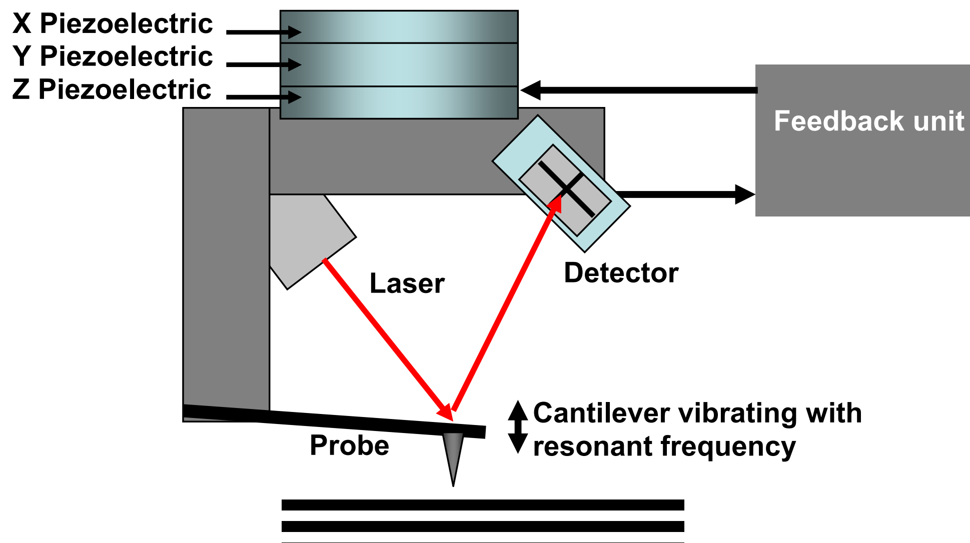

Figure 1.7 Schematic diagram of AFM in non-contact mode

AFM is used in tribology for various different characterization such as

1. topography observation
2. surface roughness measurement
3. surface feature measurement (step height measurement, wear particle size measurement)
4. phase imaging
5. friction mapping.

1.7.4 X-Ray Photoelectron Spectroscopy (XPS)

XPS was developed in 1960. It is also called as Electron Spectroscopy for Chemical Analysis (ESCA)[39]. It is used for surface analysis. In XPS, the surface of sample under high vacuum (pressure less than X 10^{-9}) is irradiated with monoenergitic soft x-rays. Mg Kα (1263.6 eV) or Al Kα (1486.6 eV) are used as source. This photon interacts with the sample surface and emits the electron called as photoelectron. Figure 1.8 shows the schematic of this emission. Kinetic energy KE of the emitted electrons is proportional to the energy of the irradiated photon energy hν. The equation is given as

$$KE = h\nu - BE - \phi s \quad [1.6]$$

where BE is the binding energy of the atomic orbital from which the electron originates. ϕs is the spectrometer work function. Binding energy is the energy difference between the initial and final states after the photoelectron has left the atom. The binding energies of electrons in different orbitals of the atom can be detected in XPS. Each element has a unique set of binding energies. These elemental binding energies vary depending on the chemical potential or polarizability of the chemical compound. These chemical shifts can be used to identify the chemical state of the material.

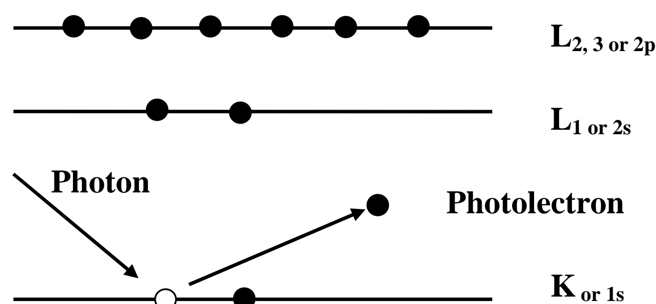

Figure 1.8 Schematic of photoelectron emission

In the process of photoelectron emission, during relaxation of excited ions, Auger electron emission also takes place. As the electron in outer shell falls in to inner orbit al vacancy, an Auger electron is emitted. Kinetic energy of the Auger electron is equal to the difference between energy of initial ion and the doubly charged final ion. The schematic of the Auger electron emission is shown in figure 1.9.

Auger electrons or photoelectrons emitted have a high interaction with matter and hence those originate from only top few angstroms depth from surface are available for

analysis. These electrons which leave the surface without loss produce the peaks in the spectra.

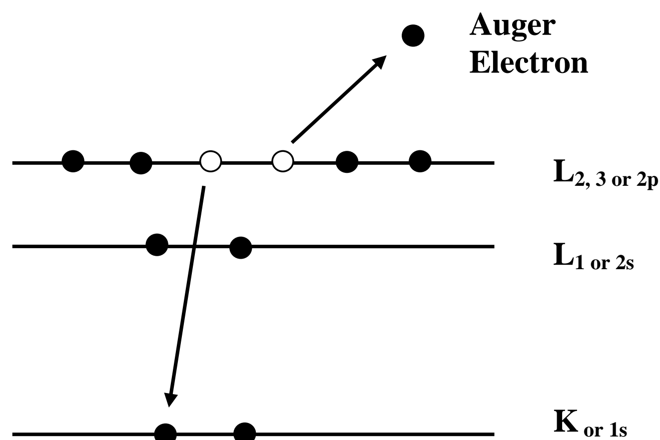

Figure 1.9 Schematic of Auger electron emission

Energy of the electrons leaving the sample is detected by the detector. The number of electrons detected for a particular energy is displayed as spectra which are later used for analysis.

A very careful sample preparation and sample handling is necessary as a very surface characterization is done. Any contamination from the environment will end up giving incorrect analysis. Foe depth profiling of the surface or also for removing surface contamination, plasma etching or oxygen etching of the surface can be performed while the sample is still inside the analysis chamber.

Data interpretation in XPS is an important step. Spectrum is displayed as number of electrons versus electron binding energy. Several types of peaks are observed in the XPS spectra. They are mainly photoelectron lines, Auger lines any x-ray satellites. The overlapping energy peaks add up to the intensity and can merge in to one peak with wide

energy lines. Also depending on the other elements and the chemical state of the elements, these peak positions can shift to some extent. Hence, calibration and right interpretation of observed values is very important. Standard values for binding energies for different orbitals for particular elements, for Mg Kα or Al Kα can be found in handbook. These values can be used as a reference to determine the binding energies for the chemical states for the observed peaks. One such list of binding energy values for copper 2p3/2 orbital is given below (Table 1.2).

Table 1.2 XPS binding energies (eV) for Cu 2p3/2 for different oxidative states[40,41,42]

State of Copper	Binding energy (eV)
Cu	932.6
CuO	933.7
Cu_2O	934.5
$Cu(OH)_2$	935.1
$Cu(CH3COO)_2$	934.2

XPS provides a most suitable tool for investigation of tribofilm – a surface film formed because of tribological interaction. It provides qualitative information of this surface film.

CHAPTER II
TECHNOLOGICAL DEVELOPMENT OF CHEMICAL-MECHANICAL POLISHING

2.1 History of CMP

As a step towards future development, IBM invented CMP in 1983 for oxide layer in the Integrated Circuit (IC).[43] Until 1988, research and development on CMP was exclusively performed within IBM. IBM shared some CMP data with Intel's interconnect technology. Subsequently, in mid-1980s IBM collaborated with Micron Technology, CMP for dynamic random access memory (DRAM). In 1989, IBM published the first paper which publicly discussed CMP of oxide films.[43] Since then a significant amount of publication on CMP appeared. The research and development of the process is continuously carried out to enable the advent of the new technology.

At the same time, in 1983, when IBM was developing the CMP technology, at Base Technology Lab, New York, inlaying of copper in trenches made in metal was being done for jewelry purpose. This process was adapted from the Damascus therefore it is referred as damascene pattern. The similar technique of making trenches, filling it with copper and polishing off the excess was then adapted by IC manufacturers for making interconnect or wiring of components. This is the development of metal CMP.[43]

CMP development hence was lead by IBM and then followed by Intel and Micron. IBM further extended the knowledge and expertise to the Sematech. The Sematech is an organization that sets the industry direction. It accelerates the semiconductor industry's development.[44]

2.2 Evolution of Integrated Circuit Technology

A semiconductor device such as an IC (integrated circuit) generally has electronic circuit elements such as transistors, diodes, and resistors fabricated integrally on a single body of semiconductor material. The various circuit elements are connected through conductive connectors to form a complete circuit which can contain millions of individual circuit elements. Advances in semiconductor materials and processing techniques have resulted in reducing the overall size of the IC while increasing the number of circuit elements.

These transistors are made by deposition of metal oxides and etching them in the required regions. A typical structure is shown in figure 2.1. As designated by IBM, this is a structure of a transistor called a CMOS (Complementary Metal Oxide Semiconductor). A polysilicon (SiO_2) dielectric layer deposited on this structure is then planarized by oxide CMP. Flow of electric current from source to drain through gate is controlled by applying excitation potential. This is a switch type transistor used in the electronic circuit.

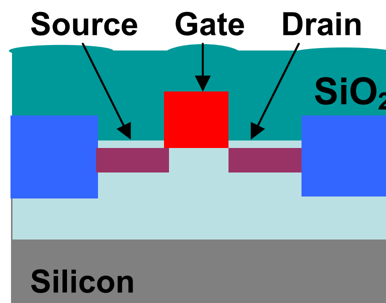

Figure 2.1 Section of component of a Complementary Metal Oxide Semiconductor (CMOS)

Additional miniaturization is highly desirable for improved IC performance and cost reduction. Interconnects provide the electrical connections between the various electronic elements of an IC and they form the connections between these elements and the device's external contact elements, such as pins, for connecting the IC to other circuits. Typically, interconnect lines form the horizontal connections between the electronic circuit elements while conductive via plugs form the vertical connections between the electronic circuit elements, resulting in layered connections. A typical section of this damascene structure of IC is shown in figure 2.2. Atomic layer deposits (ALD) are used to separate the copper from dielectric, to avoid the electromigration of copper in to the dielectric materials.

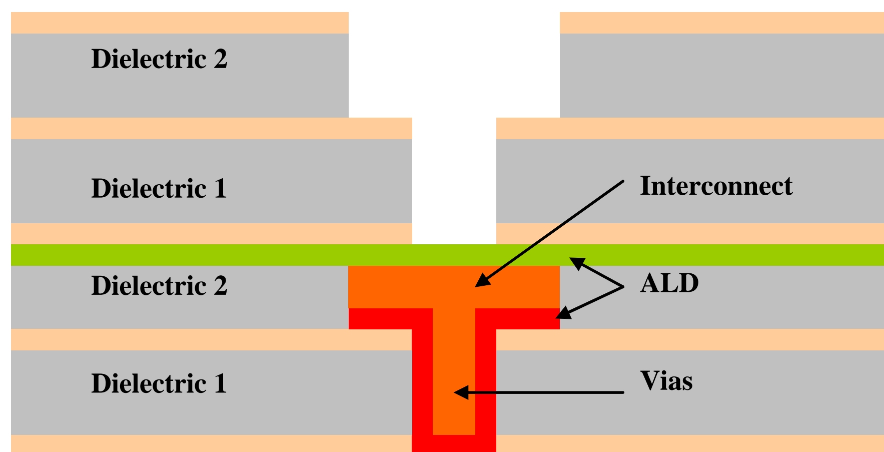

Figure 2.2 Section of integrated circuit showing copper damascene pattern

A variety of techniques are employed to create interconnect lines and vias. One such technique involves a process generally referred to as dual damascene, which includes forming a trench and an underlying via hole. The trench and the via hole are filled simultaneously with a conductor material. The evolution of IC manufacturing is driven by three major requirements of the market

1. Density: number of components (like transistors) per square inch of circuit.
2. Speed: number of processes/ operations performed per second, and
3. Reliability: reliability of the product for large production volumes.

High device density is a tool for miniaturization of the electronic circuit. Increase in the density increases the difficulty in the process and needs technological advancement to achieve it. High processing speed is an outcome of smart circuit design and processing approach. Use of fast response materials in the design is also the criteria for high processing speed. And the reliability is the parameter conclusive of the technology, tooling, process and expertise.

In 1965, Intel co-founder Gordon Moore predicted that the number of transistors on a chip doubles about every two years. This is popularly known as Moore's Law.[45] This observation about silicon integration, made a reality by Intel, has fueled the worldwide technology revolution. The law is also applied to other aspects such as transistor size, cost of memory, processing speed, etc. It seems that the miniaturization of device is reaching the physical limits of the nature even then the research is showing the advancement with time. As on today, Intel and AMD have started manufacturing product with 65 nm node size of the transistor. The future is that in 2007 it will be 45 nm, in 2009 it will be 32 nm and in 2011 it will be 22 nm node sizes. This trend is targeting towards the few atoms wide node size. This is the physical limit. Also at this device dimensions, interconnect size shrinking is not possible. It needs radical solutions. The research efforts are now exploring the use of photonics in place of electric current for transistor switching operations.

2.3 Role of CMP in IC Manufacturing

CMP is performed for the oxide (silicon dioxide) and metal deposits. Metal deposits are typically of tungsten, copper and aluminum. The applications of this planarization is required in three major product areas as

- Integrated Circuit (IC)

- Dynamic random access memory (DRAM) and
- Micro-electromechanical systems (MEMS)

Amongst these functional applications, IC manufacturing is the most difficult. Most of the research and development activities are performed in this area. Manufacturing of an IC in bulk process usually takes several hundred steps. A few of these steps are shown schematically in figure 2.3, emphasizing the copper CMP. As described above, the process starts with making silicon wafers from silicon single crystal. Next the devices are fabricated on the silicon surface. Then the trenches are made on this surface with steps as photoresist coating, photolithography and etching. These trenches are filled with copper by deposition. The over deposited copper is removed by CMP leaving interconnect circuit on the surface.

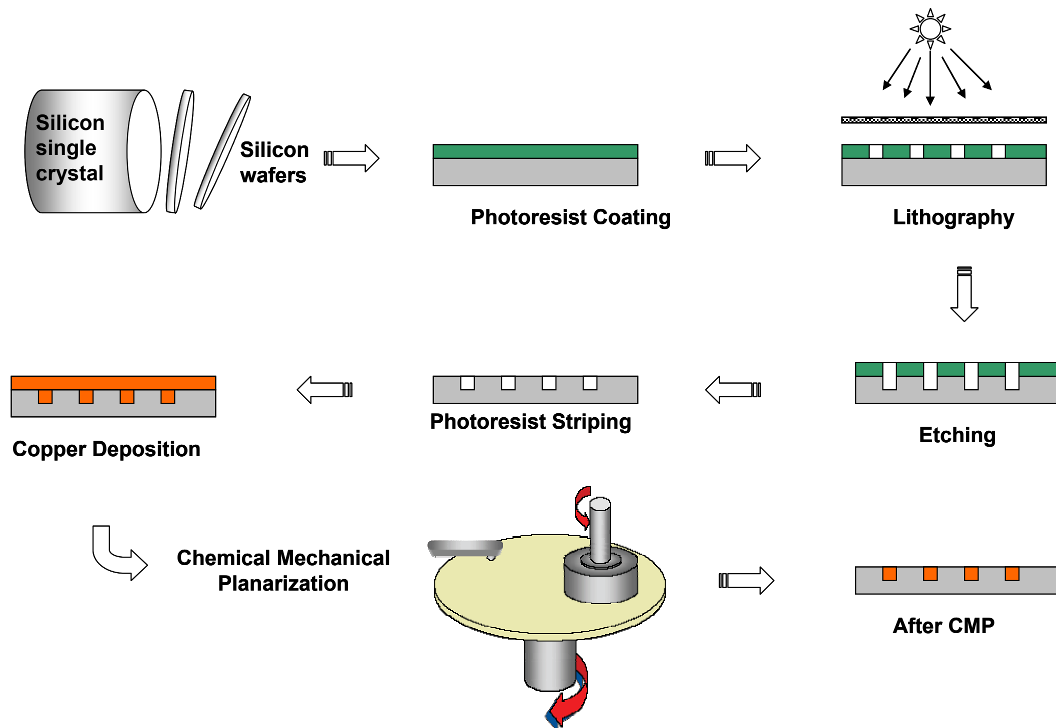

Figure 2.3 Schematic of the steps in IC manufacturing

2.4 Research Areas in CMP

The word chemical-mechanical polishing (CMP) is also used as the chemical-mechanical planarization. The CMP in polishing means making a smooth surface. The CMP in planarization means making a flat surface. In this work CMP means polishing. It is because the focus here is on removal mechanisms from atomic to micrometer length scales.

Table 2.1 Interdisciplinary research areas in CMP

Mechanical Engineering	Fluid dynamics of slurry and slurry particles, force measurements, CMP machine tool design, material handling, automation, etc.
Tribology	Wear, erosion, friction, lubrication, contact mechanics, metrology, etc.
Materials Science	Material and surface properties, microstructures, materials characterization, e.g., residual stress measurements, surface chemistry, etc.
Electrical engineering,	Electrical properties measurement for defect identification, engineered designing for efficient CMP processing.
Chemistry	Slurry composition and achieving desired etch rates, maintenance of slurry, slurry handling, environmental issues, corrosion and passivation, post CMP cleaning solutions, etc.
Physics	Material removal mechanism, surface properties, characterization.
Electrochemistry	Surface charges, electrochemical studies in CMP.

Polishing has long been used in manufacturing to make smooth or flat surfaces for optical lens, metal finishing, integrated circuits, and memory disks. CMP researchers include

chemists, electrochemists, electrical engineers, materials scientists, mechanical engineers, physics, and tribologists, among others. The CMP is an interdisciplinary area. Major perspectives studied by those scientists in these areas can be roughly listed as in table 2.1. This table is far from being complete and research areas are not restricted to the areas shown. Being an interdisciplinary field, CMP requires different approaches to solve the related issues.

The question arises here is why this field of research is so interdisciplinary in nature? A simple answer to this question is that the CMP process is complex in nature. The reason can be found from the history and technological development path of the CMP.

2.5 Copper CMP Challenges

Integrating copper with low dielectric constant (low-k) materials is critical to the development of next-generation ultra-large-scale- integrated circuit (ULSI) technologies[46]. CMP is facing the same rate of advancement as the IC industry, for high speed, high reliability and high circuit density.

To reduce device resistance and capacitance (RC), copper will be coupled with low-k interlayer dielectric (ILD) materials in dual-damascene architectures, thereby reducing RC time constant delays in interconnect devices.

A variety of copper and low-k approaches and integration schemes are currently being explored, as there are many different types of low-k ILD materials available. The two main classes of these low-k ILD materials are chemical vapor deposition (CVD) and inorganic or organic spin-on dielectric (SOD) films. Each type of low-k material poses a unique set of challenges. The introduction of copper and low-k materials demands better CMP consumables and integrated metrology to meet the upcoming requirements for 300 mm wafer manufacture.

2.6 Business in CMP

Business in CMP can be classified as the users and providers or suppliers. Users are the semiconductor industries involved in the manufacturing IC using CMP in it. Suppliers are those who make tools and consumables for the process. The growth of business in CMP is showing healthy rise. In 2003 worldwide market for CMP and post-CMP equipment and materials was $1.7 billion. This is expected to reach $3.2 billion by 2008.

The largest share of the market is for CMP and post-CMP equipment, which was $925 million in 2003. CMP slurries have a share of 24% followed by CMP pads with 15% of the market, the rest being other consumables as per the market research done by BCC.[47]

CMP business is associated with the demand of the IC and memory chip in the market. This is why the CMP business shows similar growth and recessions in the market trend. Some of the companies performing CMP are listed in Appendix I.

2.7 International Roadmap for Semiconductors

The International Technology Roadmap for Semiconductors (ITRS) is an assessment of the semiconductor technology requirements. The objective of the ITRS is to ensure advancements in the performance of integrated circuits. This assessment is called the roadmap. The purpose of the ITRS documents is to provide a reference of requirements, potential solutions, and their timing for the semiconductor industry. Its objective is to provide a forum for international discussion, cooperation, and agreement among the leading semiconductor manufacturers and the leading suppliers of equipment, materials, and software, as well as researchers from university, consortia, and government labs. The ITRS identifies the technological challenges and needs facing the semiconductor industry over the next 15 years.[48]

The development cycle of the IC industry is driven by the node size of the transistor. ITRS reviews the past present and future of the technology, around the world, considers

the research strengths and forecasts the future development of IC fabrication. The focus areas considered are listed below.

- Design
- Test and Test Equipment
- Process Integration, Devices, and Structures
- Emerging Research Devices / Emerging Research Materials
- Front End Processes
- Lithography
- Interconnect
- Factory Integration
- Assembly and Packaging
- Environment, Safety, and Health
- Yield Enhancement
- Metrology
- Modeling and Simulation

This list covers issues of technology, research, development, tooling, process integration as well costing. The ITRS identifies the principal technology needs to guide the shared research, showing the “targets” that need to be met. These targets are as much as possible quantified and expressed in tables, showing the evolution of key parameters over time. This quantification is listed below.

- Manufacturable solutions exist, and are being optimized
- Manufacturable solutions are known
- Interim solutions are known
- Manufacturable solutions are NOT known

ITRS also summarizes the production cycle of a typical node size product identified as research, development and production. The summarization is done based on the annual production volume of the industries worldwide. ITRS specifically discusses the challenges, issues and solutions related to the IC industry.

CHAPTER III
INVESTIGATION OF CHEMICAL MECHANICAL PLANARIZATION

3.1 Motivation

In spite of recent development in CMP technology, complete understanding in CMP mechanisms has yet to achieve. The major challenges remain in existing surface defects. These include pits, scratches, erosion, dishing, etc. leading to interconnect failure. During CMP, the mechanical forces, such as friction and its combined chemical reactions are the cause of those defects. In order to develop a defect-free CMP process, a good understanding is essential.

This research is to first understand the frictional behavior of CMP processes involving different abrasive particles. Beside standard oxide ceramic based particles, polymeric particles are investigated. The polished surface quality as well as the interactions between particles and chemical additives in slurries is studied. The relationship between the mechanical-chemical removal and surface roughness is explained.

3.2 Approach

This research uses experimental approach combined with a simple theoretical analysis in order to understand the effect of abrasive particles on CMP. The main emphasis was given on post CMP surface roughness. The experiments include the polishing tests followed by surface characterization. Friction forces in polishing were correlated to the polishing quality in terms of surface roughness. An overall model describing removal mechanisms are provided.

3.3 Materials Used in CMP

The chemical mechanical planarization (CMP) is applied to various manufacturing processes. Materials involved in CMP are wide in range. In IC fabrication, these

materials include, silicon (substrate wafer material), silicon dioxide, aluminum, tungsten, copper (interconnect), polymers, and recently developed low-k dielectrics. In this research we are focusing on copper.

Copper has an atomic number of 29. Its outermost energy shell has one free electron. This makes copper a good conductor. Copper is the most widely used material in IC industry today. Beside its good electrical conductivity, it is also resistant to electron migration, and thermoconductivity. Copper has good corrosion resistance in ambient environment. This is due to the high density of the passivation film or oxide film on bear copper surface.

In ICs, copper is used as an interconnect material for electrical connection. By using lithographic techniques, trenches are made in a silicon wafer. Copper is deposited using techniques such as sputtering or electroplating. Copper in direct contact with silicon wafer can cause an electromigration effect that causes failure in wires. It is avoided by depositing a thin layer of titanium on silicon wafer before copper deposition. Usually a thin seed layer of copper is first deposited using the physical vapor deposition technique. After that, the electrolytic deposition is used to coat the remaining copper. The method enables good adhesion. After deposition, heat treatment (annealing) is performed to reduce the internal stresses. It is then followed by CMP.

Comparing with other structural metals, copper is a ductile material. It has low Vicker's hardness (369 MPa)[49] and tensile strength (240 MPa)[49] Copper alloy, such as bronze, is ideal as a wear resistant material.

3.4 Material Removal Rate

Material removal rate (MRR) in CMP is usually measured in terms of height or the thickness reduction in polishing per unit time. It can be measured with techniques such as weight loss and direct thickness change. It is known that the contact stress across a wafer

is not uniform, i.e., the edge effect. Therefore, the removal rate is often seen uneven. Usually, the MRR in the edge area of wafer is higher than that in the centre. There are several possible reasons, such as fluid pressure displacement, elastic deformations in the holding fixtures and wafer, and non-uniform speed across the wafer, among others.

Factors affecting material removal rate are several. The factors can be classified into three different categories. They are mechanical – down pressure, speed, abrasive; chemical – pH, oxidizer, corrosion inhibitor; electrochemical – anodic or cathodic impressed potential. In order to understand MRR mechanisms, different approaches have been applied. These include direct separation of mechanical wear, chemical dissolution, and anodic interaction.[90] The following sections discuss wear aspects of CMP.

3.5 Down Pressure

Pressure applied to the polishing pad introduces a close and conformal contact of the polishing pad and the wafer surface. The material removal rate MRR is directly proportional to the applied pressure P and can be represented by Preston's equation. However, Preston equation does not consider some of the aspects such as chemical activity, tribochemical interactions, abrasive and material hardness. Some efforts have been made by researchers to modify the Preston equation[50,51] as shown below:

$$MRR = KPV + MRR_{chemical} \quad [3.1]$$

where K is a proportionality constant and V is linear velocity of the wafer relative to the polishing pad. The other constant, $MRR_{chemical}$ is to accommodate the chemical effects. As observed by Guo et al.[52] in copper CMP, initially with increment of pressure, the removal rate increases rapidly up to 150 kPa and then stabilizes. This phenomenon is probably related to the formation of copper oxide on the copper surface.

Applied pressure dominates the interfacial contact between the pad and the surface to be planarized. The interfacial force, i.e., friction in this study, is a function of sliding velocity. The relation between the friction coefficient and the sliding velocity is shown in

figure 1.4 for a sliding system similar to a thrust bearing. This curve is called as the Stribeck curve and was firstly discovered by Stribeck in 1902. The slurry flows through in between contact areas like a lubricant. Reports on contact mechanics[53] and fluid mechanics[54] aspects have shown that the achievement of planarization is not possible with mechanical action alone. If a continuous layer of liquid is present on the surface, slurry transportation plays an important role in material removal. In this situation, the pad itself does not contact with the surface directly. It is the collision of abrasives that is responsible for the mechanical action on the wafer surface. Therefore, the kinetic energy of the abrasive particles and the attack angle of these particles on the surface determine the material removal rate in the CMP. Nevertheless, it is proved that the hydrodynamic lubrication condition does not exist[55] and the polishing pad is in close contact with the surface. The lubrication regime is mixed: viscoelastic. When the slurry layer is not continuous on the surface, the pad comes in direct contact with the surface. The abrasives are pressed against the surface which will cause material removal action. A Hertzian contact model is usually used to estimate this material removal on surface by abrasives in the slurry. Asperity contact forces are higher than the applied pressures. They are responsible for cutting actions. These forces cause mechanical dislodging of material from the surface. Various atomistic removal models have been developed to understand the mechanisms in this process.[56,57,58]

3.6 Speed

Speed is another aspect affecting material removal. It is the relative motion between the pad and surface being polished. As seen in the Stribeck curve and in the Preston equation, at high speed of polishing the material removal rate is high. The abrasive particles attack the surface with higher kinetic energy, more quantity of abrasive particle-surface interactions occur, and higher amount of slurry is transported. As observed by Luo et al.[51] for copper CMP, with increase of velocity up to 70 cm/s, MRR increases linearly and then levels off. Normally used speeds in the CMP studies and industry are about 150 cm/sec.[90]

3.7 Slurry Abrasives

3.7.1 Abrasive Types

Abrasive is one of the important constituents of slurry, which is responsible for mechanical interaction with copper surface during CMP. Alumina, ceria, and silica have been used for copper CMP.

Silica has a Moh's hardness of 6. It is most widely used abrasive for CMP. Some studies[59] of colloidal silica have suggested its application as slurries for copper CMP in low k dielectric substrate materials. Colloidal silica manufacturing provides a better control of particle size distribution of silica. Meanwhile, the zeta potential of particles in low pH slurry helps the particles to remain in suspension, resulting in a better particle distribution in the slurry.

Alumina has a Moh's hardness value of 8 - 9 in scale. In the slurry, a thin hydrolyzed layer, aluminum hydroxide, is formed that is less hard (3-4 Moh's hardness). This in consequence reduces its scratching tendency and maintains the material removal capability.[90]

Ceria (CeO_2) is one of the major abrasive materials used for copper CMP. Ceria has a low hardness (6 in Moh's hardness scale)[59] compared to alumina and silica. It shows better uniformity and planarity than conventional abrasives for copper CMP.[60,61]

Some efforts have also been made in order to use low abrasive content i.e. less than 0.5 %wt or no abrasive slurry for copper CMP.[62,63] According to Nishioka,[64] polymer resin can be used in replacement of conventional abrasives. His investigation proved that the problems of surface erosion and dishing can be reduced with the utilization of a low or no

abrasive slurry over the conventional one. He also noticed that material removal rates are reduced compared to the conventional slurries.

3.7.2 Particle Size

Particle size and size distribution of abrasive particles in slurry and their effects on the material removal have remained contradictory. Jairath,[69] has stated that increase in size and concentration of particles in slurry showed increased oxide CMP. However, the investigation by Izumutani,[65] has suggested the opposite. His studies show that the decrease of abrasive size provides better material removal. Chandrasekaran,[66] has reported that the removal rate increases with decrease in size of abrasive particles and then saturates. According to his study, the removal rate depends on the distribution of particle size. Cook[67] proposed that particle size distribution had no effects on material removal.

3.7.3 Abrasive Concentration

The quantity of abrasives in slurry also has influences on the material removal rates. Luo et al.[68] has suggested that with the increase of the abrasive weight concentrations, three regions of material removal exist: (a) a chemically dominant and rapidly increasing region, which range is determined by the generation rate and hardness of the surface passivation layer; (b) a mechanically dominant linear region, where the material removal is proportional to the weight concentration; and (c) a mechanical dominant saturation region, where the material removal saturates in that the total contact area is fully occupied by the abrasives. In practice, 3 to 5 %wt loading of abrasive particles are used in making CMP slurry.

3.8 Polishing Pad

Polishing pads are normally made from polyurethane material which has thermosetting ability. According to Jairath et al. 1994[69], polyurethane can be tailored to have chemical resistance and mechanical performance for the CMP process. It is necessary that pad

material should be hard enough to endure the abrasive actions and be chemically resistant to high or low pH slurry environments. At the same time it should not be hard enough to scratch the surface during polishing. If the pad is too soft, it will form a conformal contact on the surface, which leads to material removal from high as well as low points on the surface. Kim et al.[70] studied the effects of pad properties on material removal. Deshpande et al.[71] observed that the shear resistance and elastic modulus of the pad material could be modified by surface coating technique that would provide improved performance. However, this effect did not result in good planarization.

The structure and surface morphology of the pad is also important. Usually the surface has a texture with fibers or pores and is considerably rough. Pores help transporting the slurry to the surface during polishing. The edges of pores collect the dislodged material from the surface and carry it away.[72] Sometimes pad with large sized texture like grooves or pores on surface is used for efficient operation. In the recent studies by Feo et al.[73], it is postulated that the surface textured pads can be used for advanced low k dielectric material processing which requires low down pressure. Such surface texture can be manufactured by nanolithography technique. Some novel materials such as thermoplastic polyurethane with better performance due to less water interaction have also been suggested recently by Prasad et al.[74]

As observed by Ng et al.[75] during initial 10 minutes exposure of the pad to water, the hardness of the pad varies. This is called as initial conditioning of the pad. The friction coefficient of the pad changes during this conditioning which is due to water absorption at the polyurethane surface.[90]

Surface structure of the pad, like the surface pores, is important for action of material removal. During its usage over a period of time, pores are clogged or fibers are oriented in the opposite direction of sliding. This drastically reduces the material removal ability of pad. This condition is known as pad glazing.[55] The properties of the pad are able to be

recovered by scratching the glazed pad with hard diamond crystals attached to a metal disk which is known as pad conditioning. It removes the byproducts from the pores of pad and recovers its performance. However, in this process, the pad has to undergo high amount of wear and its life is generally reduced.

3.9 Methods and Materials

CSM® Tribometer was employed to replicate the CMP process tool. The schematic diagram of the experimental setup is shown in figure 3.1. A copper-coated-silicon-wafer sample was mounted in a container. The sample was kept immersed in the slurry throughout the polishing cycle.

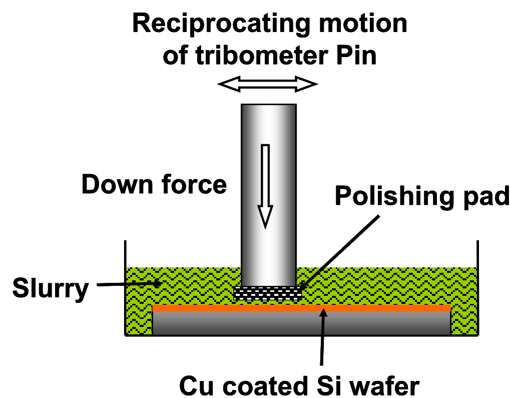

Figure 3.1 Experimental setup for slurry tests on Cu coated Si wafer

Polishing pad was fixed at the end of tribometer pin. Rodel® make, polyurethane pad of 1 cm^2 surface area was used for polishing. The down force used was 3 N/cm^2. Polishing was conducted for 3 hr. Relative speed between polishing pad and copper surface was kept 15 cm/sec during polishing. The friction coefficient as a function of polishing time was recorded during polishing.

Five different slurries were made, using 3 %wt loading of alumina abrasive particles in deionized water, by weight. The slurry composition for different slurries is listed in table 3.1. The slurry components are detailed as below.

Table 3.1 Slurry composition

Abrasive Alumina	Oxidizer H_2O_2	Polymer additive Latex	Polymer additive Teflon
3 %wt	---	---	---
3 %wt	0.5 %wt	---	---
3 %wt	1 %wt	---	---
3 %wt	0.5 %wt	---	0.5 %wt
3 %wt	0.5 %wt	0.5 %wt	---

3.9.1 Alumina Abrasives

The slurries were made with α-Alumina powder (Buehler® grade C Micropolish) with nominal size 0.05 μm in deionized water. Selection of alumina abrasives is based on its advantages mentioned in first part of this chapter.

3.9.2 Polymer Additives

Two types of polymer particles were selected. The selection criteria were based on mechanical property and chemical behavior. These particles were latex and Teflon®. The details of these particles are as given below.

3.9.2.1 Latex

Latex is an aqueous suspension of rubber particles. These particles have a rubber core size of about 90 nm in diameter and are covered with a copolymer of shell thickness of about 10 to 20 nm.[76] These particles are used as additives in epoxy based polymers, for improving their toughness and tensile strength.[77]

3.9.2.2 Teflon

Teflon® fluoroadditive is a white free-flowing polytetrafuoroethylene (PTFE) powder. It has low-surface energy. It provides improved lubricity and wear resistance. It can be used at temperatures from –190 to 250°C (–310 to 480°F). It has low molecular weight. The particle size varies from 0.3 to 4 µm. Teflon is a good electrical insulator, does not absorb water, and is highly resistant to weathering. It tends to form clumps of particles, but it can be deagglomerated during mixing and blending operations. Agglomerates of the resin are friable, a characteristic that helps in producing an intimate mixture with host materials.

3.9.3 Oxidizer

Role of oxidizer in the slurry is to enhance the oxide forming tendency of copper. Hydrogen peroxide was used as an oxidizer in making slurries. In the present research, the purpose of oxidizer in the slurry is to study its effect on friction and post CMP roughness. The optimum condition from this study was used in determination of the oxidizer content for the next experiment of polymer particle addition. Details of the chemical nature of the CMP are discussed in the next chapter.

3.10 Characterization

3.10.1 Scanning Electron Microscopy

The Scanning Electron Microscopy (SEM) studies were conducted to see the topographical features of the abrasive particles and surface after CMP. Topographical studies were performed on wear track, and abrasive particles, using JEOL JSM 6400® SEM, before and after polishing. EDS was done for the particles, to confirm the occurrence of abrasive type.

3.10.2 Transmission Electron Microscopy

The Transmission Electron Microscopy (TEM) studies were conducted on some select slurry particles, before and after CMP. JEOL EM 2010® TEM was used to study the

crystal structure and morphology of slurry particles. About 1 gm slurry sample, containing 3 %wt alumina and other additives, was drawn from the bulk. Slurry was diluted in about 10 ml of DI water. The diluted slurry was then sonicated for 4 hr, to obtain a good suspension of the slurry and deagglomeration of the alumina abrasive particles. This step is also useful for uniform distribution of the sample ingredients in the diluted slurry. A small quantity of the slurry solution was then placed on the 400 mesh copper grid and allowed to dry in the air. The grid was placed on filter paper, to allow drying. Drying was performed in the ambient atmosphere. The sample was then sputter coated with carbon (4 Å thickness) for stabilization. TEM studies were then performed for getting transmission images and electron diffraction patterns, using JEOL 2010 transmission electron microscope. Electron diffraction patterns were recorded at camera length 60 cm. Scale bar in the electron micrographs was drawn using the calibration with standard images for SiC, showing atomic fringes. Acceleration voltage of 200 KV was used in the TEM operation.

3.10.3 Atomic Force Microscopy

An atomic force microscope (AFM) (Pacific Nanotechnology, Nano-R®) was used for surface characterization. The non-contact mode was used for observation of topography. A standard silicon probe was used for scanning. The software (SPM-Cockpit2002 (3.1.2)® and Nanorule+ (2.12 Beta)®) were used for image capturing and analysis. The topography data of the AFM scan image was used for determining the surface roughness. The surface roughness (Ra) measurement was done over a scan size of average 90 micron.

3.11 Observations

Experimental work followed by the characterization is based on two themes of parameter effect. The first theme is the effect of oxidizer content and the second theme is the effect of the polymer additives. Observations of friction data and characteristics are discussed below.

3.11.1 Friction Coefficient for Slurries

The friction coefficient as a function of polishing time is shown in figure 3.2. In this figure the X-axis is the polishing time and the Y-axis is the friction coefficient. This figure also contains the information of the oxidizer content. The average values for coefficient of friction are plotted in figure 3.3. It is shown that the coefficient of friction is the highest (0.45) when an oxidizer is not present in slurry. With the addition of 0.5 %wt H_2O_2 as an oxidizer, the friction coefficient dropped to 0.41, and then further dropped to 0.38 with increase in oxidizer content to 1 %wt.

Figure 3.4 shows the graphs for coefficient of friction with reference to time for slurries with and without polymer additives. The average values of friction coefficient for the entire polishing time for polishing in different slurries are plotted in figure 3.5. CMP with only alumina and 0.5 %wt oxidizer content of slurry show the friction coefficient 0.41. When latex additive was used in slurry, then the friction coefficient increased to 0.51. With Teflon additive in slurry, the friction coefficient dropped to 0.16.

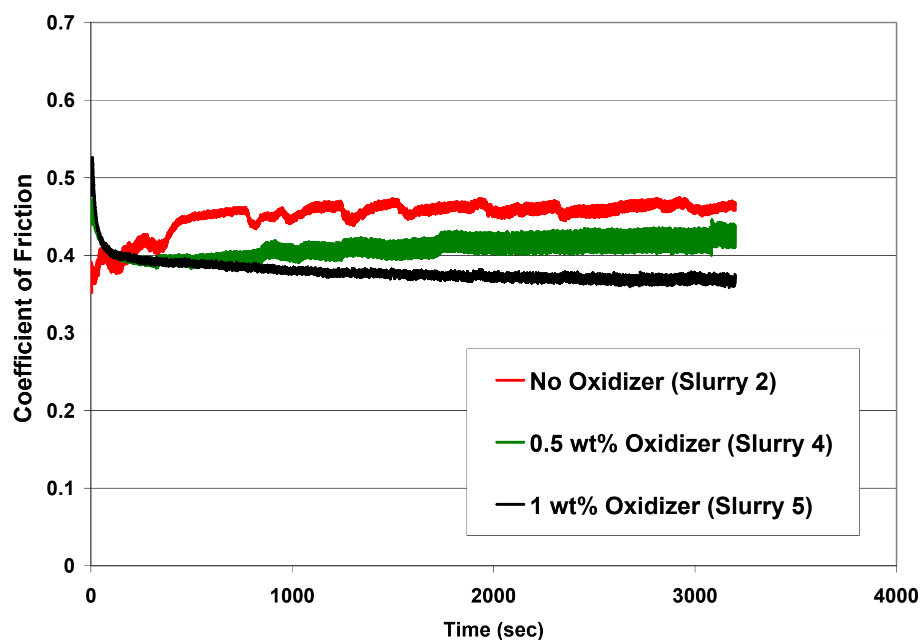

Figure 3.2 Friction coefficients as a function of time, for CMP in slurries with different oxidizer content

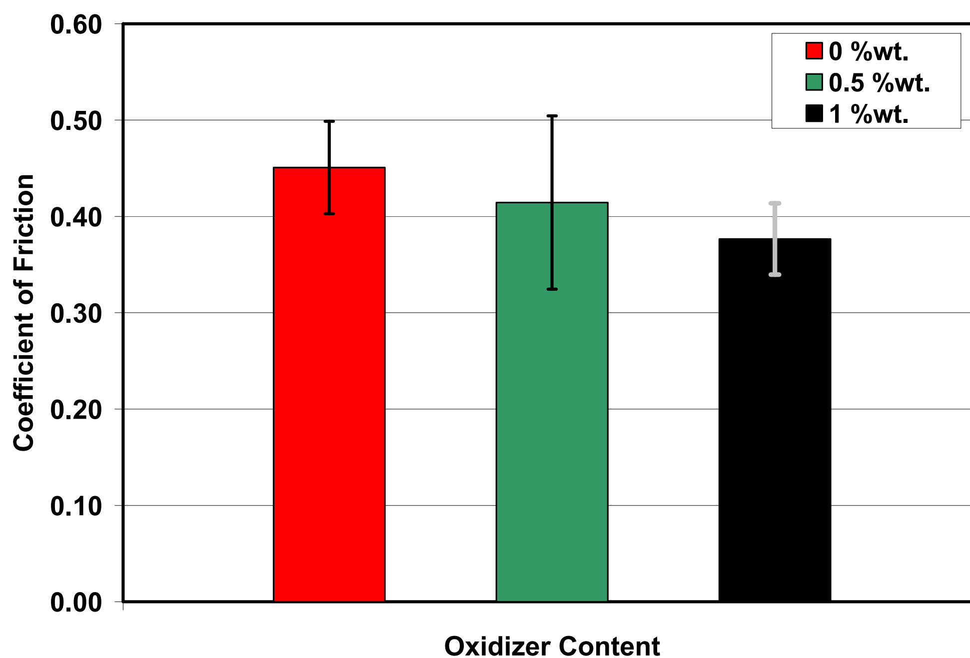

Figure 3.3 Average friction coefficients during CMP with different oxidizer content

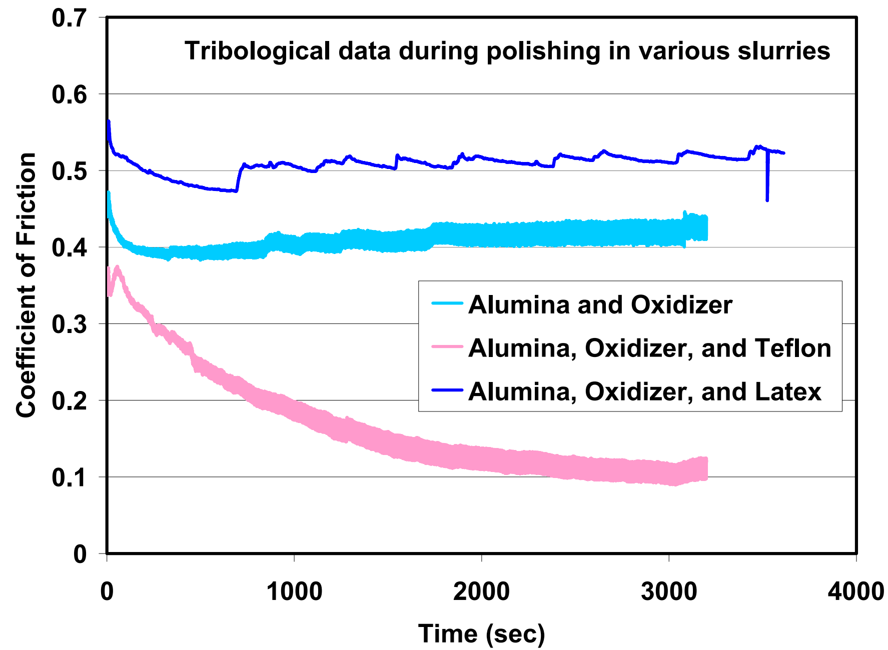

Figure 3.4 Friction coefficients as a function of time, for CMP in slurries with different polymer additives

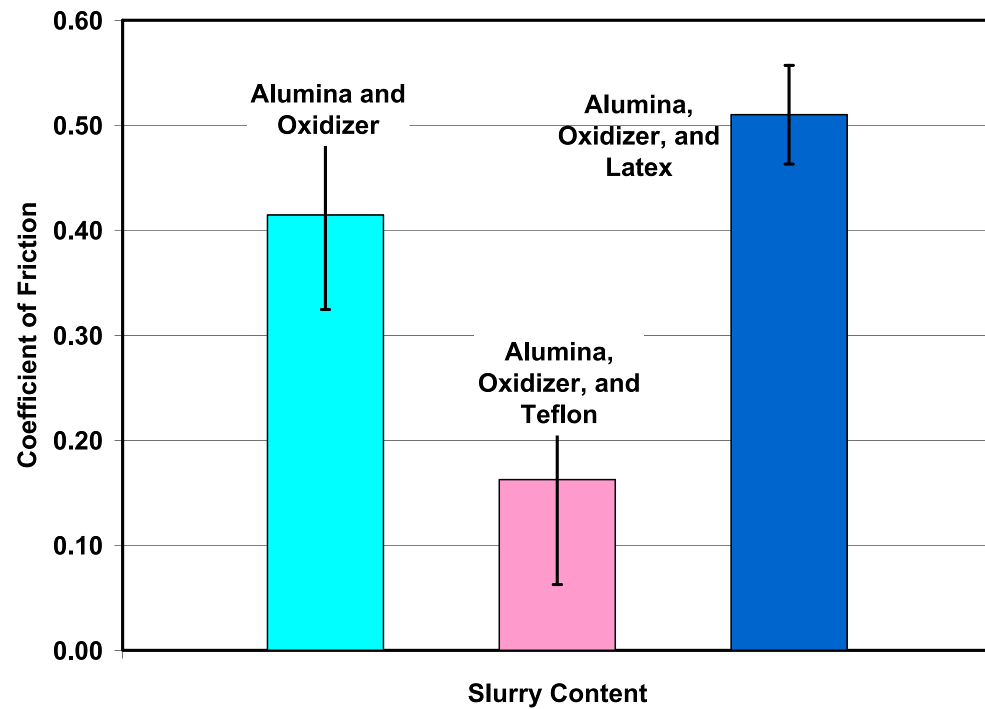

Figure 3.5 Average friction coefficient during CMP with different polymer additives

3.11.2 SEM Analysis of Slurry Particles

Alumina and latex slurry particles were observed under an SEM, in conditions before and after polishing. Figures 3.6a and b show the SEM micrographs for alumina particles before CMP. The particles have rounded edges in a shape with angularity. Figures 3.7a and b show the SEM micrographs of the alumina abrasive particles, after 3 hr CMP. The particles show the rounding of edges, and reduced angularity, as compared to the shape before CMP. To confirm the presence of alumina particles, EDS analysis was conducted. The results are shown in figures 3.8a and b. Figure 3.8a is the EDS data for the alumina particle. It confirms that the particles under observation are alumina. The background is copper, which is confirmed as per the observation in figure 3.8b.

Figures 3.9a and b show the SEM micrographs for Latex particles before CMP. The Latex particles are spherical in shape. The surface of these particles, as seen in the image, is irregular having more surface area.

SEM micrographs of latex particles after 3 hr CMP are shown in figures 3.10a and b. Some of the particles observed are totally smeared off, under the polishing force, as seen in figure 3.10b. The particle also shows brittle fractured surfaces.

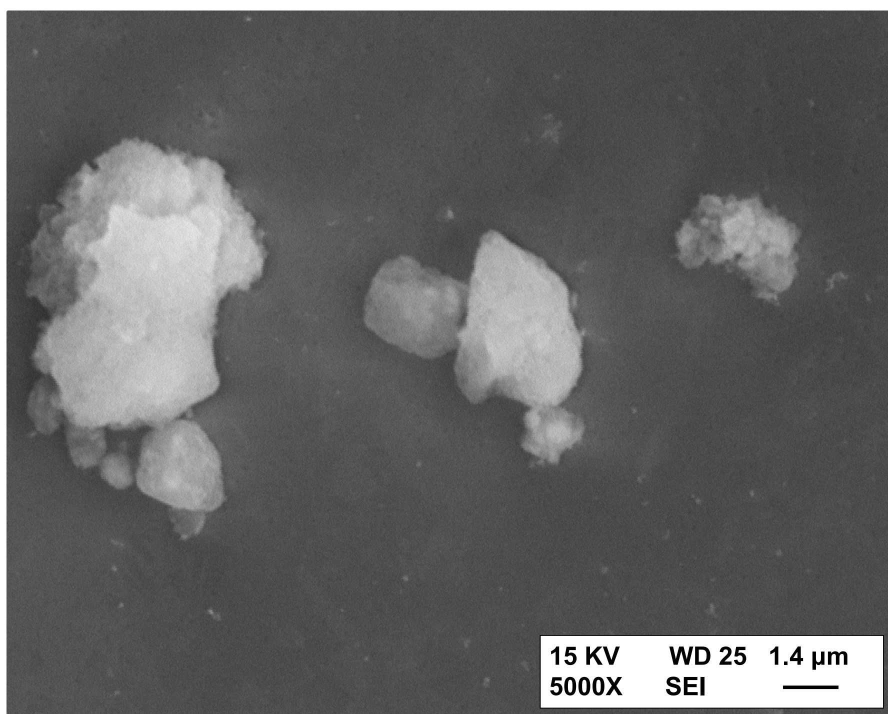

(a)

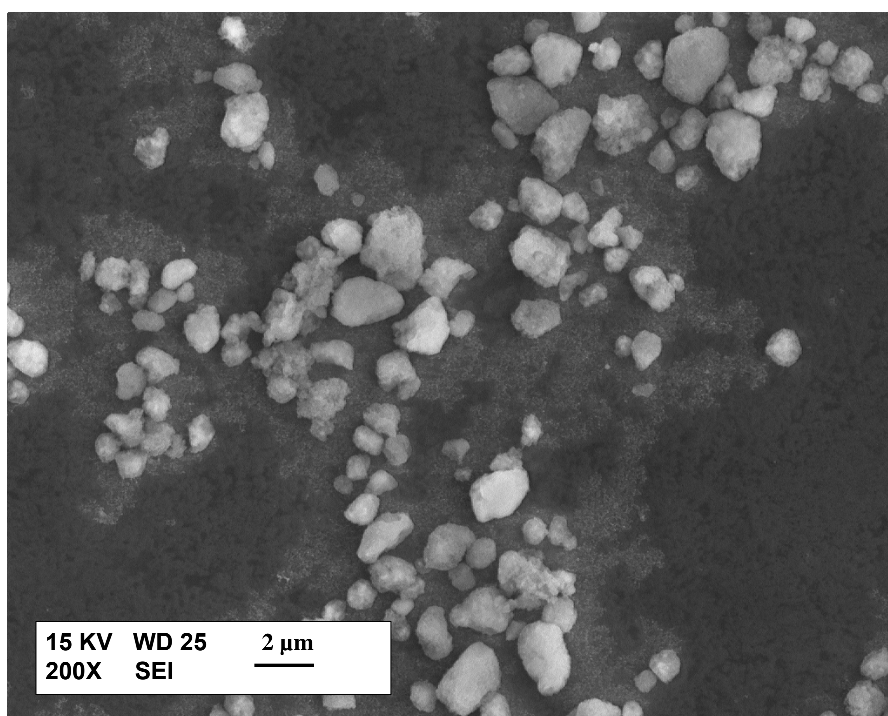

(b)

Figure 3.6 Alumina abrasive particles before CMP

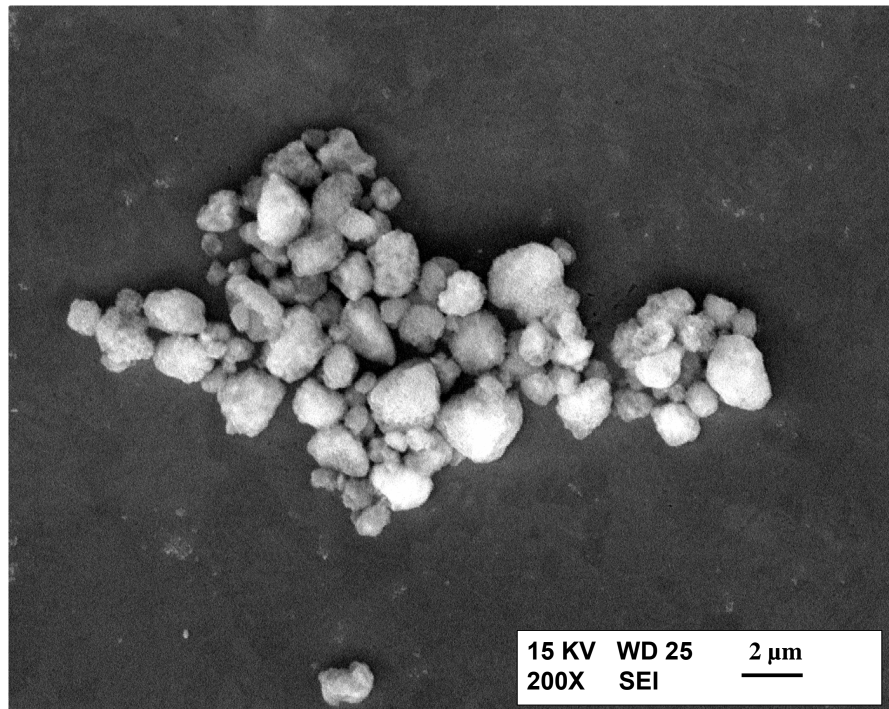

(a)

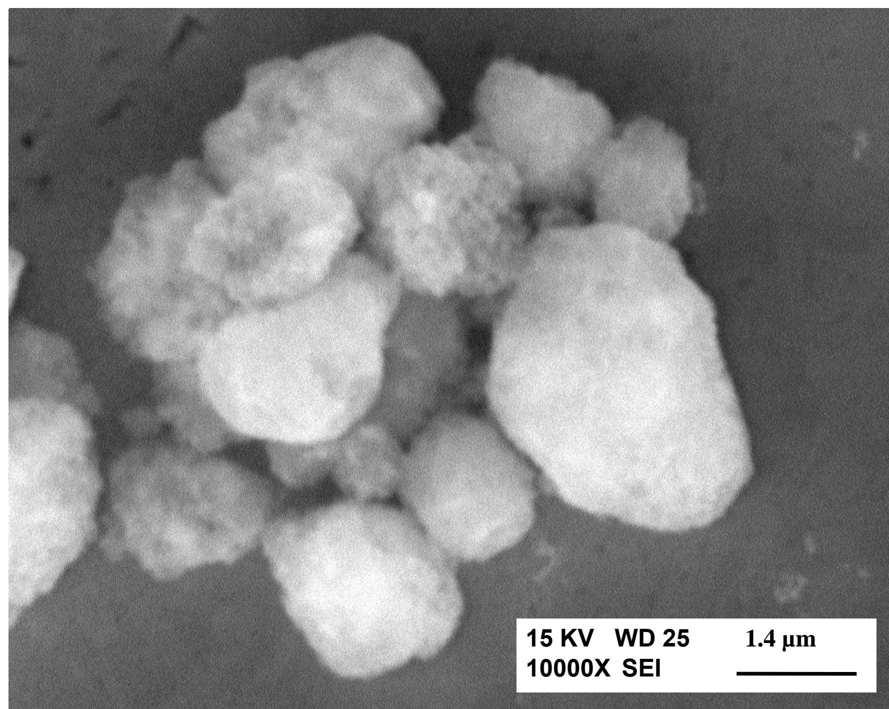

(b)

Figure 3.7 Alumina abrasive particles after CMP

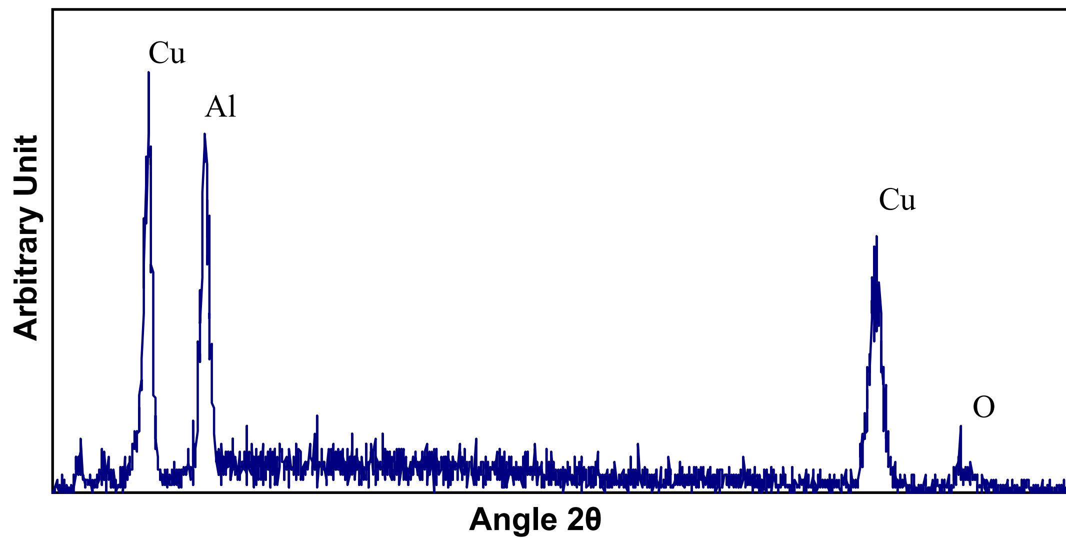

(a)

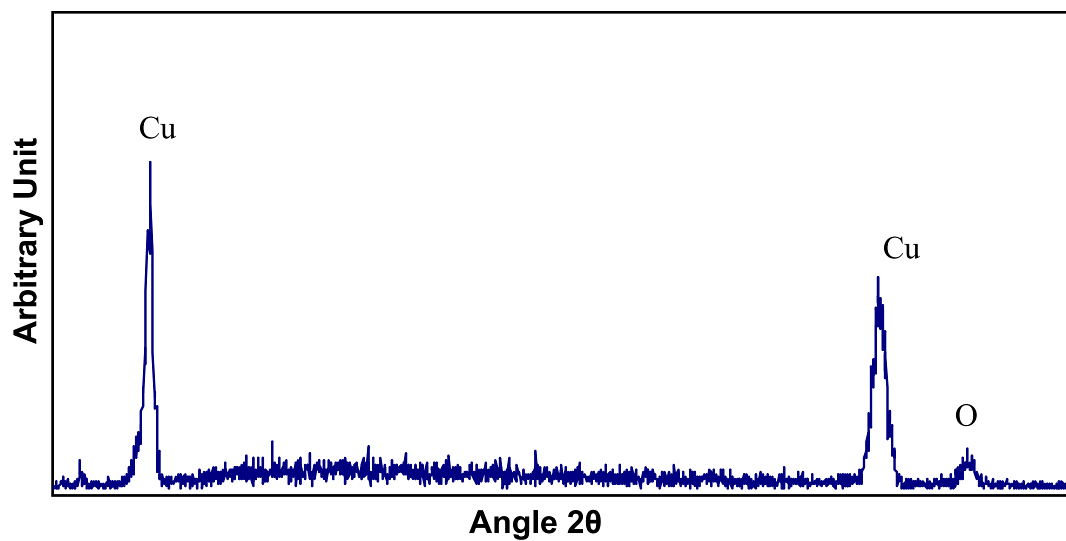

(b)

Figure 3.8 EDS data for (a) alumina particle, and (b) copper surface

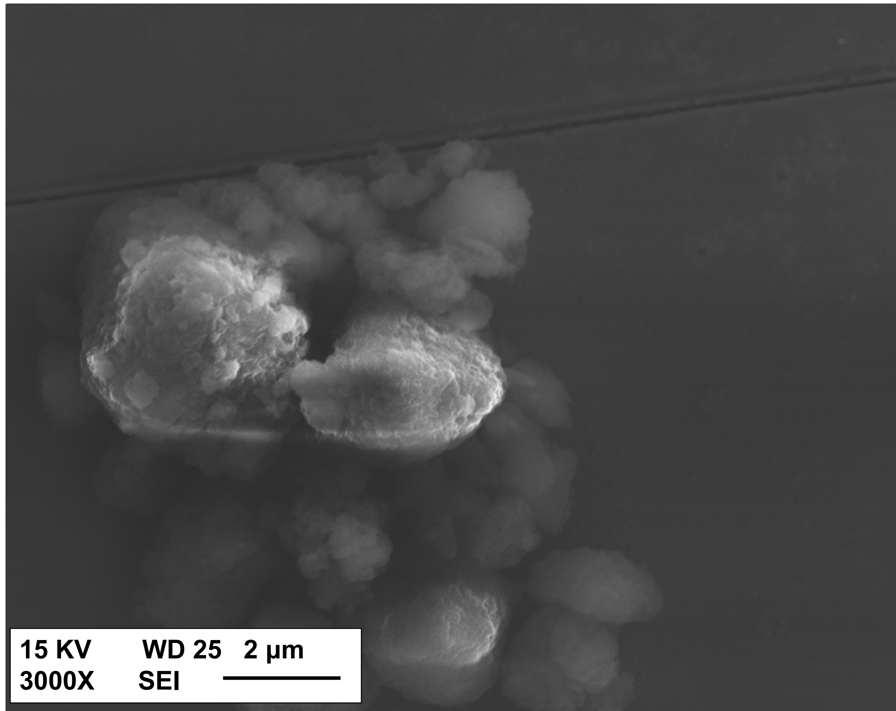

(a)

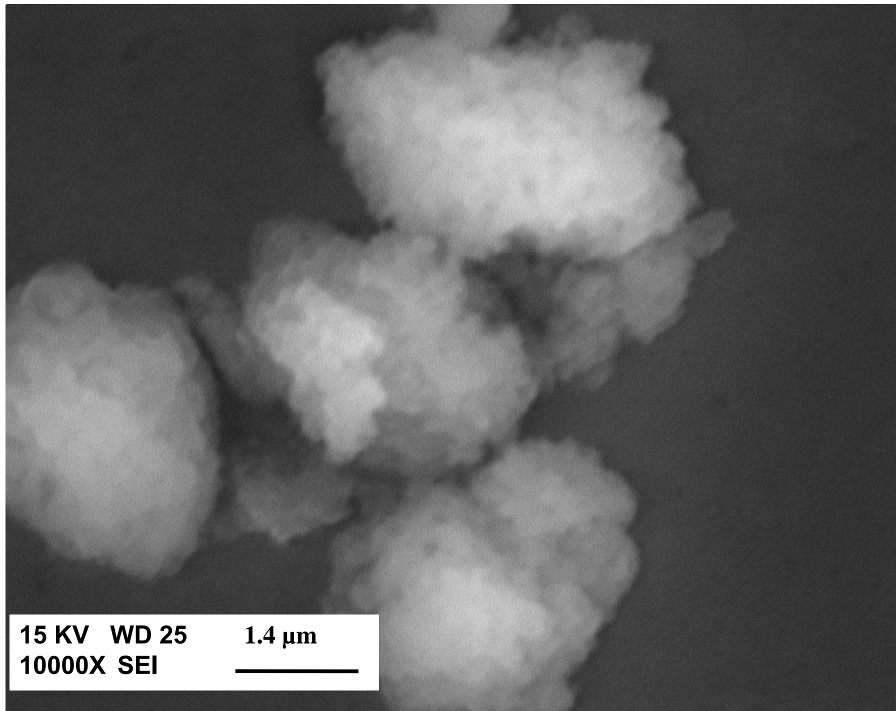

(b)

Figure 3.9 Latex particles before CMP

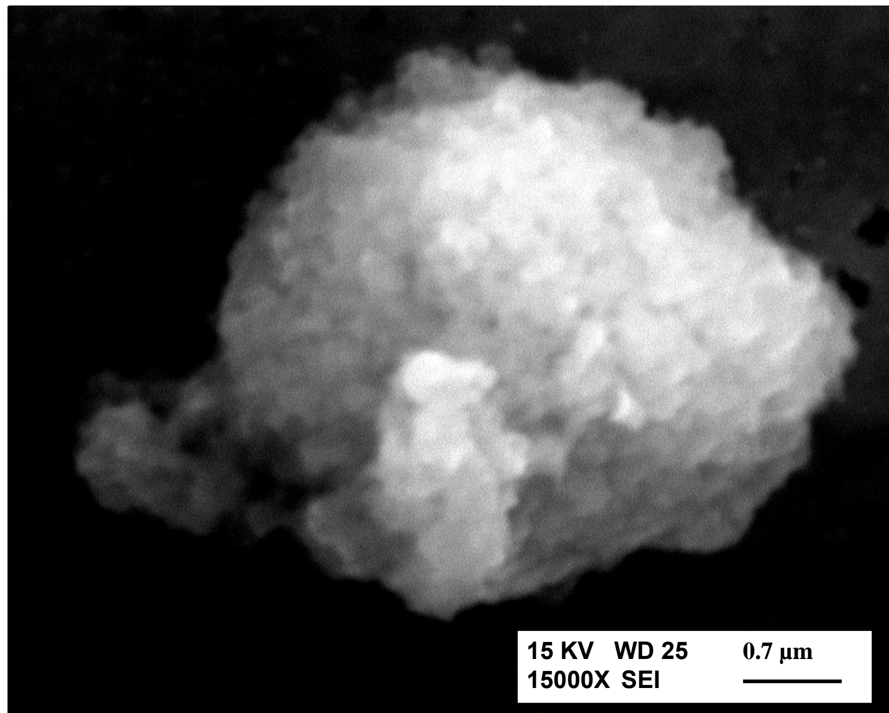

(a)

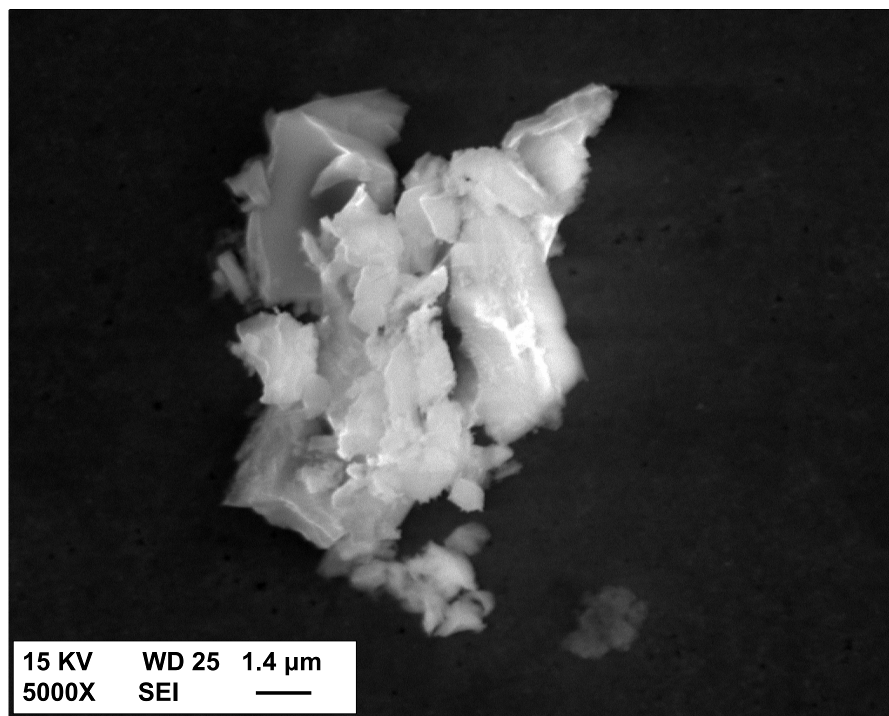

(b)

Figure 3.10 Latex particles after CMP

3.11.3 TEM Analysis of Slurry Particles

The TEM analysis of alumina and Teflon particles were performed before and after CMP for 3 hours. Results were compared with those in the literature. Diffraction patterns and TEM micrographs are shown in figures 3.11a to c.

The TEM images of alumina particles are shown in figure 3.11a. These particles are rounded without sharp edges. This is beneficial for reducing scratches. According to the images, it is seen that that the size of alumina powder particles is ranged from 5 to 50 nm. There is no coarse alumina particles seen.

Figure 3.11a shows the electron diffraction pattern for alumina. The diffraction pattern shows the diffraction spots forming a ring at 2θ (Bragg) angles. The ring formation confirms the polycrystalline nature of the alumina particles. The indexing of the electron diffraction pattern was done using the formula $d = L\lambda/r_1$ where d is interplanar spacing, $L\lambda$ is camera constant and r_1 is the radius of the diffraction ring. $L\lambda$ was used as 14.4 mm.Å for the camera length 60 cm. The software developed by Luo[78] was used for the calculation of r. From the diffraction pattern, the value of r is 11.1 mm. From the results of computer program, r is 11.07 mm for index h,k,l (0,0,1) and the lattice parameter for the alumina particles is 13.003 Å. This confirms the lattice parameter c to the standard value. These observations show that the slurry particles are alumina with the desired structure.

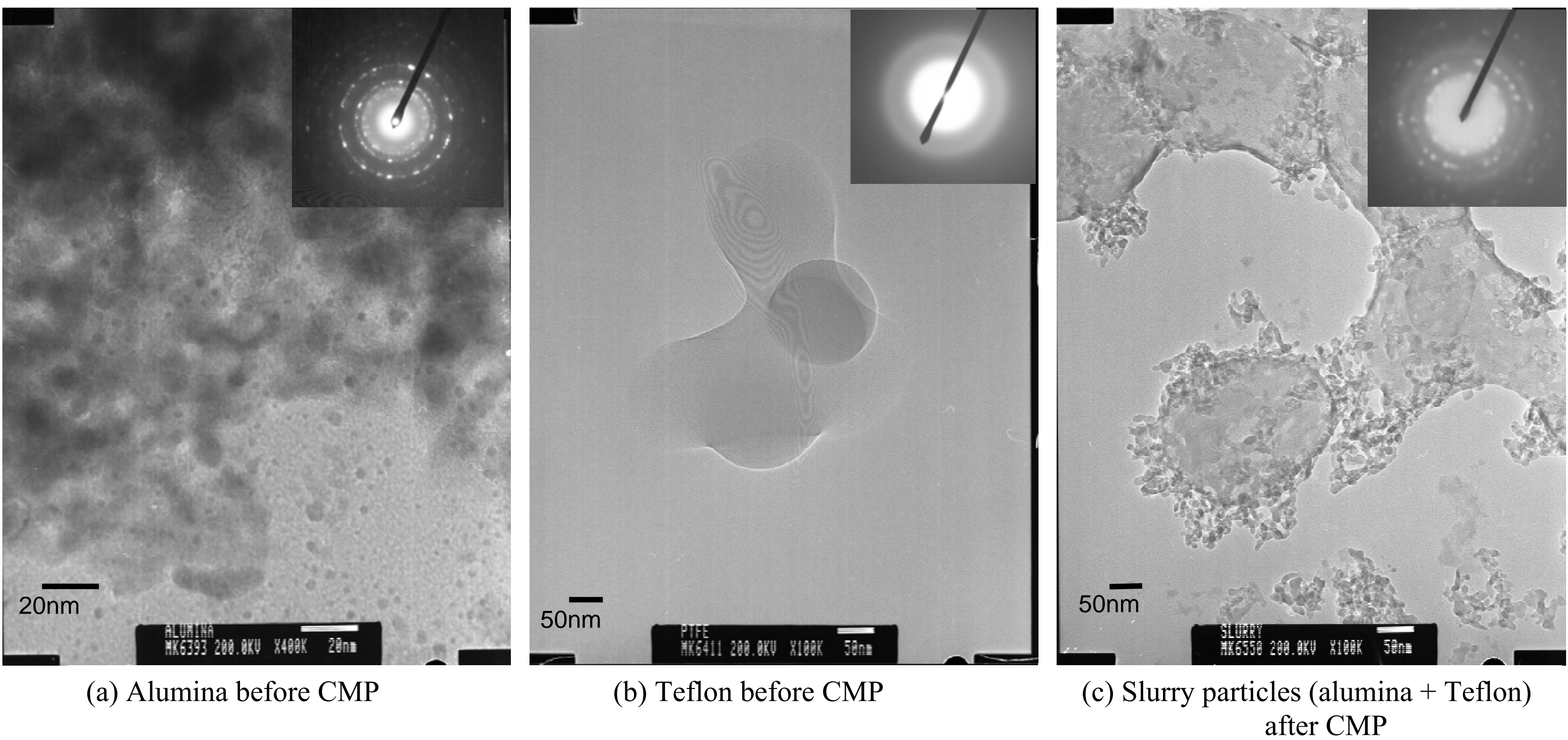

(a) Alumina before CMP

(b) Teflon before CMP

(c) Slurry particles (alumina + Teflon) after CMP

Figure 3.11 TEM and XRD of abrasive alumina and Teflon slurry particles

Electron micrograph shown in figure 3.11b is for Teflon particles. The shape of the Teflon particles is round and the diameter is 200 to 400 nm. The electron diffraction pattern of Teflon particles in figure 3.11b is a typical of an amorphous structure.

Figure 3.11c shows electron micrograph and electron diffraction pattern for slurry particles with alumina and Teflon. These particles were drawn after the CMP for 3 hrs. The micrograph shows that alumina particles are adhered to the Teflon particles. The electron diffraction pattern confirms the combination of and the presence of both alumina and Teflon particles.

Figure 3.12 shows the atomic fringes in the electron micrograph of alumina particles. This image can be used for characterization of the lattice parameters of alumina. Alumina has trigonal structure. The lattice parameters are a = 4.761 Å and c = 12.991 Å as cited in the literature [79,80,81]. The atomic fringes as seen in figure 3.12 show the lines making 120° angle. This suggests that the zone axis is [001] which is later confirmed. Using calibrated scale bar, the lattice parameter a was measured as 4.545 Å. This confirmed that the type of the alumina used for slurry is α.

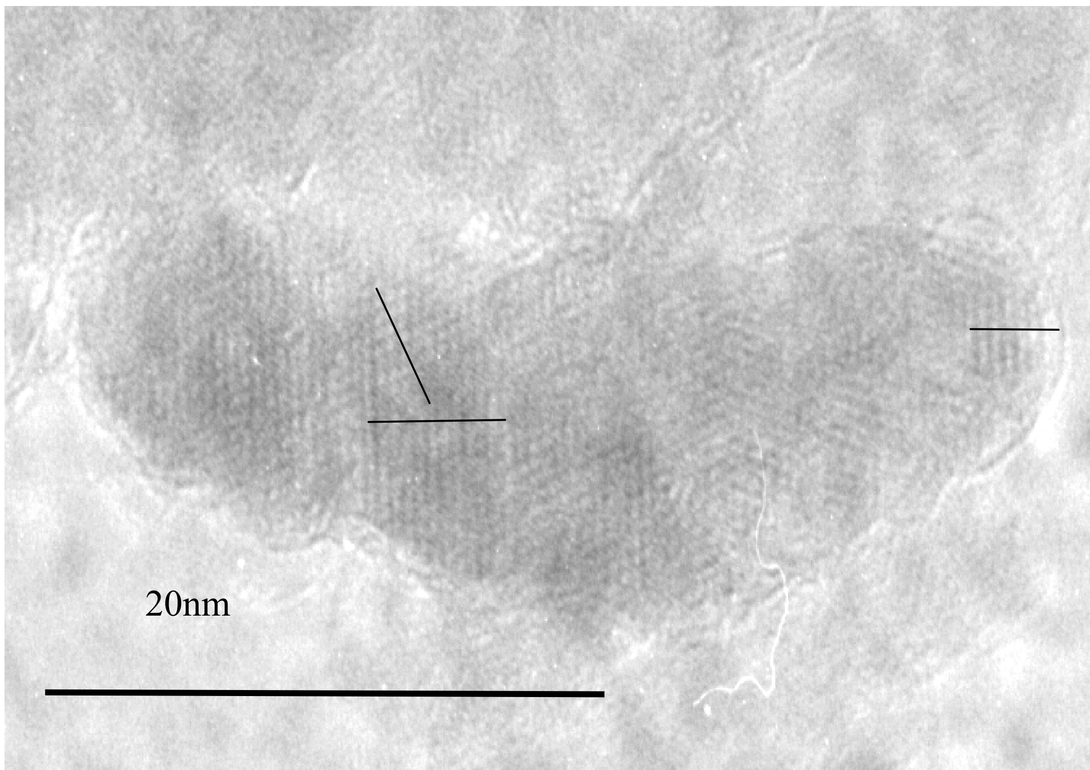

Figure 3.12 TEM micrograph of alumina particles at 400000X magnification

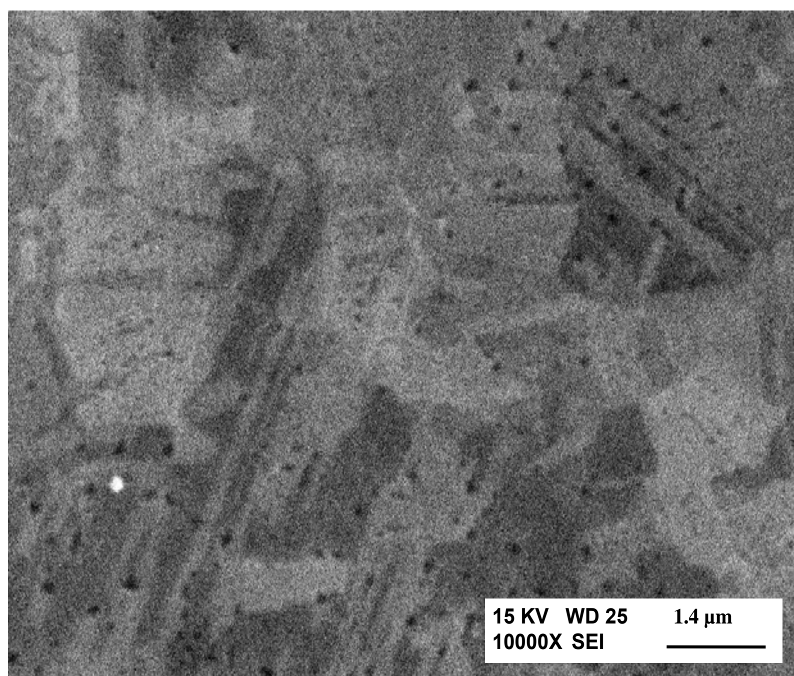

Figure 3.13 Copper surface after CMP using alumina slurry

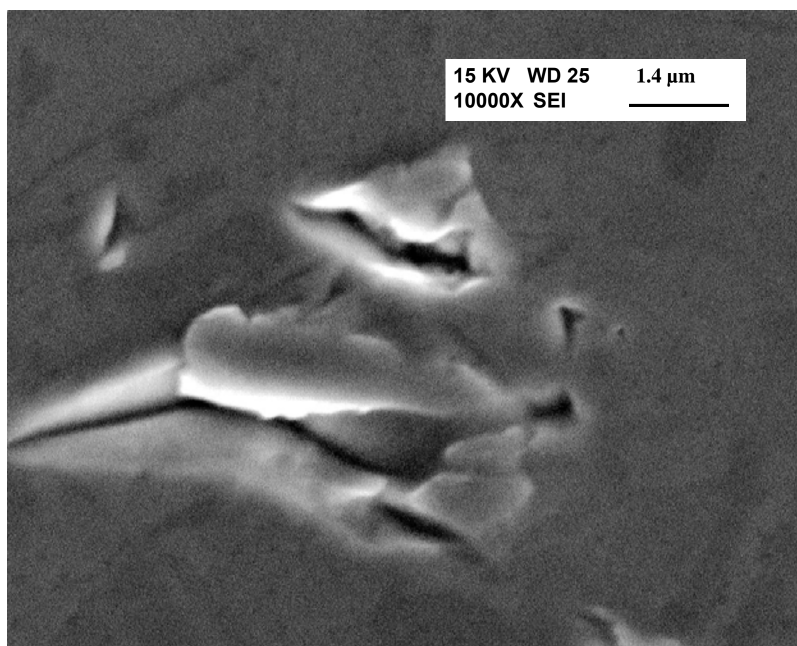

Figure 3.14 Copper surface after CMP, using abrasive slurry with Latex additive

3.11.4 Post-CMP Surface Analysis Using SEM

SEM observation of the copper surfaces was performed after CMP. Two different slurries containing alumina particles and Latex additives were analyzed. Figure 3.13 shows the SEM micrograph of copper surface after CMP with alumina abrasive. The copper grain structure with twinning is revealed. Scratches and groves formed on the surface show the evidence of the poor planarization quality. In case of Latex additive abrasive polishing, as shown in figure 3.14, delamination of copper coating from silicon substrate is observed.

3.11.5 Post CMP Surface Analysis Using AFM

Non-contact mode AFM topography of the post-CMP copper surface were used for surface roughness (Ra) measurement. The values of roughness Ra (nm) is plotted with reference to the polishing slurry composition. In figure 3.15, the average surface roughness value is the Y-axis and the slurry composition the X-axis. Effect of oxidizer on the post CMP surface roughness is seen from this chart. Without the presence of oxidizer, the roughness value is as high as 48 nm. With the oxidizer, the surface roughness is decreased to 27 nm for 0.5 %wt H_2O_2 and to 36 nm for 1 %wt H_2O_2. Best surface finish was obtained with 0.5 %wt H_2O_2 in slurry.

Effects of polymer additives on the surface roughness can be seen from the chart shown in figure 3.16. The Y-axis is the post-CMP roughness values and the X-axis the slurry contents. It can be seen from the chart that without polymer additives, a slurry made of plain alumina and oxidizer provided a surface roughness of 27 nm. With the Latex additive, the surface roughness is increased to 64 nm. With Teflon additives the surface roughness is 17 nm.

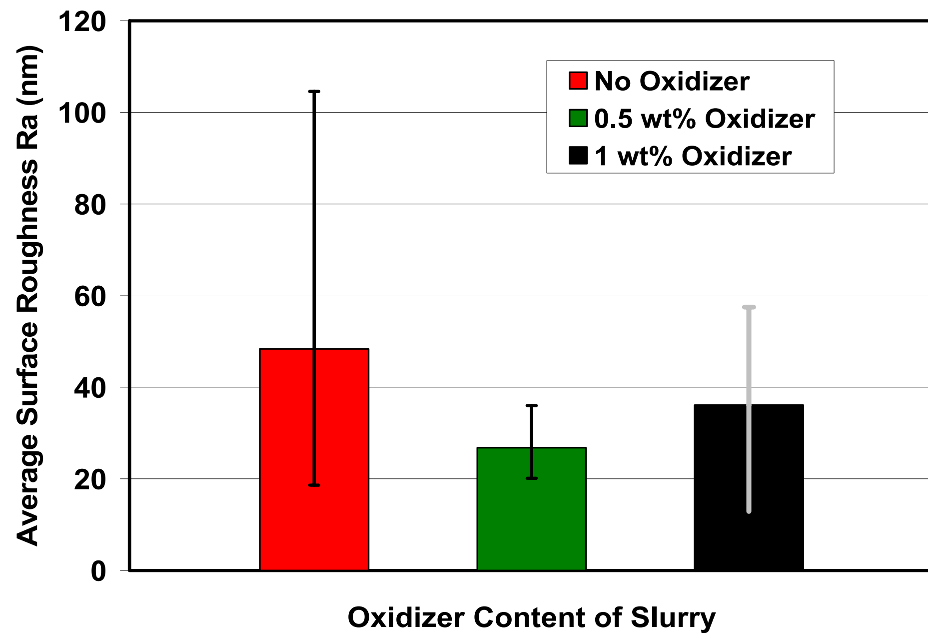

Figure 3.15 Average surface roughness after CMP with slurries containing variation in oxidizer

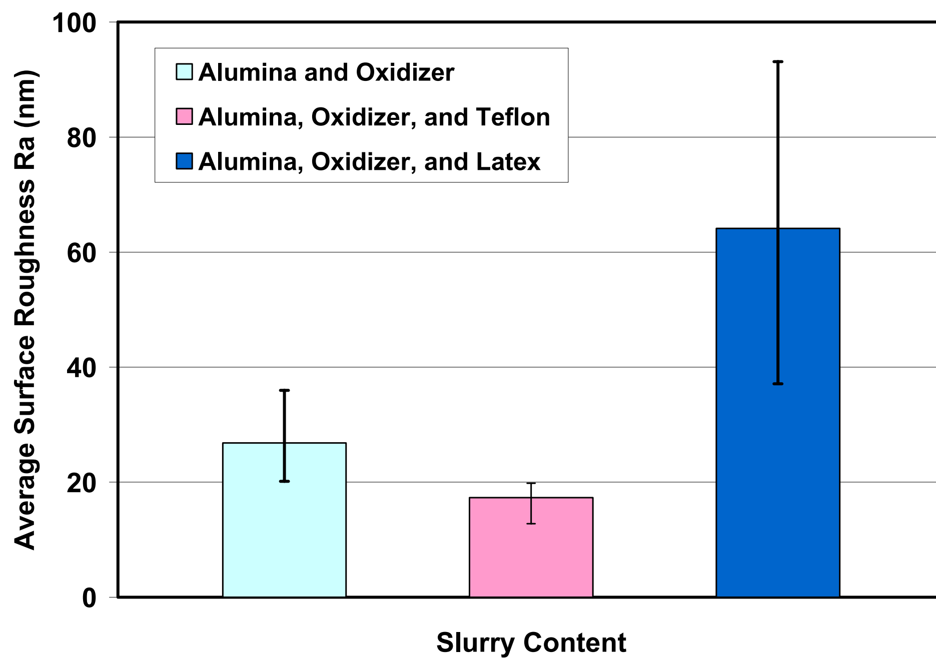

Figure 3.16 Average surface roughness after CMP with slurries containing variation in polymer additive

3.12 Discussion

3.12.1 Oxidizer in Slurry

The friction data in figure 3.2 has shown that the addition of oxidizer in alumina slurry has significant effects on frictional force. The role of oxidizer here is to react with the copper surface and to form a copper oxide layer. This layer is fragile in nature (Steigerwald et. al, 1997) and reduces the frictional forces by breaking it. This has reflected in the observation of reduction in friction with increase in oxidizer content.

With the increase in oxidizer content, copper on the surface is removed with increased chemical actions. This provides a smoother surface finish up to a critical level. Furthermore, the increase in oxidizer content does not result in a high smoothness. The reason for this is that the severe chemical reaction on the copper surface causes intense chemical attack.

The details in effects of chemical interactions in CMP are discussed in depth in the next chapter. Here it can be seen that oxidizer content in alumina slurry can be optimized to 0.5 %wt, keeping other process parameters as down force, speed, among others consistent.

3.12.2 Polymer Additives in Slurry

The SEM and TEM observations of the alumina particles, before and after CMP, have revealed that there is deterioration of the particles during the CMP. High surface roughness achieved after CMP with alumina slurries indicates that there is severe surface abrasion of copper. This is in agreement with the change in the morphology of alumina particles (shown in figure 3.16)

The use of polymer additives has shown variation in friction (figure 3.2) and post CMP surface roughness (figure 3.16). Latex particles as additives have shown increased

friction. It can be inferred that the latex particles, with spherical shape and larger surface area, provide more contact area with the copper surface. It results in a high friction force which causes brittle fracture of particles. Fractured particles have sharp cornered surfaces as seen in the SEM image (figure 3.10). However, since the hardness of these particles is less than that of copper, the sharp edge is not expected to make scratch on the copper surface.

The latex particles provided poor surface finish and caused delamination of copper (figure 3.14). The poor surface finish is a result of extreme mechanical interaction with the copper surface. SEM observation has revealed this interaction at several locations. Delamination of the copper shows a strong adhesive interaction between hydrophilic Latex particles and copper.

Teflon additives on the other hand have shown improved results. Reduced friction is the result of hydrophobic nature of the polymer and round shape of the particles. Adhesion between the Teflon particles and alumina particles provided limited surface abrasion. This resulted in a better surface finish (figure 3.16). The cause of the surface adhesion between hydrophilic alumina particle and hydrophobic Teflon particle is a result of tribological interaction during CMP.

As discussed earlier, the surface roughness is apparently affected by the polishing conditions and surface chemistry. Figure 3.17 summarizes the different removal mechanisms resulting different surface integrity. Details will be summarized in the conclusion session 3.13.

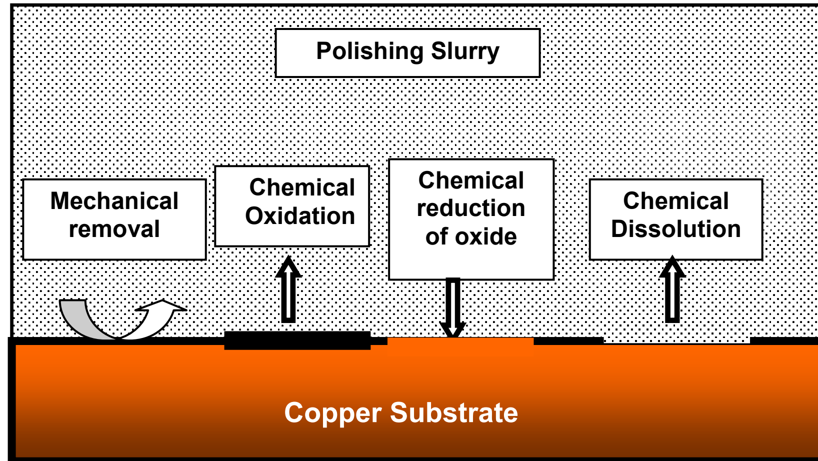

Figure 3.17 Schematic showing chemo-mechanical actions in CMP

3.13 Summary

Mechanical action on the surface is one of the important mechanisms in the chemical mechanical planarization. It is controlled by several components such as abrasives and the pad. Abrasives in the slurry, a major component, control the performance of the process. Selection of abrasive type, size and concentration are critical.

Presence of surface oxide changes the dimension of the CMP. Experiments were conducted with variation in oxidizer content of slurry. Results proved that the oxidizer content show optimum performance at 0.5 %wt.

Furthermore, a series of copper CMP experiment was conducted, using polymer additives in the alumina slurry. Latex particles are hydrophilic in nature, with high surface areas. They show adhesive type interaction with copper surface, shear during polishing, increased friction and poor post-CMP surface finish.

Teflon particles are hydrophilic in nature with low coefficient of friction. They show adhesion with alumina abrasive after long interaction. Teflon additives improve the post-CMP surface finish.

The role of polymer additives in the material mechanisms due to mechanical action in polishing is understood in this research. The nature of surface property of the polymer material controls the post CMP surface finish. Control over chemistry and abrasive together has shown even better optimization. Control over slurry pH and electropotentials during polishing will add another dimension to the optimization process. A better understanding of the entire process in steps is necessary. Beyond the mechanical action, other parameters leading the synergy in CMP are discussed in the next chapter.

CHAPTER IV
ELECTROCHEMICAL-MECHANICAL PLANARIZATION MECHANISMS

The electrochemical-mechanical planarization (ECMP) process is composed of electrolytic, chemical and mechanical actions on the surface. In Chapter III, we reviewed research in mechanical action during CMP. The mechanisms of chemical, electrochemical and synergistic effects of all these actions on surface are discussed in this chapter.

4.1 Brief Background

4.1.1 Chemistry in CMP

Chemistry of a slurry plays as important role as the mechanical action in CMP. Chemical action on a surface under friction changes the form of wear from abrasive wear to corrosive wear or other complex conditions. The synergistic effect of mechanical and chemical actions on a surface leads to planarization of a surface.

A slurry has various functions. As illustrated by Kaufmann's[82] model of oxide tungsten CMP, polishing occurs by the formation and removal of tungsten oxide on the surface. Chemical activation due to the slurry should be strong enough to rebuild the oxide on the surface. Preferentially, the oxide in the high regions is removed with the faster rate than that in the lower regions. So as the process continues for a period of time, the planarization can be achieved. A schematic of this material removal process is shown in figure 4.1. The rate at which the material is removed with time is called as static etch rate.

Another function of the slurry is to digest the mechanically dislodged particles. This digestion is similar to chemical dissolution of metal particles from wear debris. At the

same time, the slurry should not be corrosive to attack the copper surface with high static etch rate. Usually high rates of static etching also cause defects like pitting resulting high surface roughness.

4.1.1.1 Slurry pH

Copper CMP is performed with different chemistry combinations either based on acidic or basic compositions. The chemistries include application of acids- nitric, citric, acetic or bases- potassium hydroxide, sodium hydroxide, and ammonium nitrate.

As per the studies by Steigerwald et al.[90] water, acetic acid, and ethyl alcohol show similar static chemical etching rate. Nitric acid shows higher etching rate, while ammonium hydroxide shows lower etching rate. This means that acetic acid does not have etching action on copper like nitric acid does.

The process of material removal and dissolution is a complex process. Strong acids like nitric acid need ways to reduce their high etching rate since it generally results in high surface roughness. This can be achieved by adding protective agents like the Benzotriozole (BTA) which works like an inhibitor. The BTA forms a very thin layer on the copper surface and protects it against the active dissolution of copper. During mechanical sweeping of a pad, this film at the high points on the copper surface is removed and the surface in this area shows high etching rate. A good planarization can be achieved.

On the other hand, acetic acid or potassium hydroxide has low rate of chemical activity on copper. These chemicals along with oxidizing agent show a high rate of chemical activity on copper surface. Usually hydrogen peroxide or glycine is used as oxidizer. According to ellipsometric studies by Nishizawa et al.[83] approximately a 20 nm-thick film of CuO is formed on copper surface within 100 seconds of exposure to 10% hydrogen peroxide solution. As per the studies by Du et al.[84] the material removal rate

increases with increment of hydrogen peroxide in slurry up to 1 %wt. With further increment of peroxide content in slurry the removal rate drops. The initial increase in material removal is associated with the rapid passivation. Further reduction in removal rate is due to stabilization of the growth of copper oxide layer. Seal et al.[85] have shown that when glycine is used along with hydrogen peroxide, removal rate does not show this drop with increase in peroxide content in slurry.

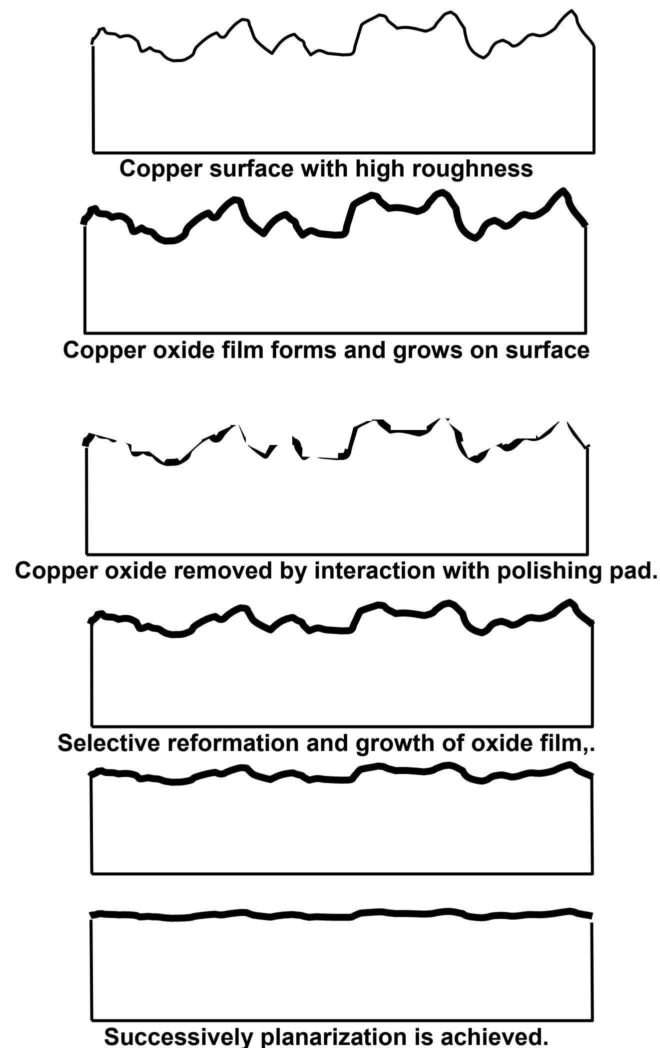

Figure 4.1 Schematic of oxide formation and removal process to achieve planarization in CMP

Tsai et al.[86] have tried to use urea as an additive to the slurry containing hydrogen peroxide and BTA. They found that urea provided controlled degradation of peroxide and stabilization of the passivation tendency on copper surface over a long period of time. They also suggested that ammonium hydroxide slurry with above combination showed a good control of oxidation and removal process. According to Kim et al.[87] phosphoric acid additive in slurry enhanced the stability of hydrogen peroxide. Tsai et al.[88] reported that the use of glycolic acid showed similar effects as urea.

The solubility of copper in slurry can be increased using complex agents such as ammonia.[90] Copper ions are isolated in slurry through interactions with a complex agent. The effect provides a consistent chemical etching rate.

As reported by Chen et al.[89] citric acid alone has no etching effect on copper surface. Instead, the citric acid works as a chelating agent that complexes the copper oxide in the slurry. The citric acid alone produces a high surface roughness.

It has been observed that the use of acetic acid for copper CMP slurry has unique performances because of its interaction with copper. This topic is discussed in detail in the following section.

4.1.1.1.1 Acetic Acid and Copper

Pure acetic acid is a colorless, corrosive, flammable liquid that freezes at 16.6 °C. Since pure acetic acid freezes only slightly below room temperature and will show an ice-like appearance, it is generally called glacial acetic acid.

In aqueous solution, acetic acid can lose the proton of its carboxyl group, turning into the acetate ion $CH3COO^-$ as shown in equation 4.1. The viscosity ρ Ka of acetic acid is about 4.8 at 25 °C, indicating that about half of the acetic acid molecules are in the acetate form

at a pH of 4.8. When heated above 440°C, it decomposes to produce carbon dioxide and methane, or to produce ketene and water.

$$CH_3COOH \leftrightarrow CH_3COO^- + H^+ \quad [4.1]$$

Experiments of copper polishing have been conducted with alumina containing slurry, containing acetic acid for pH value of 2 by Steigerwald et al.[90]. It was observed that the polishing rate is 1,000 nm/min. Compared to polishing in neutral slurries, the polish rates are similar to that obtained in water. This suggests that acetic acid alone has no effect on Cu polishing. This means that there is no copper etching[91 92]. Acetic acid removes various forms of copper oxides such as CuO, Cu_2O, and copper hydroxide ($Cu(OH)_2$) without attacking copper. Copper oxides react with acetic acid to form copper acetate as shown in equation 4.2 and 4.3

$$CuO + 2CH_3COOH \rightarrow CuH(CH_3COO)_2 + H_2O \quad [4.2]$$

$$Cu_2O + 4CH_3COOH \rightarrow 2CuH(CH_3COO)_2 + H_2O + H_2 \quad [4.3]$$

Presence of oxygen or water along with acetic acid has shown interesting behavior[93]. These oxidizing elements cause formation of $Cu(OH)_2$ or other species of copper oxide on the surface. It is then subsequently followed by removal of these compounds by the reaction of acetic acid. Thus the corrosion can be observed with mixture of oxidizer and acetic acid, resulting in the oxide free surface in the end. The etch rates in presence of acetic acid increase with increment of oxidizer (H_2O_2) content.[89] The etched surface roughness is observed to increase or decrease[89]**Error! Bookmark not defined.** depending on the concentration of other contents.

After removal from the acetic acid or its mixture with oxidizer, the surface is free of oxides. However, if the copper surface is rinsed with water, cupric oxide or copper hydroxide will form on the surface.[93]

Electrochemical studies were done for understanding copper behavior in nitric acid based slurries by Carpio et al.[94] in 1995. They did polarization test in which they found that there is no passivation of the copper. They also observed that the corrosion current

decreased and corrosion potential increased with abrasion on copper surface. However, in the presence of hydrogen peroxide, the corrosion potential decreases and corrosion current increases with abrasion. The results were further confirmed by Steigerwald et al.[90] Carpio et al.[94] and Steigerwald et al.[90] further studied and found that with use of corrosion inhibitor (benzotriozol - BTA) the corrosion potential and corrosion current decreases. Their observations concluded that copper shows dissolution type chemistry for nitric acid slurry and is consistent with the Pourbaix diagram of copper.

Xu and Liang[103] have done some path finding studies in copper ECMP. Their studies include copper ECMP studies with high anodic potentials up to 8 V in citric acid and KOH based slurries. They observed that pH of the slurry does not remain constant during polishing. pH changes towards the neutral value. They also found that material removal increases with increase in applied anodic potential.

Huo et al.[95] experimented with electrochemical polishing of copper using hydroxyethylidenediphosphonic (HEDP) and phosphoric acid solutions. They found that copper smoothening can be improved by addition of phosphoric acid. They also found that material removal rate can be controlled by controlling current density.

4.1.1.2 Oxidizer in Slurry

Zeidler et al.[96] studied the effect of on-copper surface by measuring corrosion potentials. They observed that with increase in oxidiser content of slurry, corrosion potential of copper increases upto 8 %wt. oxidiser content and then stabilises. The static etch rate of copper decreases with increase in oxidiser content of slurry upto 8 %wt. and then stabilises. The decrease in etch rate can be correlated to formation of passive oxide layer and increases in potential. They found that during ECMP, corrosion potential is less than potential under static conditions, because of the reason that abrasion results in a partial or complete removal of the surface oxide layer which makes the surface less noble.

Eli et al.[97] studied copper ECMP in slurries containing peroxide, BTA and glycine. They found that copper undergoes strong passivation below 0.2 V. Above 0.2 V, protective layer of BTA is destroyed. Peroxide in addition to BTA provided a strong passivation even beyond 0.2 V. In absence of peroxide, pitting at copper surface is observed at high anodic potentials. They also found that glycine has no effect on electrochemical behavior of copper surface in presence of BTA and peroxide.

Du et al.[98] studied electrochemical characterization for copper CMP with variation in oxidizer content of slurry. They observed that corrosion current increases up to 1 %wt. hydrogen peroxide (oxidizer) in slurry and then drops with further increase in hydrogen peroxide, whereas corrosion potential increased up to 3 %wt. hydrogen peroxide in slurry and then stabilized with further increase of hydrogen peroxide.

Du et al.[99] conducted electrochemical studies for copper CMP with potassium iodide (KIO_3) oxidizer. They found that at low pH (pH = 2), KIO_3 containing slurries interact very strongly with copper surface and hence show high corrosion current density.

Overall, these studies on oxidizer content in slurry leads to the benefits of using the oxidizer for the material removal. It also mentions the efficacy of the oxidizer along with the other variables in the process. This also leads us to the understanding that individually oxidizer in slurry does not lead us to the required planarization as it shows no selectivity over the high and low regions on the copper surface. This make us to decide the use of oxidizer in our slurries used for the ECMP experiments.

4.1.2 Electrochemistry and CMP

As the name suggests, the Electro-Chemical-Mechanical Polishing (ECMP) is a CMP with applied electro potential. Electropolishing or electromachining is a similar term in which material removal is achieved only by the electrolytic interaction between electrodes. The component to be polished or machined is made anode, immersed in a

suitable conductive electrolyte and a suitable cathode is placed in the circuit. The role of electrolyte here is to support the movement of metal ions away from the surface where they are released. When the chemistry of the electrolyte is aggressive, there is a static chemical action on the metal surface. In such the material removal is a combined interactions between chemistry and electropotential. The reaction rate in electrochemical interaction is that at which ions are going to electrolyte. Studies of material removal due to electrochemical interactions have been carried out using open circuit measurement and polarization test. The observations from these tests predict the surface interaction for a particular slurry chemistry and electropotential. The information can be correlated to the material removal mechanism. Information is obtained in the form of surface activation, passivation and change in the nobility of the material with reference to different components of the slurry. Brusic[100] evaluated ECMP studies for different materials such as low-k dielectric, copper, gold and others. She concluded that electrochemical studies in CMP provide information for the following:

1. selection of slurry components that controls chemical activity of metals
2. mechanism of material removal
3. measurement of corrosion rate
4. determination of reaction product

Material removed in process of these electrochemical interactions in such a way that materials from both the peak and valley areas are removed. As a result the planarization does not meet requirement. With the assistance of mechanical impact, materials at peak areas can be removed effectively. In such a good planarization is desirable. The synergy of electro-chemical-mechanical in ECMP plays an important role. Below is a literature review related to the static electrochemistry and ECMP studies.

Electrochemistry is a science in which electrons and ion movements are concerned. Chemical reactions incur the charge transfer as the exchange of electrons or sharing of electrons. The reaction kinetics can be studied with the potential and current

measurements. The electrochemistry consideration is important for applications in areas of electroplating, electropolishing, electrowinning, electromachining, corrosion, and electrical storage (such as batteries). Understanding material removal mechanisms in electrochemical wear and electrochemical testing is described in the following.

Electrochemical reactions occur in pairs termed as cathodic and anodic interactions. Anodic or oxidation reaction is the one in which the electron is lost by formation of a metal ion as shown in the equation 4.4.

$$M \rightarrow M^{+} + e^{-} \quad [4.4]$$

The cathodic or reduction reaction constitutes with the gain of electrons resulting in reactants like metal deposition or hydrogen gas evolution as shown in the equation 4.5.

$$2H^{+} + 2e^{-} \rightarrow H_2\uparrow \quad [4.5]$$

The loss of metal ions at the surface, by the oxidation reaction, in presence of electrolyte, is considered as corrosion or electrochemical wear of surface. In this reaction, electrons are generated. The flow of these electrons generates an electric current, I. The rate at which the metal ions are lost to the solution can be represented by a simple equation 4.6, where F is the faraday's constant (96,487 coulomb $equiv^{-1}$) and n is the equivalent weights reacted per second.[101]

$$I = F\,n \quad [4.6]$$

This reaction is thermodynamically favored only when the free energy of the system is lowered. The free energy of the reaction is ΔG. It is related to the electrochemical potential ε in equation 4.7, n is the number of electrons transferred and F is the Faraday's constant (95,600).

$$\Delta G = -\,nF\varepsilon \quad [4.7]$$

Equation 8 is a most simplified version of the reaction. The kinetics of the process is complex. It can be explained with a Tafel plot. Tafel (1950) found that current I is related to the potential ε of a metal with a single reaction on a surface. The relation is given by:

$$\varepsilon = a + b \log |I| \quad [4.8]$$

where a and b are constants. If the graph is plotted for potential with reference to log $|I|$, the slope of the curve is given by b. The curve is called as the Tafel plot. A typical graph is shown in figure 4.2. Value of b is the characteristic of cathodic or anodic process occurring on a metal surface. The slope of the Tafel plot is the rate at which the metal ions are formed. With time, there could be more than one anodic reaction occurring on the electrode surface. The resulting potentials observed is the sum of all reactions occurring in the process.

4.1.2.1 Potentiodynamic Polarization Test

As discussed earlier, any electrochemical reaction occurs in pairs of cathodic and anodic reactions. The amount of charge transferred in these individual reactions is the same. Individual reaction is called as the half reaction. The potential generated at the metal surface is called as the electrode potential denoted as E in equation 4.9. This is also called as an over-potential or half-cell potential. The over-potential (alternatively called polarization) is associated with a chemical reaction (without charge transfer) step that is an elementary step in the overall electrode reaction.

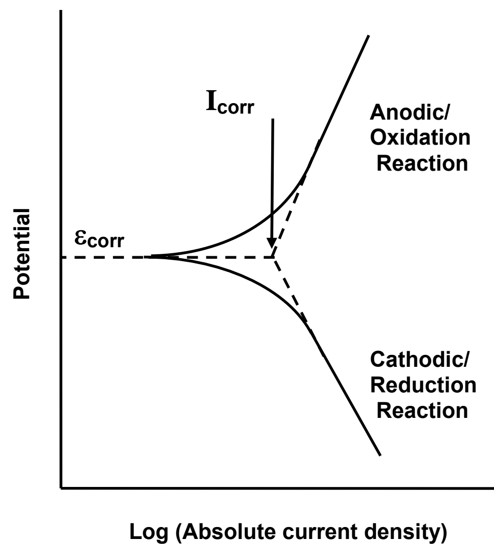

Figure 4.2 Typical graph for Tafel plot

This half-cell potential is usually measured with reference to a standard half cell called reference electrode. A reference electrode should have a stable electrochemical potential as long as no current flows through it. The most common laboratory reference electrodes are the Saturated Calomel Electrode (SCE) and the Silver/Silver Chloride electrodes. They can be calibrated to standard hydrogen electrode (SHE) which is referred as a standard half cell.

Electrochemical tests are conducted using a standard set up called as electrochemical cell shown in figure 4.3. A potentiostat or galvanostat is used for controlling the reactions in cell either controlling the potential or current in the cell.

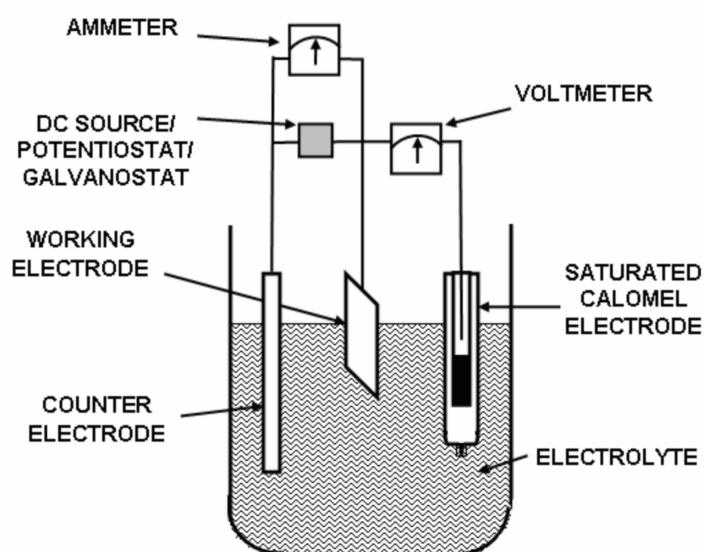

Figure 4.3 Construction of electrochemical cell

In polarization test, potential is varied in steps from cathodic interaction to anodic interaction or negative to positive potential values. The potentiostat can be programmed for the step intervals and potential steps. The current values are measured for each step.

These measurements provide the data for getting the Tafel plots and reaction rate calculations.

Polarization tests provide us the information about the active passive transitions of the material surface in different test conditions such as electrolyte chemistry, temperature, etc. For example if an oxidizer is added to the electrolyte, then the curve shifts to the higher current and potential values. As an effect of this, if the surface oxide film formed is protective type, then the curve shows the passivation as shown in figure 4.4. If the surface is abraded while testing, high activity on the surface causes metal to be more active and the curve shifts to lower potential values as described in figure 4.4.

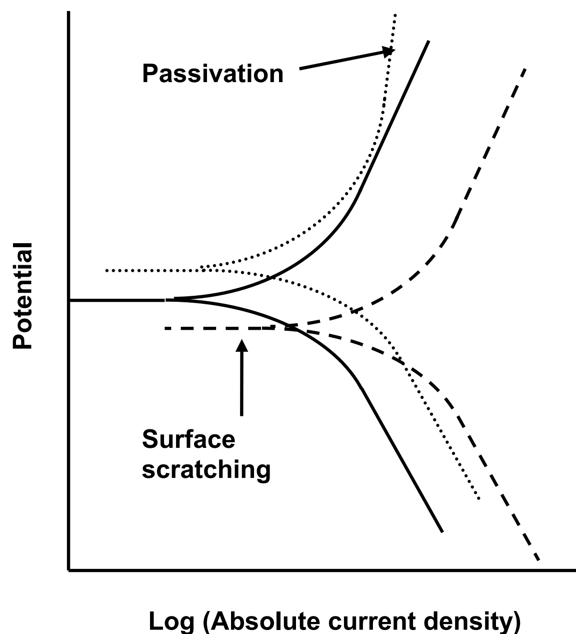

Figure 4.4 Effect of oxidizer and active scratching on the polarization curve

4.1.2.2 Pourbaix Diagram

In balancing redox equations, many electron-transfer reactions involve hydrogen ions and hydroxide ions. The standard potentials for these reactions refer to the pH, either 0 or 14, at which the appropriate ion has unit activity. Because multiple numbers of H+ or OH–

ions are often involved, the potentials given by the Nernst equation can vary greatly with the pH. It is useful to see what combinations of potential and pH allow the stable existence of a particular species. This information is most usefully expressed by means of an E-Vs.-pH diagram, also known as a Pourbaix diagram.[102]

4.1.2.3 Stability of Water

As was noted in connection with the shaded region in figure 4.5, water is subject to decomposition by strong oxidizing agents such as Cl_2 and by reducing agents stronger than H_2. The reduction reaction can be written as:

$$2H^+ + 2e^- \rightarrow H_{2(g)} \qquad [4.9]$$

or as well in neutral or alkaline solutions:

$$H_2O + 2\,e^- \rightarrow H_{2(g)} + 2\,OH^- \qquad [4.10]$$

These two reactions are equivalent and follow the same Nernst equation:

$$E_{H^+/H^-} = E^0{}_{H^+/H^-} + \frac{RT}{nF}\ln\frac{[H^+]^2}{p_{H2}} \qquad [4.11]$$

The Nernst's equation, at 25°C and unit H_2 partial pressure becomes:

$$E = E° - 0.059\text{ pH} = -0.059\text{ pH} \qquad [4.12]$$

Similarly, the oxidation of water in equation given below is governed by the Nernst equation.

$$H_2O \rightarrow O_{2(g)} + 4\,H^+ + 2\,e^- \qquad [4.13]$$

It can also be represented by equation 14 above. From this information we can construct the stability diagram for water shown below in figure 4.5.

This diagram has special relevance to electrochemical corrosion. Thus metals above H_2 in activity series tend to be oxidized (corrosion) by reducing H^+ ions. The unity partial pressures are of course purely arbitrary criteria; in a system open to the atmosphere, water can decompose even at much lower hydrogen partial pressures.

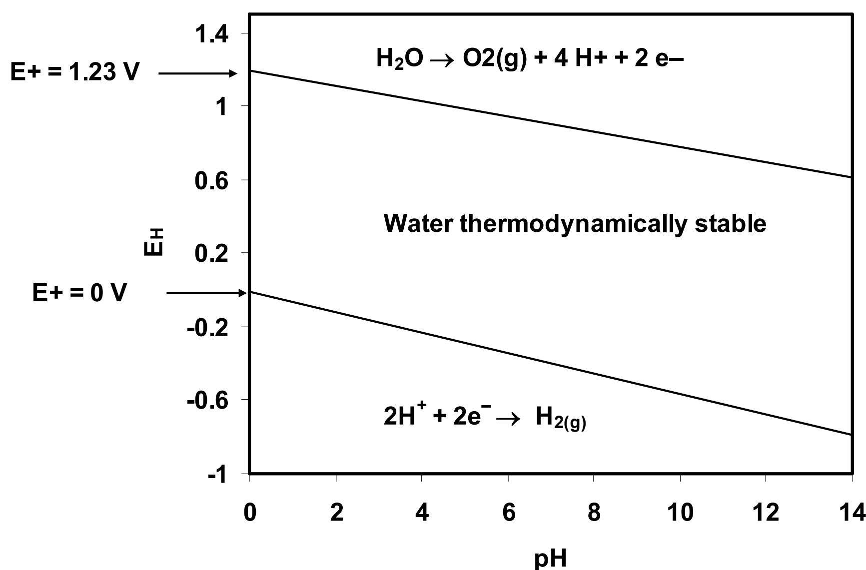

Figure 4.5 Stability (Pourbaix) diagram for water

Similar to water hydrogen system discussed above, water copper system stability diagram also can be plotted as shown in figure 4.6. Copper ion stable stage shows the region where active dissolution or corrosion of copper takes place. CuO and Cu_2O formation shows corrosion but protection in further corrosion because of oxide film on the surface. This region can be called as passive region. Passivity is the temporary loss of activity. $Cu(OH)_2$ region shows active corrosion and the stable copper region shows stable state. This information can be used for predicting the behavior of copper at different potentials and pH with water as an electrolyte for the reactions given below.

$$Cu = Cu_2^{+} + 2e^{-} \quad [4.14]$$

$$CuO + 2H^{+} = Cu_2^{+} + H_2O \quad [4.15]$$

$$Cu_2O + 2H^{+} = 2Cu_2{+} + 2e^{-} + H_2O \quad [4.16]$$

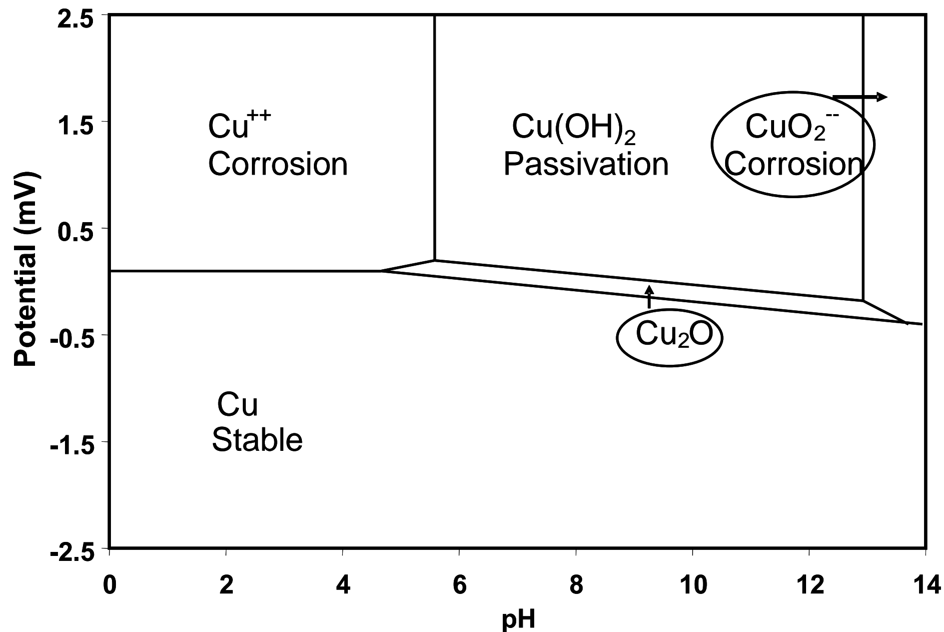

Figure 4.6 Pourbaix diagram for copper water system at room temperature

4.1.2.4 Dynamic Test

Dynamic electrochemistry means measurements when the electrochemical process under study is active. For example in case of corrosion studies, current measurement during active corrosion. This information provides the information of the kinetics of the surface interaction. In ECMP studies, current measurements provide the quantitative evaluation of the material removal process. The setup however needs to be modified for the active current measurement.

4.2 Motivation for Research

In CMP, material removal occurs through movement of atoms, particles, ions and oxides. There are synergistic effects of mechanical, chemical, and electrochemical interactions. The current practice is to use an equilibrium state of surface materials to guide CMP process design. However, the CMP process itself is a non-equilibrium process. The motivation of this research is to gain understanding of this synergy. It is necessary to understand triboelectrochemical interactions which are expected to lead towards the

formation of nonequilibrium oxide phases on the copper surface. Further more, it is necessary to pinpoint friction as surface forces and to understand its tribological effects on CMP, as well as material removal mechanisms.

4.3 Approach

The approach includes three steps, experimentation, characterization, and analysis. Design of experiments accommodated the parameters affecting the tribological interactions. Characterization is planned for surface topography and chemical nature. The output of experimentation is used for empirically deriving the physical nature of mechanisms in CMP. The analysis of these data is done to understand the scientific reasoning solving the complexity in the process. Existing standard static interaction and expected dynamic tribo-chemical interaction are compared. This concluded in fundamental understanding of tribological and tribochemical interactions.

4.4 Methods and Materials

4.4.1 Static Electrochemistry (Open Circuit Potential Measurement)

An electrical grade pure copper strip of 0.8 mm in thickness and 62.5 mm^2 square was used for polishing. Polishing slurries were made of 1 μm sized alpha alumina (grade C, Buehler Micropolish) in deionized water. Abrasive powder loading was 5 % by weight. Slurries were made to have two variables, pH and oxidizer content. The pH of the slurry was adjusted to values 3, 5, 7 and 9 respectively using acetic acid (CH_3COOH) and potassium hydroxide (KOH). The oxidizer content was maintained to 0.09, 0.15 and 0.21 % wt, using hydrogen peroxide (H_2O_2).

Open circuit electrochemical potential for each sample was measured, with reference to the Saturated Calomel Electrode (SCE), after 10 min of immersing the sample in slurry. The SCE is often used as a reference electrode in electrochemistry to measure the surface potential in an aqueous medium. It consists of a Hg/Hg_2Cl_2 electrode in a saturated solution of KCl_2. The electrode makes contact with the electrolyte via a porous frit.

4.4.2 Polarization Test

Potentiodynamic polarization tests were conducted on copper samples in the same slurries mentioned above, after OCP measurements. Potentiostat (Amel 2053) was used for this purpose. To complete the electrical connection, platinum counter electrode was used. This wire-shaped electrode was immersed in the slurry.

Tafel plots were generated for analysis. A Tafel plot is the potential versus current density. Values for current are measured over the surface area, exposed to the slurry, while the potential is varied from cathodic to anodic side with potential steps of 0.16 mV/sec. Current values were measured against pH and H_2O_2 contents.

4.4.3 ECMP (Dynamic Test)

A series of polishing experiments were conducted in the conditions mentioned below. The current measurement was carried out while the sample was being polished. The current density was obtained using the current value divided by the surface area.

4.4.3.1 Applied Potential and Slurry pH Variation ECMP

The sample was glued to the specially designed sample holder. The sample holder was made of nonconductive polymer, with an internal electrical connection, as shown in figure 4.7 for experimental setup. The polishing experiments were conducted on a table top polisher (Buehler Minimet 1000®). The applied pressure was 1 N/cm^2 for all samples polished. The purpose of using this pressure is to highlight electro-chemical effects. A soft stop option was used during polishing to avoid scratches. Each polishing cycle was set for 10 min.

The same slurries as for OCP were used for polishing experiments. Polyurethane pad (Rodel IC1000®) was used for polishing and it was soaked in polishing slurry for 30 min before experiments. No pre-polishing treatment was used.

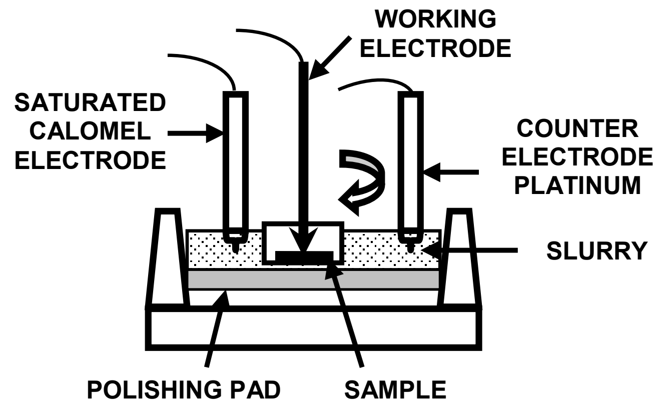

Figure 4.7: Experimental setup for copper CMP electrochemical studies

To study the electrochemical behavior under applied potentials, impressed current was applied to CMP. Impressed anodic or cathodic potential was controlled using a potentiostat (Amel 2053®). To complete the electrical connection, a platinum counter electrode was used. This wire-shaped electrode was immersed in the slurry. Applied potentials were +400, +200, 0 and -200 mV for different samples polished. After CMP, the samples were thoroughly rinsed with deionized water.

4.4.3.2 Variable Applied Potential ECMP

A series experiments were conducted on copper coated silicon samples. The experimental setup is shown in figure 4.8. The slurry was made in deionized water with alumina powder as abrasives. The size of the powder was 0.05 μm in diameter. The abrasive content in the slurry was 3 %wt. Hydrogen peroxide (1 %wt, H_2O_2) was used as an oxidizer. Acetic acid was used to adjust the slurry pH to 1. Polyurethane pad (Rodel IC-1000®) was used for polishing. Experiments were carried out using a disk-on-disk tribometer (CSM®), as shown in figure 4.8.

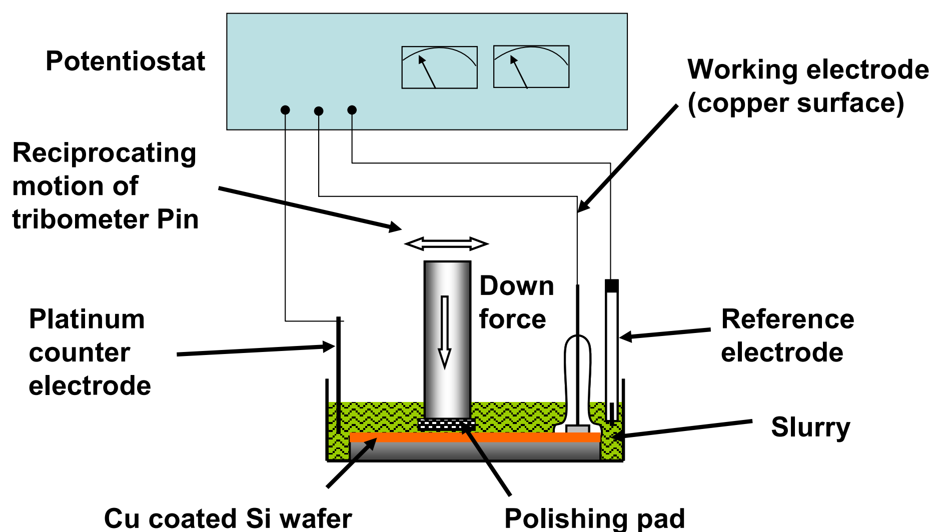

Figure 4.8 Experimental setup for Cu coated Si wafer ECMP

The sample was mounted on a substrate and polishing pad was attached on the pin of the tribometer as shown in figure 4.8. An oscillating motion (of the pin) was used for polishing and the sliding speed was 10 cm/sec. The stroke length was set to 2 cm. The pressure was applied at 3 N/cm^2. The slurry was added to the container of the sample. The amount of slurry was maintained such that the pad and the sample remained immersed throughout the tests.

Using a standard DC power supply the potential was applied to the sample. Copper surface was made a working electrode. Platinum wire electrode was used as a counter electrode and the connections were made as shown in the same figure. Each polishing cycle was conducted for 20 min in order to generate enough information for surface characterization.

Three samples were polished with three different conditions of impressed potentials as schematically described in figure 4.9. One sample was tested with constant applied

anodic potential of 2 V. The second sample was tested with constant applied cathodic potential of 2 V, while the third was with cyclic applied potential. The cyclic potential was applied at 2 V, anodic, and cathodic, reversing at each minute.

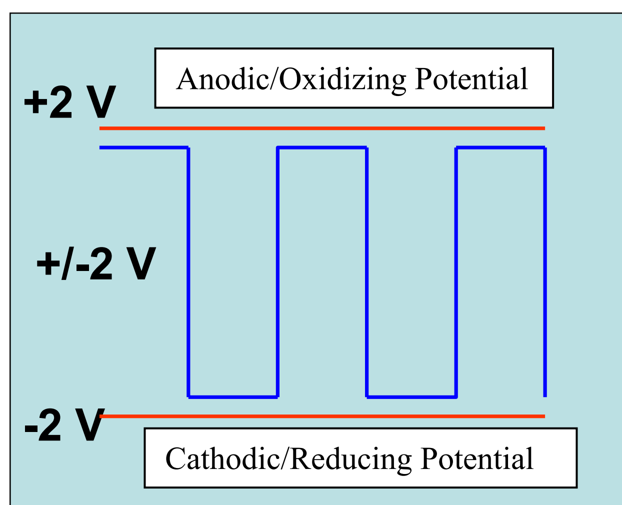

Figure 4.9 Applied potential cycle during ECMP

4.4.4 Atomic Force Microscopic Characterization

An atomic force microscope (AFM, PNI Nano-R®) was used for first step surface analysis. The AFM probe was made of silicon. A contact mode was used for topographical analysis. Usually a scan rate of 1 line per second was used. In cases where the height difference in topography was more than 1 µm, slower scan rates (as low as 0.2 lines/second) were used. A software (SPM-Cockpit2002 (3.1.2) and Nanorule + (2.12 Beta)) was used for image capturing and analysis. Image planarization and filtering were performed to reduce the image artifact and noise. Surface roughness was obtained over the topographical image data. The scanned area was 90x90 µm in average.

For the first set of experiment, where the copper plate samples were polished, a contact-mode scanning was performed. For the next set in the series, where copper coated silicon

wafers were polished, non-contact mode scanning was performed. For this second series of experiments, A novel technique for sample preparation and polishing was developed. The sample details and characterization are described below

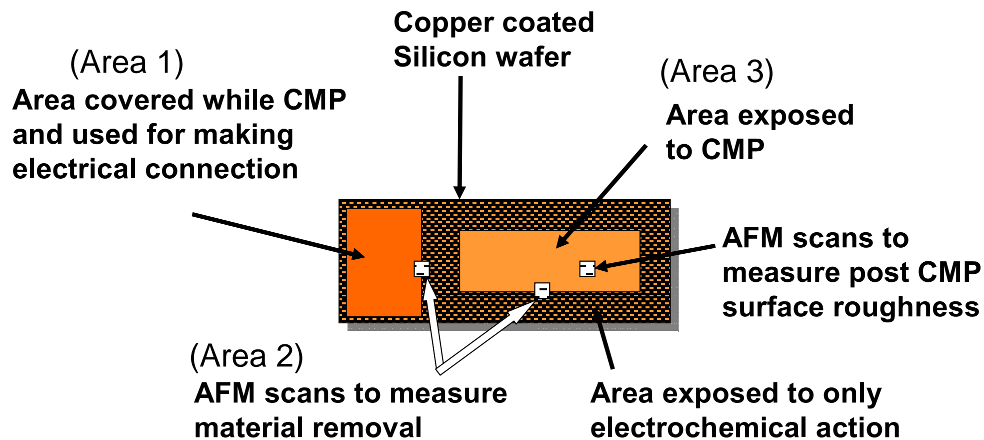

Figure 4.10 Schematic of sample surface

Samples were cut from a 200 mm copper wafer with silicon substrate to a square of 20x40 mm on each side. The Cu film was electroplated (annealed). For making an electrical connection to the copper surface, a conductive wire was attached to the sample surface and was sealed with a scotch tape.

In order to estimate the material removal rate, experiment was conducted in such a way that a polished sample has distinguishable areas. These areas were exposed to different conditions as schematically explained in figure 4.10. These areas are labeled into three regions:

Area 1, the original surface

Area 2, the area exposed to electrolytic interaction during CMP, and

Area 3, the area exposed to both electrolytic interaction and mechanical action of pad.

The Area 1, original surface, was the area where the electropotential was applied. This area was covered by using a scotch tape. During polishing, this area was free from electrochemical interactions. The Area 2, where the copper surface was exposed to slurry, underwent electrochemical interaction during CMP. Part of this area was exposed to mechanical interaction with polishing pad, during CMP. This region was marked as area 3. These areas were numbered as 1, 2 and 3 above and are shown in figure 4.10.

After polishing, the tape was removed. The surface contains an unaffected area and an electrolytically-affected area, next to each other, at a boundary region between areas marked as 1 and 2, as shown in figure 4.10. Height difference between these original and polished surfaces was measured using an atomic force microscope (AFM). This measurement provides values to be used for calculation of electrochemical removal.

Similar to the previous method, the step-height was measured in the region where areas 2 and 3 are connected to each other. This is illustrated in figure 4.10. An AFM topographical image is shown in figure 4.11. This measurement provides values to calculate the mechanical removal.

In order to obtain accurate values, neither image processing nor planarization over the AFM data was conducted. The material removal rates were calculated by averaging the surface height value at three different locations. The step height measurement at one single location was done over averaging 50 line scans.

The roughness was obtained using a non-contact mode scanning on polished surfaces. The scan size was about 90 μm. The AFM image was obtained at three locations for an average value.

4.4.5 Spectroscopic Characterization

The polished copper surface was analyzed using an X-ray Photoelectron Spectroscopy (XPS) (Kratos). The Mg Kα anode source with primary beam energy of 1.5 kV and electrocurrent 10 mA was used. The regions of interest were Cu $2p_{3/2}$ and Cu $2p_{1/2}$. The spectra were integrated for 10 scans.

4.5 Observations

4.5.1 Open Circuit Potential Measurement

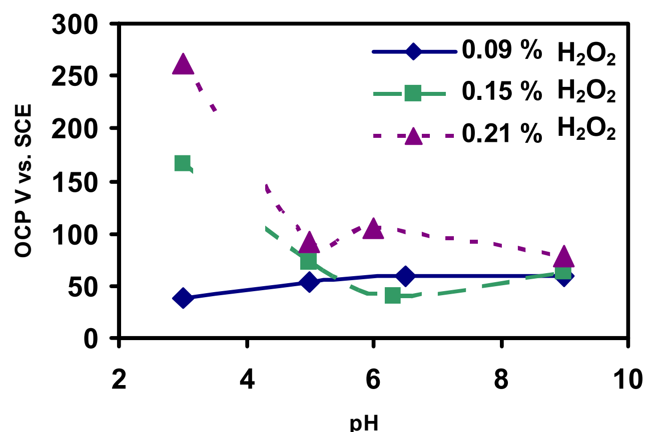

Figure 4.11 Open Circuit Potentials (OCP) of copper in CMP slurry as a function of pH

The Open Circuit Potential (OCP) for copper surface, measured in a stand alone slurry, are presented graphically, in figures 4.11 and 4.12. Figure 4.11 shows the effect of slurry pH on OCP at different oxidizer content, whereas figure 4.12 shows the effect of different oxidizer content on OCP, for different pH values of slurry. These figures show that at low pH values, variation in OCP is the highest. It is seen that at the low oxidizer content, variation in pH does not vary visibly, compared to the high oxidizer content of the slurry. Only for oxidizer content of 0.09%, it is observed that the OCP shows smaller values

than neutral pH values. For the rest of the samples, OCP values, away from the neutral pH, show an increase. The increase in the OCP values shows that a low pH and high oxidizer content of slurry increase the anodic dissolution tendency of the copper (figure 4.12). This is expected to increase the electrochemical oxidation rate. For CMP, this will provide higher material removal rate. However, this increase in electrochemical activity, which is discussed later, is not necessary for planarization.

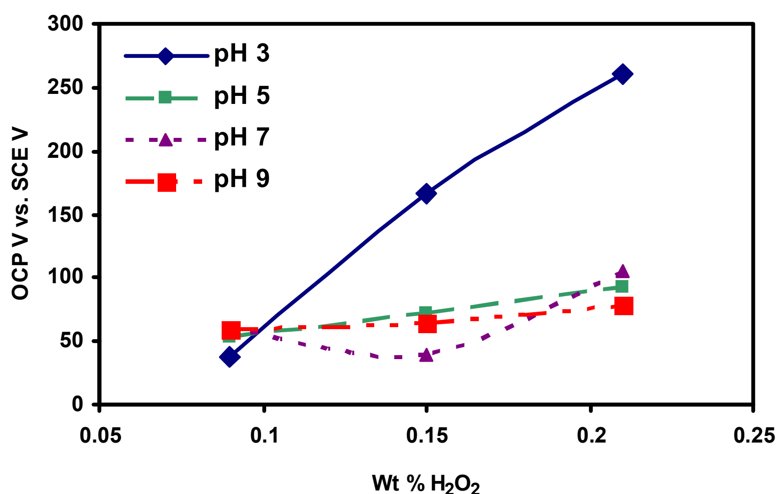

Figure 4.12 Open Circuit Potentials (OCP) of copper in CMP slurry as a function of H_2O_2

4.5.2 Potentiodynamic Polarization Test

Cyclic polarization (Tafel Plot) is useful in understanding the behavior of copper in the impressed potential condition. Polarization curves for copper in stand-alone slurries are thus obtained and plotted. Figures 4.13 and 4.14 show the Tafel plots for copper surface in slurries, at various pH values and different oxidizer contents. These Tafel plots consist of potential values on Y-axis and absolute current densities on X-axis. The anodic part of the curve shows the values of current densities, which can be correlated to the rate at which the oxidation reaction is occurring at the copper surface. The plots show that higher oxidizer content in the slurry results in higher current densities. This means that oxidation reaction rate increases with increase in the oxidizer content. However with

0.09% oxidizer in slurry, and pH value of 3, lower current densities were observed than the higher oxidizer contents at same pH. With neutral or basic slurries, the current densities observed were low. Lower current densities can be correlated to the formation of the passive oxide layer on the surface, or as such, low anodic activity rate. The passivating behavior is important to CMP that will be discussed later.

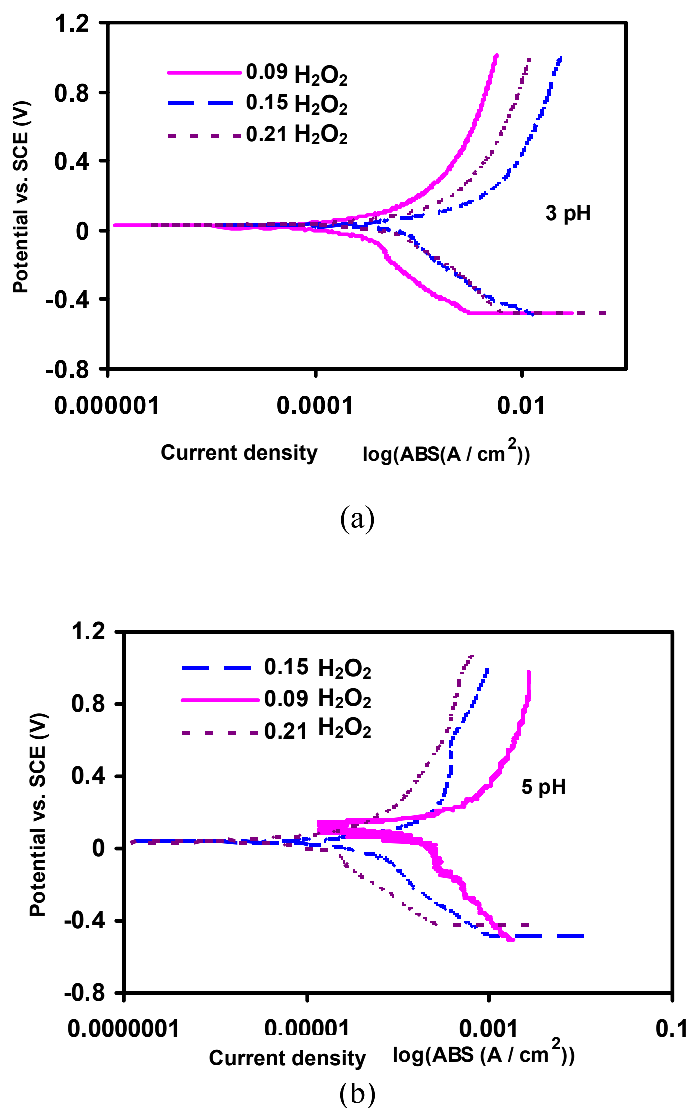

Figure 4.13 Tafel plots for copper in CMP slurry containing different level of oxidizer at (a) pH 3 (b) pH 5 (c) pH 7 and (d) pH 9, without active polishing

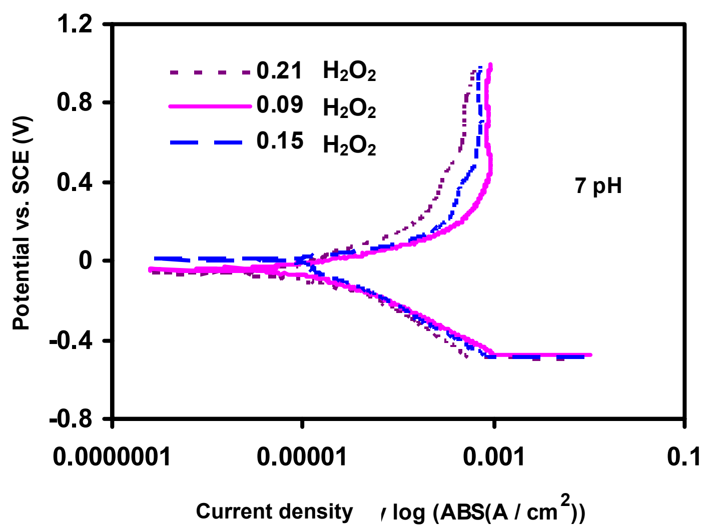

(c)

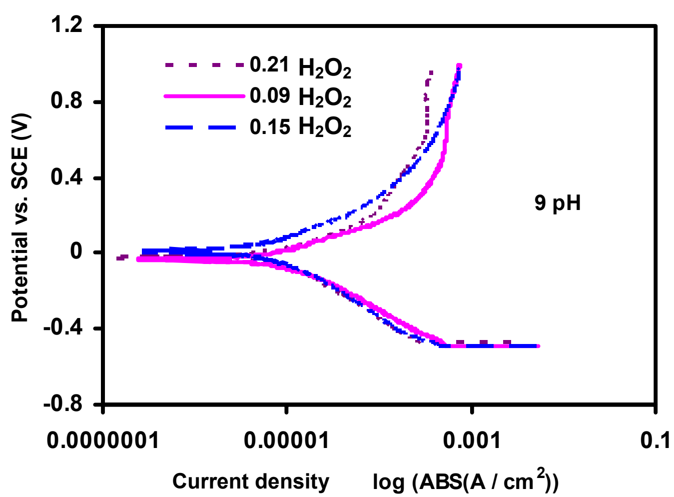

(d)

Figure 4.13 Continued

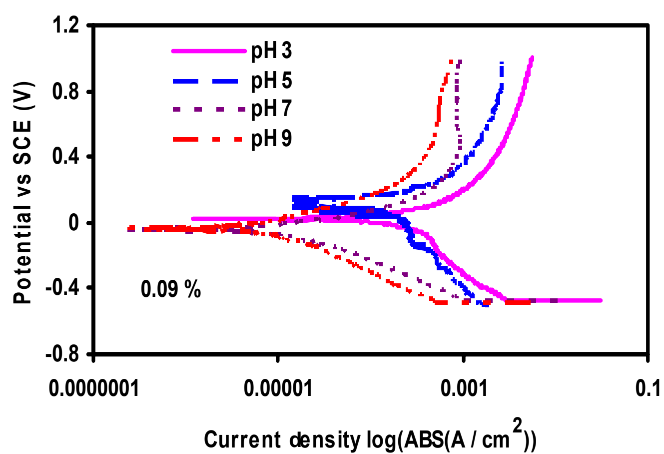

(a)

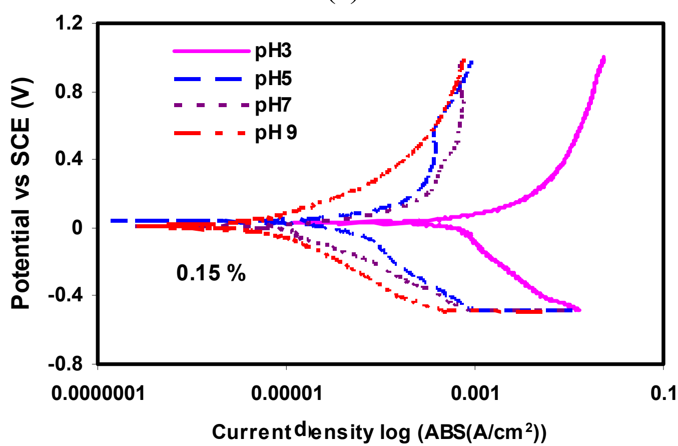

(b)

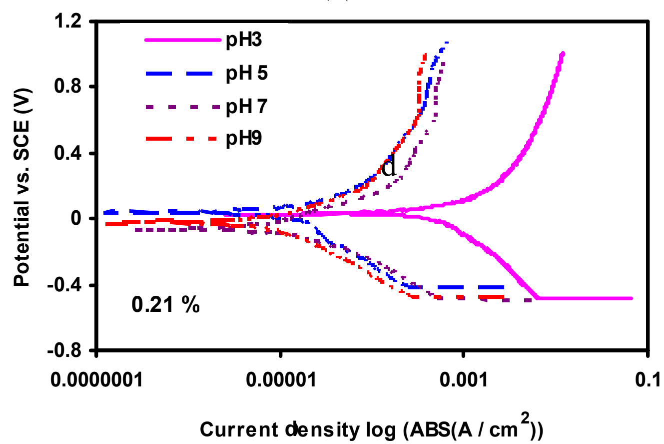

(c)

Figure 4.14 Tafel plots for copper in CMP slurry at different pH, containing (a) 0.09 % H_2O_2 (b) 0.15 % H_2O_2 and (c) 0.21 % H_2O_2, without active polishing

4.5.3 In Situ Current Measurement

Kinetically, the rate of surface reaction, in the electrochemical process can be predicted from the current densities. Current density in the anodic region is seen as the rate of anodic dissolution activity on the copper surface. To see the effect of variation in oxidizer content and pH of slurry, graphs of current densities were plotted as shown in figure 4.15 a through c. It can be seen that, with low oxidizer content of slurry, the variation in current densities is high with reference to change in applied potential and pH of slurry. At higher value of oxidizer (0.21 %), the current densities are comparatively stable. This means that the addition of an oxidizer reduces the oxidation through passivation.

4.5.4 AFM Topography: Surface Roughness

The average surface roughness achieved after CMP is expected to be a function of several variables. The abrasive particle size, shape, distribution and polishing as well as polishing time, load and pre/post cleaning techniques, were kept constant. The variables were electrochemical potential of the copper sample in polishing slurry, pH, and the amount of H_2O_2 in slurry. AFM topography images of post CMP surfaces were used for understanding the correlation between these variables and surface roughness achieved.

As an effect of impressed electropotentials and slurry chemistry, the activity at copper surface generates the electrical current. This electric current is related to the electrochemical rate kinetics on the copper surface. To understand the effect the correlation between the high and low current densities, two AFM topography images can be compared that are shown in figures 4.16 a and b. Figure 4.16a shows morphology of copper surface obtained at current density of 0.01 A/cm^2 lower than that in figure 4.16b at 0.0005 A/cm^2. The observed surface in figure 4.16a is rough because the kinetics of the process does not provide a complete and uniform oxide layer on the surface. The high rate of anodic dissolution leads to poor surface quality.

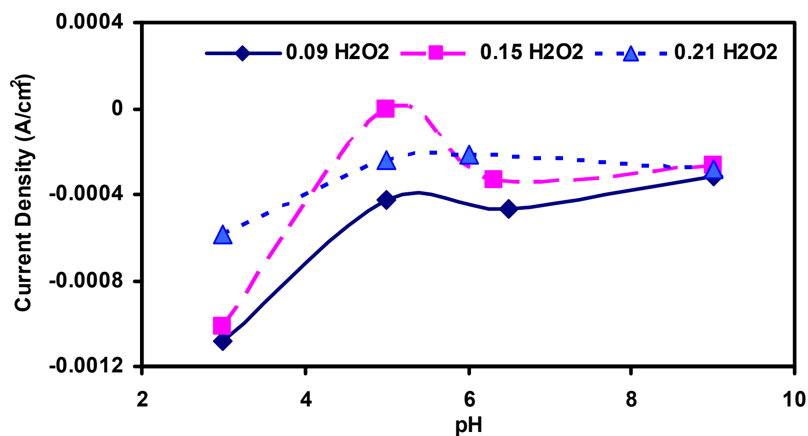

(a) Applied potential -200 mV with respect to OCP

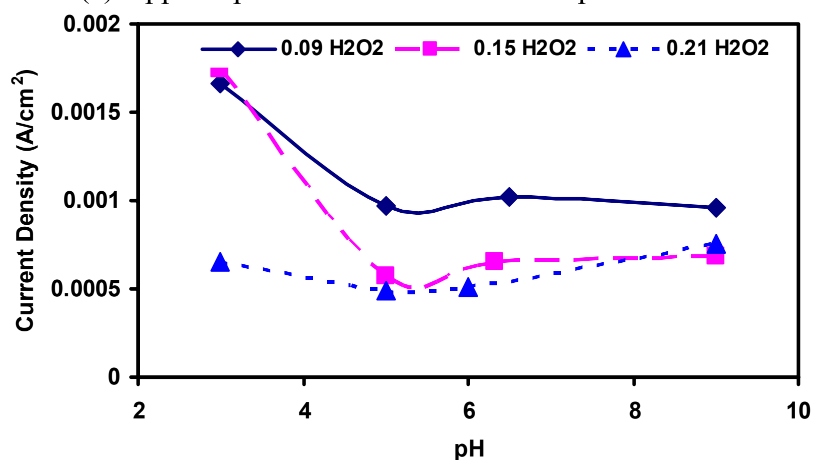

(b) Applied potential +200 mV with respect to OCP

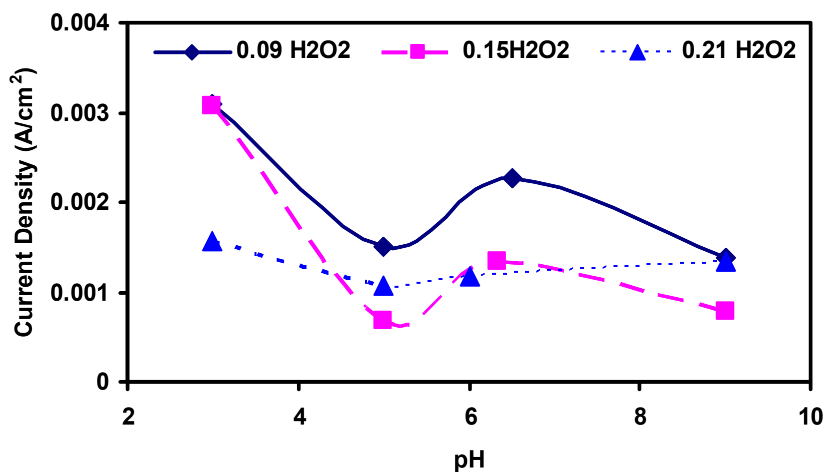

(c) Applied potential +400 mV with respect to OCP

Figure 4.15 Variation in current density as a function of slurry pH, for various weight % H_2O_2 content and applied potentials during CMP

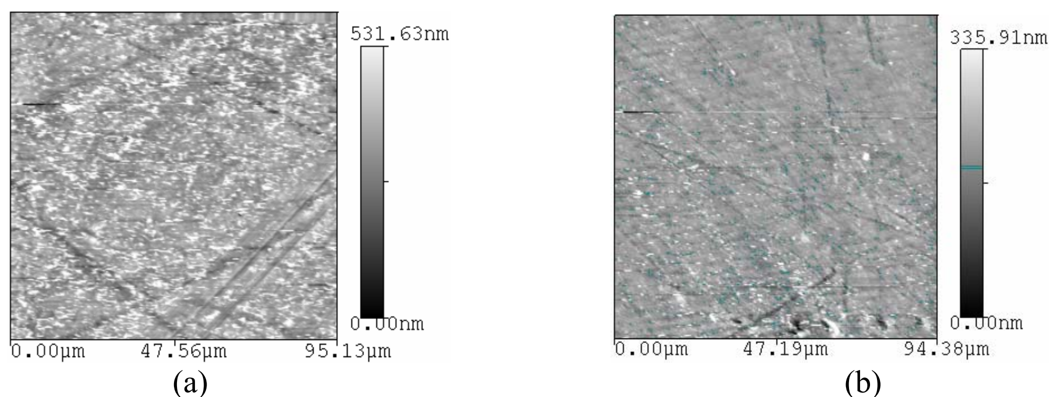

(a) (b)

Figure 4.16 AFM topography images showing topography after CMP with current densities of (a) 0.01 A/cm^2 and (b) 0.0005 A/cm^2

Effects of pH on CMP were further studied and the results are shown in figure 4.17. Figures 4.17a through c show the morphology of copper surface obtained after polishing with slurries of different pH. Figure 4.17a shows the surface after polishing with slurry of pH 3. Figure 4.17b shows the surface after polishing with neutral slurry whereas figure 4.17c shows that of pH 9. As observed from the figure, low pH and cathodic potential, or high pH and anodic potentials during CMP show better quality after CMP than other conditions. The results are for 0.09 %wt H_2O_2, i.e. low oxidizer content of slurry. With remaining parameter combinations, the surface roughness after CMP is high.

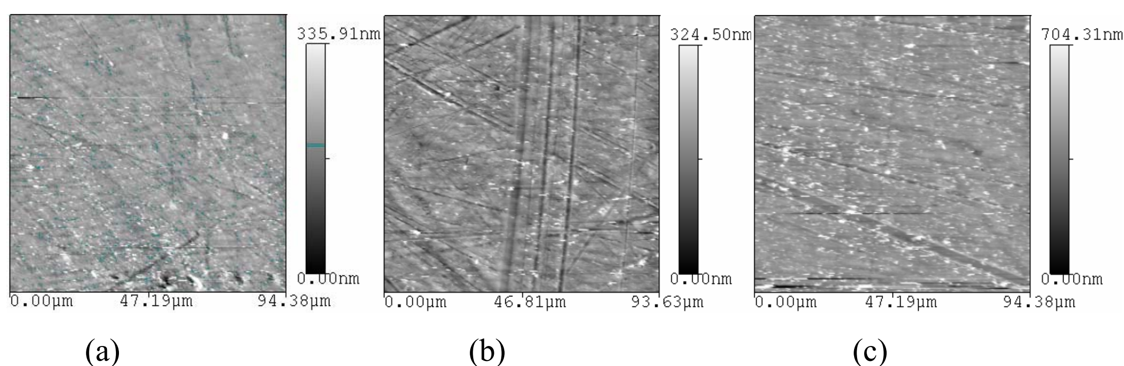

(a) (b) (c)

Figure 4.17 AFM topography images of copper surface after CMP in slurries with (a) pH 3, (b) neutral pH, and (c) pH 9

The material removal in ECMP is synergistic effect of chemical, mechanical and impressed potentials. Surface roughness achieved by this synergy can be better understood if the combination of the pH and applied potential can be understood. The surface roughness values Ra (nm) provided by the post ECMP AFM surface topographies are plotted as shown in figure 4.18. This particular plot is for slurry containing 0.09 %wt H_2O_2. X-axis of the plot is slurry pH, Y-axis is applied potential (mV) and the Z-axis is the surface roughness (Ra nm). The Ra value is plotted as color intensity referring to the scale shown in right side of the plot.

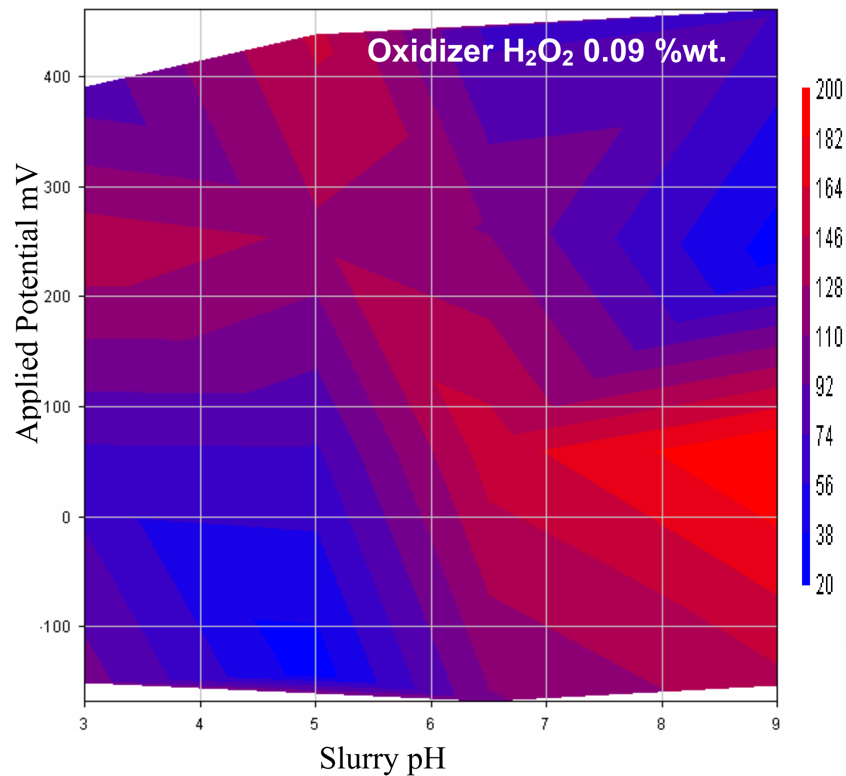

Figure 4.18 Surface plot for post ECMP copper surface roughness

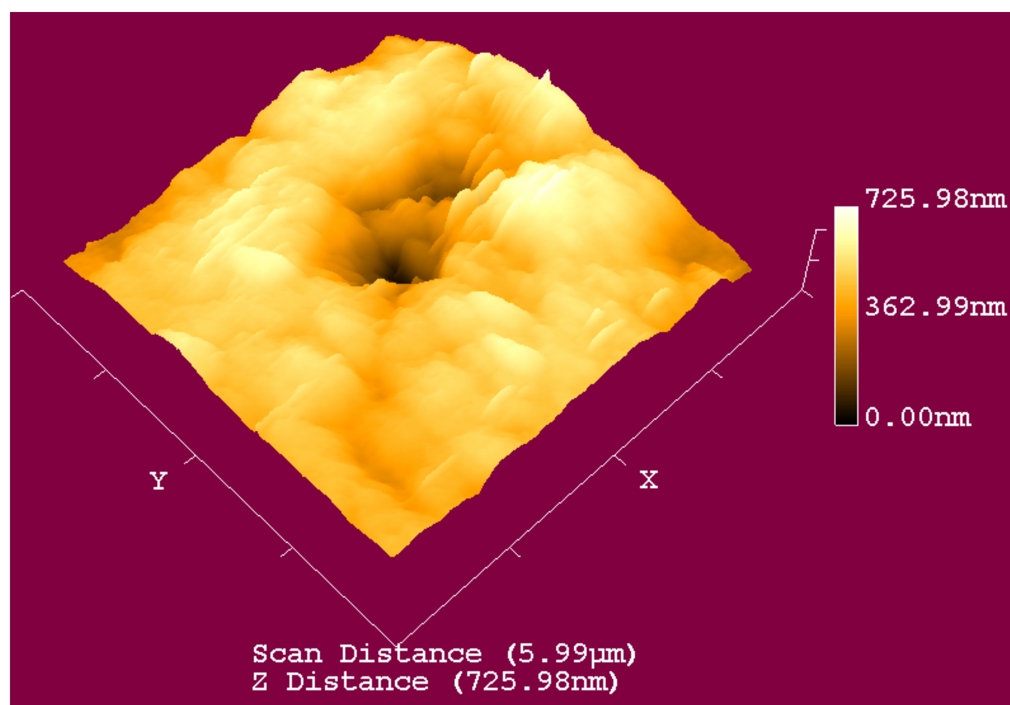

Figure 4.19 AFM scan showing a pit in a topography image

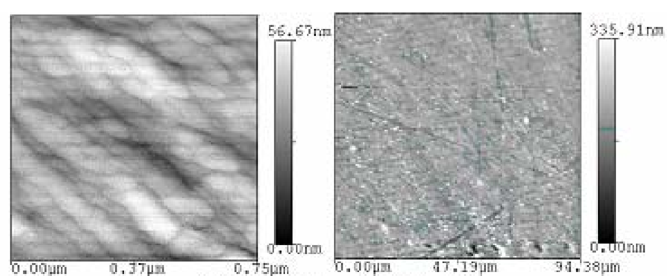

(a) Low pH Anodic Potential

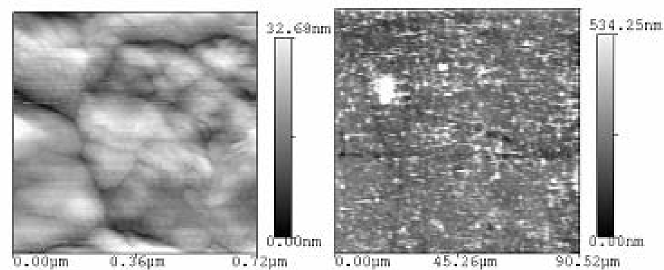

(b) High pH Anodic Potential

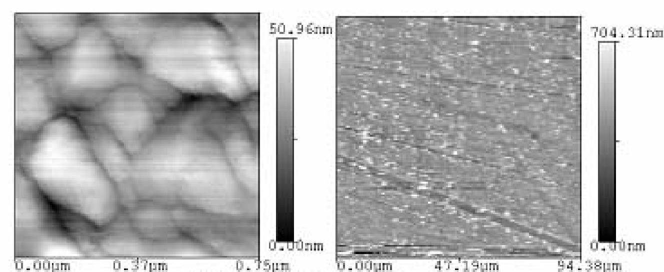

(c) Low pH Cathodic Potential

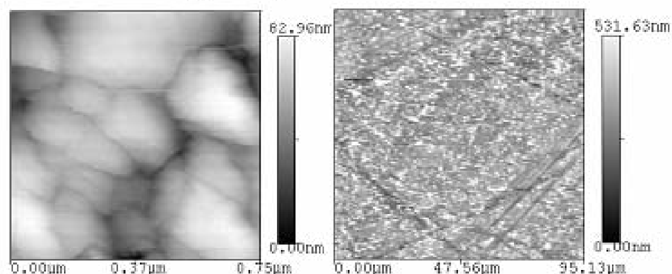

(d) High pH Cathodic Potential

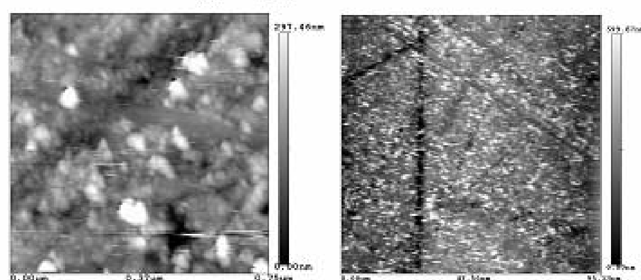

(e) Neutral pH and Open Circuit Potential (no external potential applied)

Figure 4.20 AFM scans showing topography after ECMP with various conditions

The AFM topography images in figures 4.19 and 4.20 are for the samples polished with different combinations of high and low, pH and applied potentials. Figure 4.19 shows the pitting occurred on the surface while polishing in slurry with pH 3 and applied potential of +400 mV. Figures 4.20 a through e show the AFM topography at two different magnifications for various combinations of pH and applied potentials. The details of these images are discussed further in next section of this chapter.

The second set of experiments, where the impressed potentials were of high order (2 V) and the pH of the slurry was also high (pH = 1), has generated some interesting results of surface roughness. The AFM topography for these surfaces is shown in figures 4.21 a through c. The graphical representation of the average surface roughness values is shown in figure 4.22.

Post CMP surface roughness after anodic impressed potential of +2 V has generated high roughness of 46 nm. Cathodic impressed potential of cathodic 2 V potential has provided surface roughness of 36 nm. The best average surface roughness value (10 nm) was achieved when the applied potential was cycled between anodic and cathodic 2 V.

4.5.5 Chemical Analysis Using XPS

In order to investigate the passivation and removal mechanisms, XPS analysis was conducted on polished copper surface. Figure 4.23 presents the spectra of Cu 2p3/2 and 2p1/2 from specimens polished with anodic and cathodic potentials of 2 V respectively.

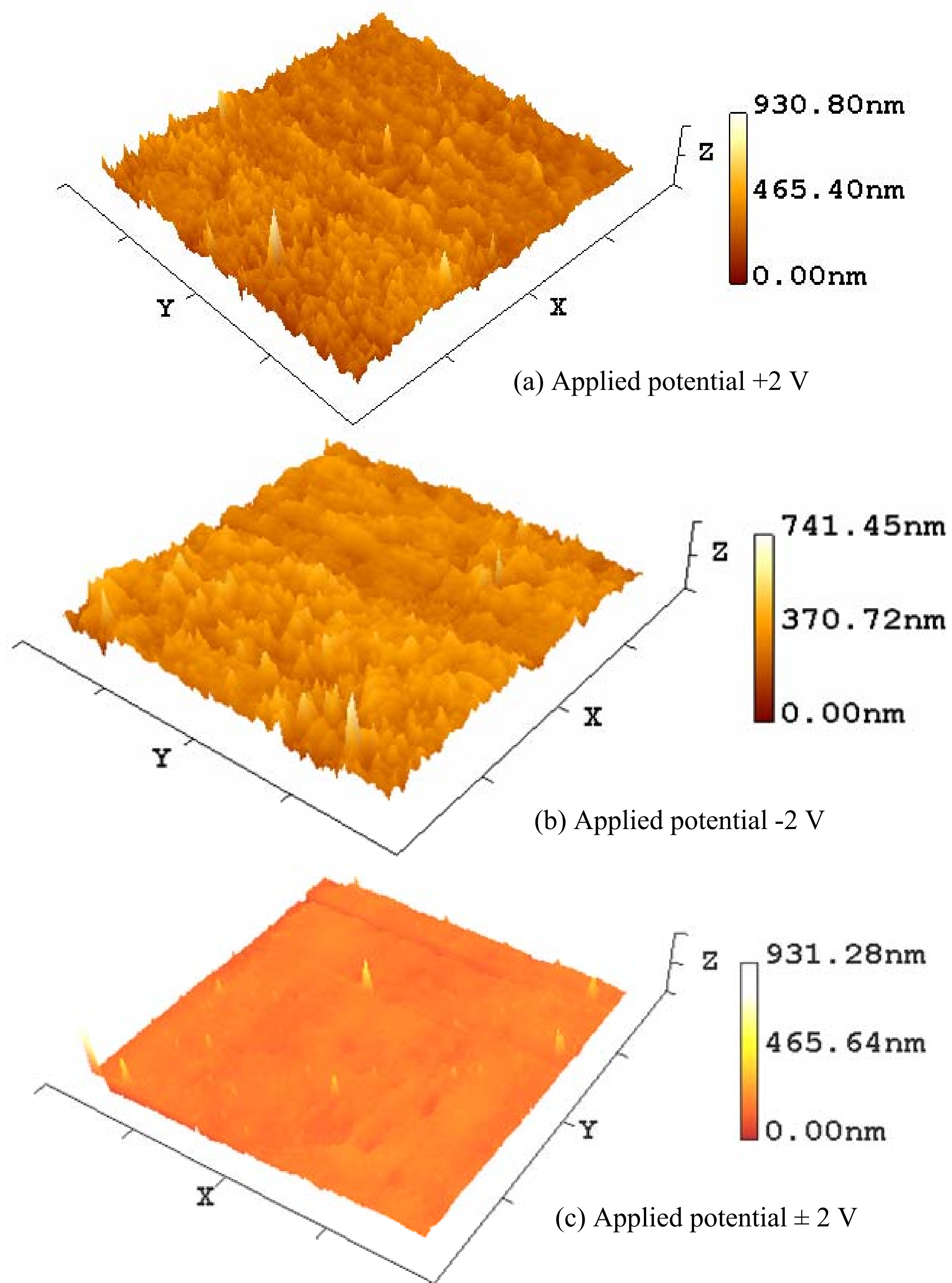

Figure 4.21 AFM surface topography of copper surface after ECMP

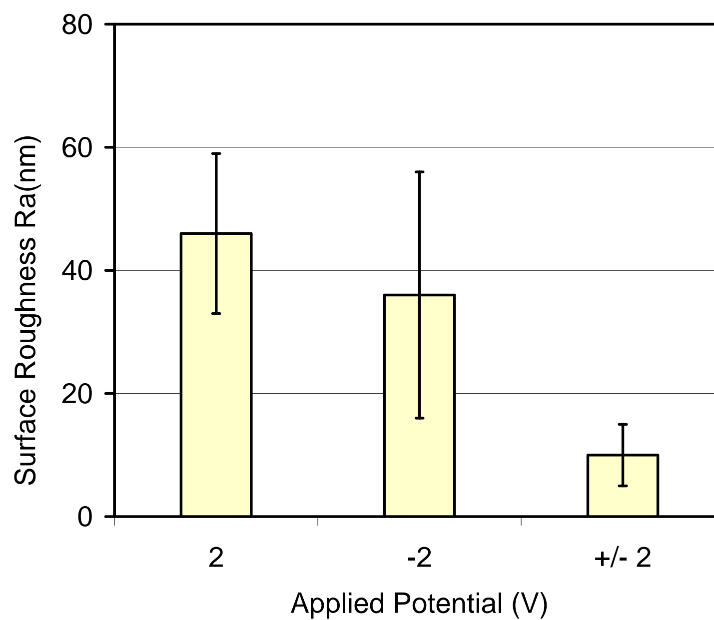

Figure 4.22 Post ECMP surface roughness for different applied potentials

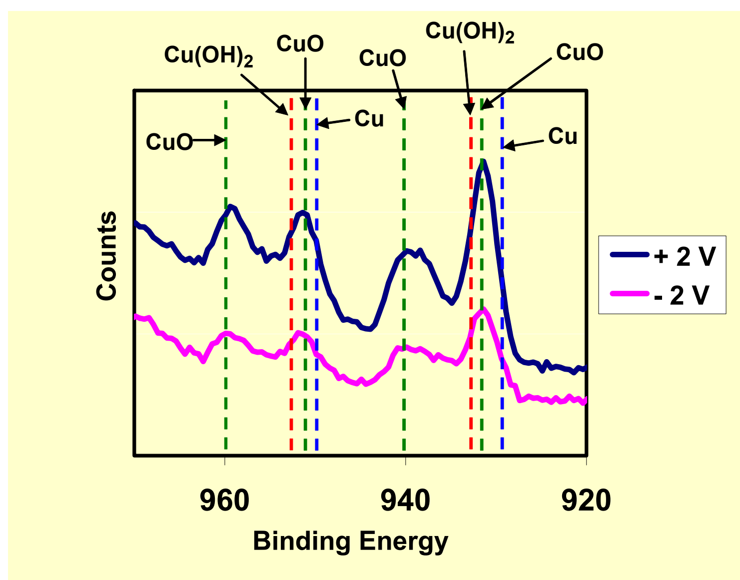

Figure 4.23 XPS spectra of Cu 2p3/2 and 2p1/2 for Cu after ECMP

For copper surface that was polished with cathodic impressed potential, the oxidation of copper is evident from the peaks observed at binding energies between 933.5 and 935.2 eV for Cu 2p3⁄2; and between 953.5 and 955.2 eV for Cu 2p1⁄2. This proves the formation of CuO and Cu(OH)2. The satellites near 943 and 963 eV confirmed the presence of CuO. For the sample polished with anodic impressed potential, the presence of CuO is confirmed. In both slurries, the peaks of 932.5 and 952.5 eV corresponding to 2p3⁄2 and 2p1⁄2 spectra for Cu were not found. This means that metallic copper does not exist. and the oxide film is present.

4.6 Discussions

4.6.1 Static Electrochemistry

OCP values observed in the figure 4.11 and 4.12 have suggested a strong correlation between the surface activation with pH and oxidizer content.

4.6.1.1 Effect of Oxidizer

It is known from basic chemistry that there are more than one type of copper oxides existing: CuO, Cu_2O and $Cu(OH)_2$. In the presence of H_2O_2, the following possible cathodic/reduction reactions take place,

$$H_2O_2 + 2H^+ + 2e^- \rightarrow 2H_2O \qquad [4.17]$$

$$H^+ + 2e^- \rightarrow H_2 \qquad [4.18]$$

$$O_2 + 2\,H_2O + 4e^- \rightarrow 4OH^- \qquad [4.19]$$

$$O_2 + 4H^+ + 4e^- \rightarrow 2H_2O \qquad [4.20]$$

The dissolution of Cu proceeds according to the following anodic/oxidation reaction:

$$Cu \rightarrow Cu^{++} + 2e^- \qquad [4.21]$$

While in case of water, according to the Cu–H_2O potential–pH diagram, Cu can be oxidized by water to form Cu_2O following the reaction:

$$4Cu + 2H_2O \rightarrow 2Cu_2O + 4H^+ + 4e^- \quad [4.22]$$

For both cases in equation (4.18) and (4.19), OCP values are related to the extent to which these reactions proceed. High value of OCP shows an increase in anodic activity on copper surface. Similarly, the high oxidizer content in the slurry shows an increase in anodic activity at copper surface. Further more, the acidic pH shows more anodic activity at the surface. The exception was found at the low pH and low oxidizer content. This suggests that a low pH and oxidizer content result in controlled anodic reaction. The acetic acid may be getting adsorbed in the copper oxide film, formed by the H_2O_2, and getting stabilized. This gives a passivation effect. As a result of the passivation effect, with 0.09 %wt of oxidizer, the values of OCP are lower in all the pH conditions.

With the increase of content of oxidizer, the oxidation rate increases. It is followed by the dissolution of copper oxide through by the acetic acid in a low pH slurry. This is seen in figures 4.13 and 4.14 with increased OCP values. With the increase in oxidizer content (from 0.09 %wt to 0.21 %wt), the anodic current densities increase showing increased material etch rate.

4.6.1.2 Effect of pH

Acetic acid (CH_3COOH), which is used for adjusting the acidic pH, is corrosive for the copper. Chemical etching is possible for copper in the presence of acetic acid. The etching is not severe. Acetic acid dissolves oxides from the copper surface. These oxides are CuO and Cu_2O. The H_2O_2 and deionized water form an oxide layer rapidly. The oxide layer can be either Cu_2O or copper hydroxide ($Cu(OH)_2$) In presence of acetic acid, copper acetate ($Cu(CH_3COO)_2$) can also be formed. With a lower concentration, acetic acid is adsorbed on the oxide film and stabilizes. With low pH values, in presence of

oxidizer, formation of copper oxide causes passivation. With the increase in oxidizer content, dissolution rate of copper should increase as the oxidizer-acid combined action cause active etching. The same increased activation is reflected in the Tafel plots for 3 pH slurries as shown in figures 4.13 and 4.14. The OCP values are shown higher than that for the neutral and basic slurries.

With neutral and basic slurries, all oxidizer concentrations show passivation. The anodic current densities are decreased by almost a decade (10^1 times) of current density than that of current densities for acidic slurries current densities as seen in the Tafel plots. The absence of acetic acid caused no change in the anodic potential nor in the current density values as observed in figures 4.13 and 4.14.

KOH, which is used for stabilizing the alkaline pH, is also corrosive for the copper. However its role varies based on the electrode potential applied. The KOH works as a catalyst, in the cathodic region, and reduce the ionic copper to the atomic copper. However, the action is not as strong as seen from the Tafel plots (figure 4.15). The variables like pH, oxidizer, and anodic potentials do not show considerable variation in current densities in the Tafel plots.

4.6.2 Roughness Measurement

It is known that in CMP, the material removal from the surface is the synergistic effect of chemical dissolution, mechanical abrasion, and electrochemical reaction. The role of oxidizer in the slurry is to stabilize the oxide on the surface to be planarized. The download of abrasive particles on wafer surface causes mechanical removal. Impressed potential provide stabilization of the ionic or oxide state with reference to the Pourbaix – E-pH (Potential – pH) diagram. In the past, it is shown that presence of the oxide provides lubrication effect on the surface. Maintaining useful oxide film on the surface is important in the CMP. Since the process of CMP is dynamic in nature, it is difficult to control the surface oxidation. Our results showed that the control of surface oxidation can

be achieved through varying the content of H_2O_2. The planarization is achieved through a balance between the formation and removal of oxide.

4.6.2.1 Roughness Map

The surface roughness over a wide range of polishing conditions is mapped as shown in figure 4.18. In figure 4.24, the X-axis is the pH and Y-axis is the applied DC potential. The solid lines outline the regions of thermodynamically stable reaction products within. This is a part of typical Pourbaix diagram. The measured roughness values at various applied potentials and pH are superimposed on this diagram. The diagram is further extrapolated into five zones as marked in the figure. The removal mechanisms in these zones are discussed below.

4.6.2.1.1 Zone 1

Acidic pH and impressed anodic current: The existing Pourbaix diagram for the water-copper system suggests the ionic dissolution of the copper. If the rate of ion dissolution is high, pitting type corrosion behavior is expected. Indeed, figure 4.19 shows the pitting observed for the copper sample polished in the pH=3 and 400 mV impressed anodic current. This shows that the accelerated corrosion along with polishing action is producing poor planarization. In Figure 4.20a, the same can be depicted as we find poor Ra values in this region.

4.6.2.1.2 Zone 2

Basic pH and impressed anodic current: This is expected to be the range of passivation by Cu_2O film formation. Observed Ra values in this zone appear to be the best. This can be seen in figure 4.20b, where better finish is observed in the AFM topography. Although the hardness of Cu_2O is higher than virgin Cu, under the abrasion of nanoparticles, this film is removed atomically. This indicates that the removal mechanism is dominated by surface modification with oxide formation removal simultaneously. .

4.6.2.1.3 Zone 3

Acidic pH and impressed cathodic current: Copper is expected to remain in the cathodic current regions. The corrosion activity is low and mechanical wear is more pronounced in the region. Observed Ra values are best among the parameter regimes studied. In this region the oxidizer H_2O_2 suppresses the direct chemical attack. Doing so, a balance between corrosion and wear is achieved. The evidence is seen in the AFM topography (figure 4.20c) where a relatively smooth surface is seen in the overall area (right). Some grooves are observed due to mechanical abrasion.

4.6.2.1.4 Zone 4

Basic pH and more cathodic current: Under this condition, poor values of Ra were obtained. This correlates with a relatively poor surface quality observed under AFM, as shown in figure 4.20d. Apparently, the effect of oxidizer is eliminated in this condition. There is no beneficial layer nor does surface modification promote an atomically flat surface. All these, in addition of lack of corrosion, mean that a higher surface roughness is mainly caused by mechanical wear,

4.6.2.1.5 Zone 5

Neutral pH and no impressed current: This region has shown very high values of surface roughness. The AFM images also show severe abrasion type wear. Deep scratches are observed as seen in the AFM scan figure 4.20e. This is typically a mechanical wear, rather than electrochemical polishing. This suggests that oxidizer alone is not affecting planarization. It can be concluded that in absence of oxide film on the surface, high quality of Cu planarization is difficult to achieve.

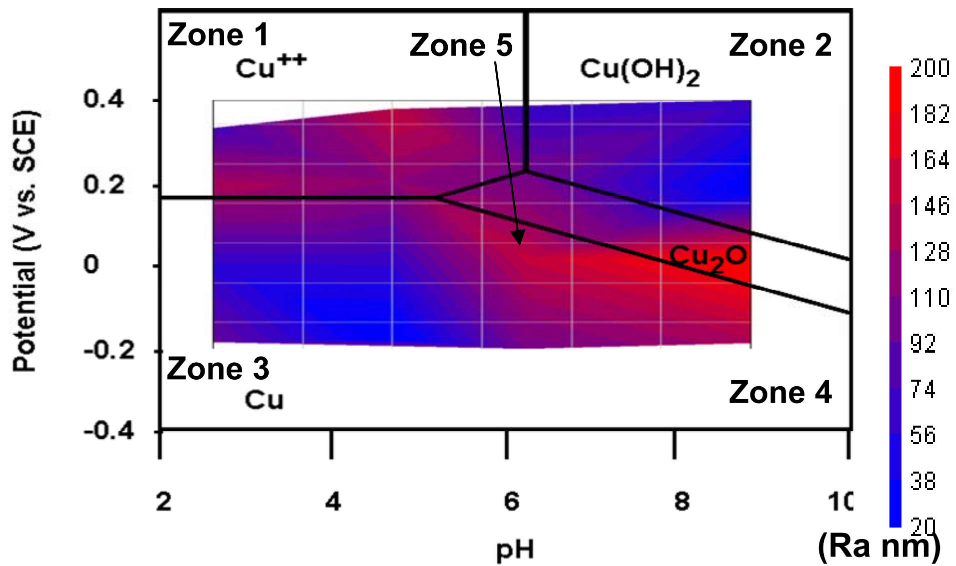

Figure 4.24 Surface roughness Ra value gradient graph superimposed on Pourbaix diagram for copper water system at room temperature

4.6.2.2 Effect of Potential Variation on Ra

The second set of experiment with high impressed potentials has generated interesting results. The surface roughness values after various impressed potential ECMP process are discussed below.

4.6.2.2.1 Anodic Potential

In the electrochemical dissolution, copper atoms are ionized and are removed from the surface by the action of electrolyte. This anodic reaction occurs under the impressed anodic potential. The electrical circuit is completed externally by providing suitable electrode platinum.

Copper layer deposited on silicon wafer was subsequently annealed after deposition. Annealed structure of this layer is polycrystalline and has a twinned microstructure. This means that copper grains have random orientation with reference to the face in contact with an electrolyte. When the copper is exposed to a current, a corresponding dissolution

rate will be generated. The dissolution rate in the grain boundary region will be higher than that in the grain due to the level of surface energy. The planarization is expected poor. As shown in the figure 4.21a, copper surface after CMP with impressed anodic potentials has revealed the grain structure of copper. The valley in the grain boundary region is 15 nm. With a higher applied potential, the current density does not show linear increase. In this region, the ionic dissolution rate is reduced by formation of passive copper oxide layer on the surface. Copper dissolution rate in this region is controlled by mass transfer. However, the mechanical action of pad will have continuous action of removal of this oxide layer. This will expose the copper surface again.

As discussed above, in anodic impressed potential condition, high dissolution rates and reduced tendency of the continuous oxide layer formation on the copper surface, material removal rates are high but the material removal is non-uniform. This results in a poor surface finish value (Ra 47 nm) after CMP. The AFM topography shows some groves and scratches resulted from direct abrasion. This surface finish is not desirable.

4.6.2.2.2 Cathodic Potential

Under the cathodic condition, the electric potential has negative charge on the wafer surface, and the positive charge on the counter electrode. In such condition, electrons intend to move towards the copper surface so that copper ions are not formed and corrosion is suppressed. This is opposite of the basic corrosive behavior just discussed in previous section.

In cathodicaly impressed current condition, the dissolution of copper ions is suppressed. The process of hydrogen evolution may occur as an effect of reduction reaction. Thermodynamically, the copper remains inert under this cathodic condition.

The passivation of copper surface is enhanced by electrons due to impressed cathodic potential. This will lead to a uniformed layer of oxide with a good final planarization.[103, 104]

The suppressed corrosive reaction, controlled oxidation, and reduced mechanical abrasion resulted in a good surface quality. This can be seen in an AFM topography image, as shown in figure 4.21b. The surface has fewer scratches and better planarization than anodic impressed potential condition. . Surface roughness (Ra) here is 35 nm. The improvement surface finish was due to the presence of surface oxide film.

4.6.2.2.3 Cyclic Potential

It can be seen in the AFM topography (figure 4.21c) that the surface has almost no scratches. The measured average surface roughness is around 10 nm.

In the electroplating and electropolishing processes, application of cyclic potential has been reported. In electroplating, the potential of an electrolyte is maintained high.[105] This enables reducing the dog-bone effect in the plating. The dog-bone effect is defined as the formation of a thick layer deposited in protruding edges over valley regions. With a cyclic potential, such non-uniformity can be reduced through a uniform ionic concentration.

In case of electropolishing, previous research has shown that if the current is reversed between anodic and cathodic potentials, the surface is smooth.[106] In this case, the overall material removal is negligible. Instead, surface atoms diffuse from peaks (during anodic cycle) to valleys (cathodic).

In the electrochemical reactions, the kinetics of the ionic dissolution or deposition is non uniform in nature. In such, uneven current distribution over the surface of electrodes is observed. This causes uneven material removal, which is the reverse of the dog-bone effect. In electropolishing, surface of anode material to be polished, that is close to the

cathode surface, will have more material removal rates than the area that is away from the cathode surface. Such uneven material removal results in a poor surface quality. To overcome this, one of the methods that can be implemented is the cyclic current reversal during CMP. A cyclic current enables a mass–transfer-controlled rather than a diffusion-controlled process. The mass-transfer–controlled process is associated with the amount of mass being moved while the diffusion-controlled one means the path being past due to the concentration change.

If the current is intermittently reversed during the ECMP process, then the ionic polarization effect can be reduced. This will lower the differential dissolution. Uniform dissolution is required for achieving a good planarization.

4.6.3 Surface Phases and Pourbaix Diagram

Copper has good corrosion resistance in the presence of acetic acid. As seen before, in presence of oxidizer, the chemical etching of copper occurs. The process includes the formation of copper oxide and its subsequent dissolution. If the copper surface is rinsed with water after this procedure, then a thin copper oxide layer is formed on the surface. However if the copper is rinsed with non-oxidizing solution like acetone, then copper is exposed with no oxide on it.

In the present study, copper surface was exposed to the slurry containing acetic acid and an H_2O_2 oxidizer. The copper surface was rinsed with acetone after the ECMP trials. It is expected that the copper surface free from oxides.

In addition, during ECMP, the copper surface was exposed to impressed potential. As seen in the Pourbaix diagram (figure 4.6), when the pH is 1 and the anodic potential is 2 V, copper ions are thermodynamically stable. The copper ions go into the slurry and the pure metal is exposed. In the case of cathodic -2 V impressed potential, the copper is thermodynamically stable. Therefore under impressed potentials, no copper oxide is

expected on the surface. Further more, mechanical action from a polishing pad and abrasive particles abrades surface materials. Bare copper surface exist momentarily.

According to our XPS results (figure 4.23), it has been proved that different types of oxide present after ECMP. Particularly, the existence of non-equilibrium Cu_2O and $Cu(OH)_2$ in originally equilibrium conditions indicates unstable state of surface chemistry. This non-equilibrium state is induced through tribochemical interactions in polishing. As it turns out, the planarization seems to be good

4.6.4 Material Removal Rate

As discussed in previous sections (4.6.1 to 4.6.3), both electrochemical and mechanical interactions contribute to the material removal. This removal can be summarized in figure 4.25. A simplified formula for the material removal rate (MRR) is listed in the equation 4.24. Electrochemical MRR is the MRR due to electrochemical interactions and mechanical MRR is the MRR due to mechanical abrasion during ECMP. In the following the kinetics of removal mechanisms will be discussed.

$$\text{Total MRR} = \text{Electrochemical MRR} + \text{Mechanical MRR} \qquad [4.24]$$

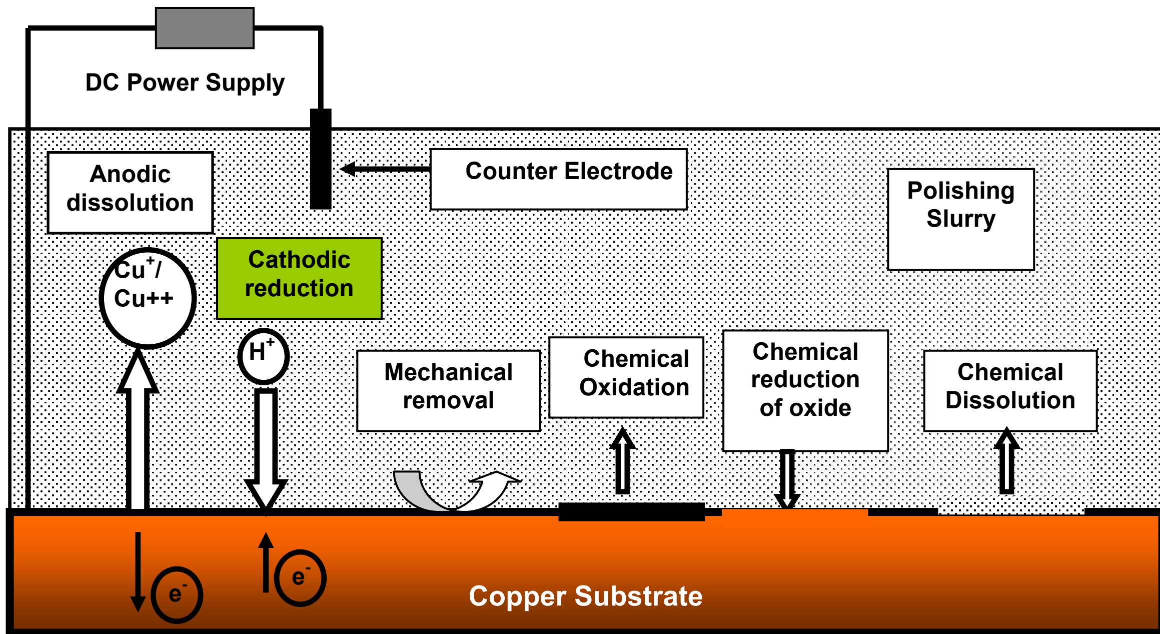

Figure 4.25 Schematic model of material removal mechanisms in ECMP

4.6.4.1 Calculated Material Removal Rate

Using the conceptual equation 4.24, the total MRR can be analytically derived, with the known operating parameters in the process. The rate of electrolytic dissolution is the number of copper atoms removed from the surface per unit time. As per Faraday's law, using the measured current density (current per unit area), the rate of copper ionic dissolution can be calculated. Here it is assumed that the copper ions have the valence of 2. On the contrary, it was reported previously that in the early stage of oxidation, copper oxidizes with the valence of 1, ½ or ¼.[107,108] The formation of CuO at initial stages can subsequently lead to formation of Cu_2O. In presence of water, the Cu_2O subsequently transforms to the form of $Cu(OH)_2$.[106] During each of these oxidation reactions, the electrons are generated. The value of valence 2 is likely to dominate the electrolytic dissolution rate of copper.

The anodic dissolution of the copper occurs follow the reaction:

$$Cu \rightarrow Cu^{n+} + ne^- \quad [4.25]$$

The copper dissolved in the form of ions is directly proportional to the electrons generated. The current values measured during CMP can be used to determine the electrochemical dissolution. The electrolytic dissolution of copper in terms of thickness t, can be calculated from the standard formula

$$t = \frac{mI}{\rho nFA} \qquad [4.26]$$

where m is atomic mass of copper (63.546), I is current measured during CMP, ρ is the density (8.96 g/cm^3), n is valence (i.e., 2), F is Faraday constant (96,500 coulomb/mol), and A is the surface area of copper exposed. The electrolytic anodic dissolution was observed only when the anodic currents are impressed. In case of cathodic currents, it is assumed that the metal dissolution does not take place electrolytically. To simplify the process, the copper re-deposition is ignored here. The calculated values for copper removal are considering for valence of 2 only. It has been shown that all forms of CuO, Cu_2O, Cu_4O, and Cu_8O can exist. [107,108] In such cases, other than CuO, the number of copper atoms oxidized is expected to be lower by electrolytic action than the calculated one.

4.6.4.2 Material Removal due to Wear

The material removed as abrasive wear can be calculated, using the values of applied load, sliding distance, and the hardness.[109]

$$V = \frac{k_{abr} L x}{H} \qquad [4.27]$$

where, V is the wear volume, L is the applied load, k_{abr} is the average tangent of the roughness angle divided by π. The value of k_{abr} typically varies from 3x10^{-3} to 6x10^{-4}. The sliding distance x in our experiment is 78.4 m for 20 minutes. H is the hardness of the material. The copper's hardness is 369 MPa, whereas, if the material removed is CuO or Cu2O, the hardness is 1,000 MPa. The applied load in the CMP experiment was 3 MPa. According to these values, the wear is 3.19 nm/min and 1.18 nm/min, in case of copper or copper oxide removal respectively, as listed in Table 4.1.

The overall removal rate is summarized in the equation below.

$$MRR = \frac{mls}{\rho nFA} + \frac{k_{abr} Lx}{H} \quad [4.28]$$

4.6.4.3 Measured Material Removal Rate

In the present work, the electrochemical MRR and mechanical MRR are precisely measured. They are listed in table 4.1. Graphical representation of these MRR is as shown in the figure 4.26. As seen in the figure 4.26, the mechanical action of the pad is causing almost similar amount of material removal under the action in all of the cases of applied potential. The electrochemical action has more pronounced effect on the material removal rate.

4.6.4.3.1 Anodic Potential

The material removal rate as listed in the table 4.1 is 34 nm/min which is the highest among all three conditions tested. This is related to the corrosive behavior in electrochemical dissolution.

In the electrochemical dissolution, copper atoms are ionized and removed from the surface by the action of electrolyte in the contact. This anodic reaction occurs under the impressed anodic potential. The electrical circuit is completed externally, by providing suitable electrode platinum.

4.6.4.3.2 Cathodic Potential

Polishing results under cathodic condition are shown in Table 4.1. The electrochemical dissolution rate of copper has dropped to 9 nm/min from 34 nm/min with the anodic condition. Under the cathodic condition, the electric potential has negative charge on the wafer surface, and the positive charge on the counter electrode. In such a condition, electrons intend to move towards the copper surface so that copper ions are not formed and corrosion is suppressed. This is opposite of the basic corrosive behavior just discussed in previous section.

Table 4.1 Observed and calculated MRR

Applied Potential (V)	Observed MRR (nm/min)			Calculated MRR (nm/min)		
	Electro-chemical	Mechanical	Total	Electro-chemical	Mechanical	Total
+ 2	34.2 +/- 0.7	9.6 +/- 5.3	43.6 +/- 6.0	28.3	3.2	31.5
- 2	9.3 +/- 0.5	7.3 +/- 0.2	16.3 +/- 0.7	17.3	3.2	20.5

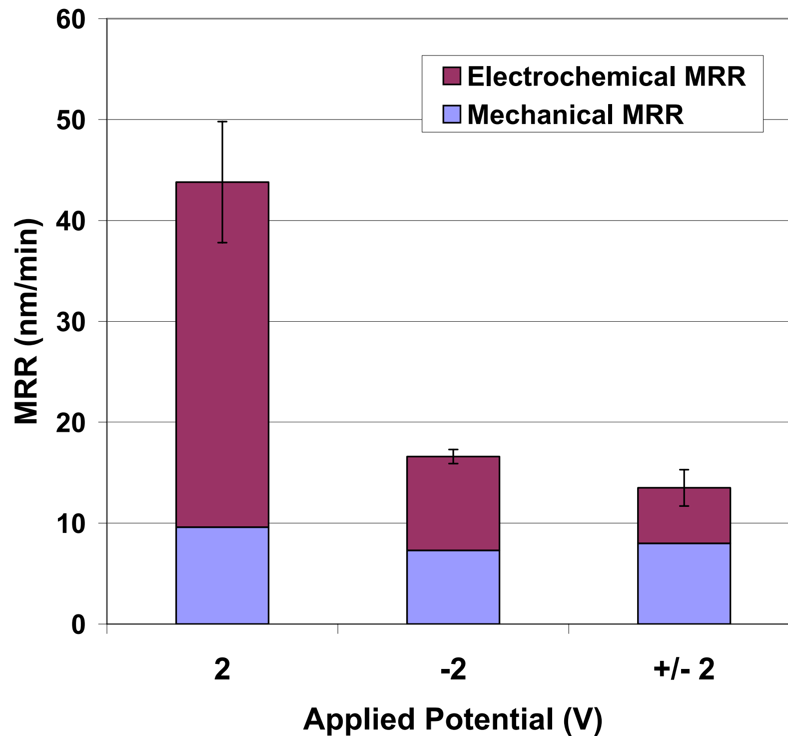

Figure 4.26 Chart showing MRR for different applied potentials during ECMP

In cathodically impressed current condition, the dissolution of copper ions is suppressed. The process of hydrogen evolution may occur as an effect of reduction reaction. Thermodynamically, the copper remains inert under this cathodic condition.

As shown in Table 4.1, mechanical material removal rate at copper surface dropped from 9 nm/min to 7 nm/min when the applied potential was switched from an anodic to the cathodic. This reduction is correlated with removal modes. Oxide film formed on the copper surface is harder than Cu so mechanical removal is less. A hard surface requires more mechanical abrasion to remove it.

4.6.4.4 MRR Model

The graphical representation of the analytically calculated and experimentally observed MRR is shown in figure 4.27. The figure shows the bars for individual set of experiment, total MRR, split into mechanical and electrochemical MRR.

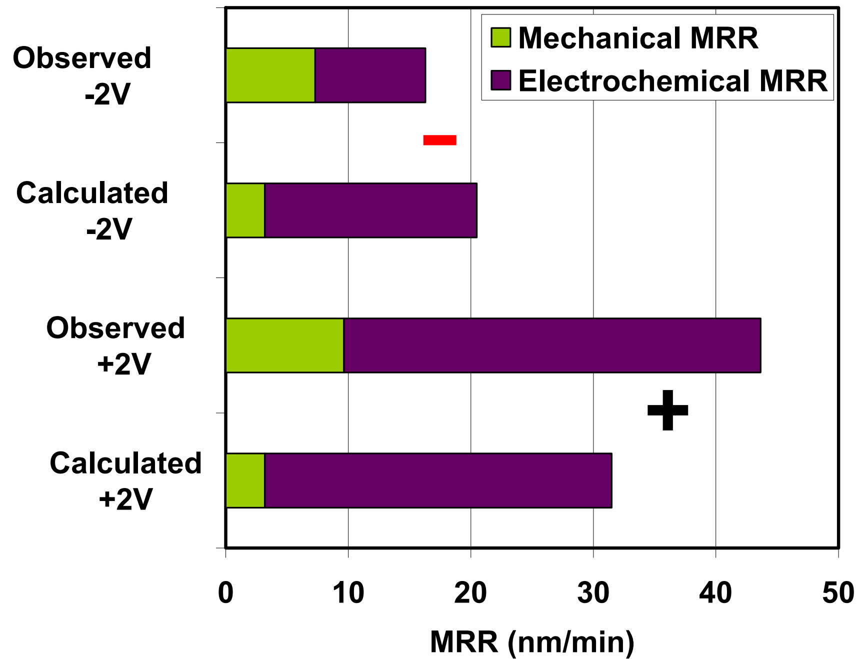

Figure 4.27 Chart evaluating calculated and observed MRR

In the anodic impressed potential, experimental wear rate is higher than the calculated one. This means that the wear due to pad sweeping is higher than expected. This can be correlated to the tribochemical interactions at the surface. The mechanical impact stimulated chemical reactions contribute additional material removal. Furthermore, the formation of copper oxide due to electrochemical reaction is less dense than copper and not strong enough to resist the mechanical action from the pad.[103] Hence the oxide removal is relatively easier and faster than the calculated value.

It was observed experimentally that the material removal value obtained in case of anodic impressed current is higher than that in cathodic one. This is however opposite to the calculated values. The reason for this is that the cathodically impressed current provides

resistance to the chemical dissolution and oxidation action of the slurry. This is not considered in the calculation.

Beyond all discussed so far, an important interaction is not to be ignored. The tribo-electro-chemical interface is a synergistic effect. Although it is experimentally impossible to directly detect the non-equilibrium interactions, the analytical model will certainly assist the prediction of the surface inter change.

4.7 Summary

In this part of the research, unique experimental approaches were used to investigate removal mechanisms of Cu ECMP. The combined electrochemical and mechanical experimental study revealed insight of copper behavior in nanometer length scales. During polishing, currents were impressed in different ways to copper surface. XPS and AFM surface characterization studies were conducted to understand the surface morphology and material removal mechanisms.

The major findings are summarized as follows:

- Oxidizer is beneficial for a good polishing surface only within a certain concentration range. It was found that a low concentration of H_2O_2 results a good polished surface.
- High rate anodic dissolution leads to a high surface roughness. Cathodic reaction on the copper surface has shown improved surface finish with reduced material removal rate. Alternating anodic and cathodic interactions on the copper surface provide excellent surface with further reduced removal rate.
- The height reduction due to electrochemical and mechanical removal can be distinguished using an AFM.
- A good surface finish achieved by cyclic current during the Cu ECMP is attributed to the mass transport and breaking down of surface charged layers.

- It was discovered that the alternating potentials have profound influence on surface integrity after polishing than purely anodic or cathodic potentials.
- The linkage between electrochemical interactions and surface quality is a synergetic approach. The superimposition of surface roughness data on the Pourbaix diagram is a powerful tool to understand the removal mechanism in CMP systematically.
- Anodic currents in acidic slurries provided high material removal rate leading to high surface roughness. The material removal rate was controlled by electrochemical interactions.
- Cathodic impressed currents in acidic slurry provided uniform material removal leading to low surface roughness value leading to planarization.
- The optimized surface quality can be obtained when the balance between electrochemistry and wear of the oxidized copper surface is observed. For good planarization, this research recommended consideration of an acidic slurry with oxidizer and cathodic impressed current.
- In order to achieve a good planarization, our research recommends that there should be a balance between electrochemical interaction, passivation, and mechanical wear. Results from this research showed that the slurry with acidic pH and cathodic impressed current was the best condition used.

This research has highlighted two major outcomes:

1. The tribo-electrochemical interactions generate the non-equilibrium oxide phases on copper surface. This effect is responsible for the synergy in the material removal mechanisms. The formation of copper oxide on the surface was proved using an XPS.
2. Experimental and analytical approaches were implemented in this research. Extensive AFM surface characterization was conducted for experimental

measurements. It resulted in the understanding that the tribo-electrochemical interaction and removal mechanisms.

The electrochemical-mechanical planarization is becoming important in microelectronics due to the high demand of low-force polishing of low-K materials. This research will help to understand the mechanisms of ECMP, as well as to provide guidelines in process development and optimization.

CHAPTER V
CONCLUSIONS AND FUTURE WORK

5.1 Conclusions

Fundamental investigation of tribochemical principles was conducted in this research. Focus was on the non-equilibrium surface phenomena. These include the friction-induced chemical reactions and non-equilibrium phase transformations, electrochemical-mechanical wear, and non-equilibrium oxidation. This research covers studies in mechanisms of electrochemical-mechanical planarization (ECMP), an important process being developed in making integrated circuits (IC) today. The following are conclusions.

1. In CMP study on the interfaces between polymeric particles and substrates, polymer particles were found to reduce friction. There was evidence of adhesion between hard alumina particles to the polymer surfaces. The addition of polymer particles was shown to reduce the surface roughness after CMP.

2. The combined electrochemical and mechanical investigation using experimental approach with AFM revealed insight of copper behavior in nanometer length scale. These include that the oxidizer is beneficial for a good polishing surface only within a certain concentration. It was found that a lower concentration of H_2O_2 results a good polished surface. In order to achieve a good planarization, our research recommends a balance between electrochemical interaction, passivation, and mechanical wear. Results from this research showed that the slurry with acidic pH and cathodic impressed current is the best condition used.

3. The linkage between mechanical interactions, electrochemical interactions and surface quality is a synergetic approach. The superimposition of surface roughness

data on the Pourbaix diagram is a powerful tool to understand the removal mechanism in CMP systematically. ECMP results showed that anodic currents in acidic slurries provided high material removal rate leading to high surface roughness. The material removal rate was controlled by electrochemical interactions.

Cathodic impressed currents in acidic slurry provided uniform material removal leading to low surface roughness value leading to planarization.

The optimized surface quality can be obtained when the balance between electrochemistry and wear of the oxidized copper surface is observed. For good planarization, this research recommended consideration of an acidic slurry with oxidizer and cathodic impressed current.

4. High voltage (2V) anodic, cathodic, and variable electro potential on the copper surface was studied. The variable potential interaction provided an excellent surface with reduced removal rate. XPS studies provided the information that the triboelectrochemical surface interaction during ECMP is leading to formation of copper oxide and copper hydroxide on the copper surface. These are nonequilibrium phases as per the Pourbaix diagram. This research was conducted at industry's early age using electrochemistry in CMP. It has potential in applications in microelectronics manufacturing.

5.2 Future Research

This research has made some path finding studies. Future investigation is suggested as following:

1. In the present study, potential reversal during ECMP has been found to improve surface quality. However, this improvement was accompanied with the reduced removal rate. This short come can be overcome if the anodic cycle is performed for longer time than the cathodic one. A high frequency of cyclic impressed potential

should be studied for two reasons. One is that the surface charge dissipation occurs in less than a minute; the second is that in industrial practice, a high speed polishing (linear speed 150 cm/sec) will further reduce the concentration gradients in polishing slurry.

2. *In situ* impedance study is recommended in terms of formation and removal of copper oxides during ECMP. This will enable understanding the triboelectrochemical interactions that are nonequilibrium in nature.

3. Effects of polymer particles as abrasives in the polishing slurry should be further explored with adequate slurry chemistry so as to achieve the combination of high removal rate and high surface smoothness.

4. Similar experimentation as performed in the present research should be conducted for patterned and damascene wafers in order to understand effects of presence of different components on the ECMP performance.

REFERENCES

1 F. P. Bowden, D. Tabor, *The Friction and Lubrication of Solids*, 2nd Ed. Oxford University Press, Oxford (1987).

2 G. P. Shpenkov, *Friction Surface Phenomena*, Ed. D. Dowson, Tribology Series, Elsevier, Amsterdam (1995).

3 N. P. Suh, *Tribophysics*, Prentice Hall, Englewood Cliffs NJ (1986).

4 E. Rabinowicz, *Scientific American*, **218(6)**, 91 (1968).

5 H. S. Carslaw, J. C. Jaeger, *Conduction of Heat in Solids*, Oxford University Press, Oxford (1959).

6 J. D. Eshelby, *Phil. Trans. Roy. Soc. London-A, Math. Phys. Sci*., **244**(877), 87 (1951).

7 S. Malkin, and A. Marmur, *Wear*, **42**, 333 (1977).

8 F. D. Fischer, W. Daves, and E. A. Werner, *Journal of Fatigue and Fracture in Engineering Material Structures,* **26**, 999 (2003).

9 J. P. Hirth, D. A. Rigney, *Wear*, **39**, 13 (1976).

10 Y. Gogotsi, V. Domnich, *High Pressure Surface Science and Engineering,* Institute of Physics Pub., London (2004).

11 H. Mishina, *Tribology International*, **1**, 39 (1988).

12 J. R. Davis, *Surface Engineering for Corrosion and Wear Resistance*, ASM International, Materials Park OH (2001).

13 R. Stribeck, *Zeitung des Vereins Deutscher Ingenieure*, **46**, 1341 (1902).

14 S. A. McKee and T. R. McKee, *Trans. ASME*, **51**, 161 (1929).

15 G. Luengo, J. Israelachvili, S. Garnick, *Wear* **200**, 328 (1996).

16 T. E. Fischer, Tribochemistry, *Ann. Rev. Mater. Sci*. **18**, 303 (1988).

17 G. E. Totten and H. Liang, *Surface Modification and Mechanism: Friction, Stress and Reaction Engineering,* Marcel Dekker, New York (2004).

18 C. K. Kajdas, *Tribology International* **1**, 17 (2004).

19 G. Heinicke, *Tribochemistry*, Carl Verlag, Munich (1984).

20 V. A. Muratov, T. Luangvaranunt and T. E. Fischer, *Tribology International* **31**(10), 601 (1998).

21 J. L. Sullivan, *J. Phys. D: Appl. Phys.* **19**, 1999 (1986).

22 H. Liang, *Tribology International* **38**, 235 (2005).

23 S. C. Lim, *Tribology International* **35**, 717 (2002).

24 Y.L. Cheng, Z. Zhang, F. H. Cao, J. F. Li, J. Q. Zhang, J. M. Wang, C. N. Cao, *Corrosion Science* **46**, 1649 (2004).

25 N. Axon, S. Jacobson and S. Hogmark, *Tribology International* **27**(4), 233 (1994).

26 H. Mishina, *Tribology International*, **1**, 39 (1988).

27 S. C. Lim, M. F. Ashby, J. H. Brunton, *Acta. Metall.* **35**(6), 1343 (1987).

28 M. Kerridge, *Proc. Phys. Soc. B* **68**, 400 (1955).

29 T. E. Fischer, *Ann. Rev. Mater. Sci.* **18**, 303 (1988).

30 P. Ponthiax, F. Wagner, D. Drees, J. P. Celis, *Wear* **256**, 459 (2004).

31 S. Mischler, A. Spiegel, M. Stemp, D. Landolt, *Wear* **251**, 1295 (2001).

32 S. Mischler, P. Ponthiaux, *Wear* **248**, 211 (2001).

33 F. Assi, H. Böhni, *Tribotest J*. **6**, 17 (1999).

34 S. W. Watson, F. J. Friedersdorf, B.W. Madsen, S. D. Cramer, *Wear* **181**, 476 (1995).

35 G. H. Xu, H. Liang, *Journal of Electronic Materials*, **31**(4), 272 (2002).

36 G. Binnig, C.F. Quate, Ch. Geber, *Phys. Rev. Letters*, **56**(9), 930 (1986).

37 G. W. Stachowik, A. W. Batchelor, G. B. Stachowik, *Experimental Methods in Tribology,* Ed. D. Dowson, Elsevier, Woburn MA(2001).

38 Y. Martin, C. C. Williams, H. K. Wickramasinghe, *J. Appl. Phys.* **61**(10), 4723 (1987).

39 *Handbook of X-ray Photoelectron Spectroscopy*, 3rd Ed., Physical Electronic Inc., Ismaning, Germany (1995).

40 E. Cano, J. M. Bastldas, J. L. Polo and N. Morra, *Journal of the electrochemical society*, **148**(11), B431 (2001).

41 K. L. Chavez, D. W. Hess, *Journal of the Electrochemical Society*, **148**(11), G640 (2001).

42 J-C Chen, W-Ta Tsai, *Materials Chemistry and Physics*, **87**, 387 (2004).

43 IBM Highlights 1970-1984, http://www-03.ibm.com/ibm/history/documents/pdf/1970-1984.pdf [May 2006].

44 H. Liang, D. Craven, *Tribology in Chemical Mechanical Planarization,* Taylor & Francis, Boca Raton FL(2004).

45 G. Moore, A Prediction Made Real Improves Billions of Lives, http://www.intel.com/technology/silicon/mooreslaw/ [May 2006].

46 Products, http://electronicmaterials.rohmhaas.com/businesses/cmpt/products [May 2006].

47 T. Abraham, Chemical Mechanical Polishing Equipment and Materials:A Technical and Market Analysis, http://www.bccresearch.com/advmat/GB288.html [May 2006].

48 International Technology Roadmap for Semiconductors 2005 Ed. Executive Summary, http://www.itrs.net/Common/2005ITRS/ExecSum2005.pdf [May 2006].

49 T. E. Reed-Hill, R. Abbaschian, *Physical Metallurgy Principles*, 3rd Ed. Thomson, Singapore (1991).

50 J. Luo and D. A. Dornfeld, *IEEE Trans. on Semiconductor Manufacturing* **14**(2), 112 (2001).

51 Q. Luo, S. Ramarajan, S. V. Babu, *Thin Solid Films,* **335**, 160 (1998).

52 L. Guo and R. S. Subramanian, *Journal of The Electrochemical Society*, **151**(2), G104 (2004).

53 W. Choi, S. M. Lee, R. K. Singh, *Mat. Res. Soc. Symp. Proc.*, **767**, 63 (2003).

54 S. Danyluk, A. Osorno I. Yoon, S. Tsiareshka, in *CMP-MIC Proc.*, Institute for Microelectronics Interconnection, p.79 Fremont CA (2006).

55 H. Liang and D. Craven, *Tribology in Chemical Mechanical Planarization*, CRC Press, Boca Raton FL (2005).

56 T. Dickinson, in *CMP-MIC Proc.*, Institute for Microelectronics Interconnection, p.220 Fremont CA (2006).

57 G. P. Muldowney, R. Palaparthi, D. P. Tselepidakis; S.G. Natu; V. Vikas, in *CMP-MIC Proc.*, Institute for Microelectronics Interconnection, p.262 Fremont CA (2006).

58 T. Dickinson, F. Stevens, S. C. Langford, *Proceedings of World Tribology Congress III,* Washington DC (2005).

59 P. Beaud, D. Bouvet, P. Fazan, E. Jacquiuinot, H. Aoki, T. Aoki, *Mat. Res. Soc. Symp. Proc.,* Ed. D. S. Boning, K. Davriendt, M. R. Oliver, D. J. Stein, I. Vos, Chemical Mechanical Planarization*,* p.141 San Francisco CA (2003).

60 J. W. Lee, B. U. Yoon, J. K. Choi, J. S. Park, H. Y. Kim, C. K. Hong, H. K. Cho, J. T. Moon, in *CMP-MIC Proc.*, Institute for Microelectronics Interconnection, p.179 Fremont CA (2006).

61 C. Yu, S. Lane, B. Mueller, S. Lawing, P. Flanagan, K. Lindemann, in *CMP-MIC Proc.*, Institute for Microelectronics Interconnection, p.175 Fremont CA (2006).

62 I. Belov, J.Y. Kim, M. Perry, P. Watkins, T. Moser & K. Pierce, in *CMP-MIC Proc.*, Institute for Microelectronics Interconnection, p.564 Fremont CA (2006).

63 D. Ng, H. Liang; K. Cheemalapati, Y. Li, in *CMP-MIC Proc.*, Institute for Microelectronics Interconnection, p. 179 Fremont CA (2006).

64 T. Nishioka, H. Yano, G. Minamihaba, D. Fukushima, S. Seta, in *CMP-MIC Proc.*, Institute for Microelectronics Interconnection, p.73 Fremont CA (2006).

65 T. Izumutani, *Treatise on Material Science and Technology*, Ed. M. Tomazawa, R. Doremus, Academic Press NY, 115 (1979).

66 N. Chandrasekaran, T. Taylor, G. Sabde, *Mat. Res. Soc. Symp. Proc.*, Ed. D. S. Boning, K . Davriendt, M. R. Oliver, D. J. Stein, I. Vos, Chemical Mechanical Planarizaation, p.153 San Francisco CA (2003).

67 L. M. Cook, *Journal of Non-Crystalline Solids*, **120**, 152 (1990).

68 J. Luo and D. A. Dornfeld, *IEEE Trans. on Semiconductor Manufacturing*, **16**(1), 45 (2003).

69 R. Jairath, M. Desai, M. Stell, R. Telles, S. Scherberbrewer, in *Mat. Res. Soc. Symp. Proc.* **337**, p.121 San Francisco CA (1994).

70 K. Hoyoung, D. W. Park, C-K Hong, W-S Han, J-T Moon, in *Mat. Res. Soc. Symp. Proc.*, Ed. D. S. Boning, K. Davriendt, M. R. Oliver, D. J. Stein, I. Vos, Chemical Mechanical Planarization, p.87 San Francisco CA (2003).

71 S. Deshpande, S. Dakshinamurthy, S. C. Kuirya, R. Vaidyanathan, Y. S. Obeng, S. Seal, *Thin Solid Films* **483**, 261 (2005).

72 H. Liang, H. Xu., J. M. Martin, T. L. Mongne, *Mat. Res. Soc. Symp. Proc.*, Ed. D. S. Boning, K. Davriendt, M. R. Oliver, D. J. Stein, I. Vos, Chemical Mechanical Planarizaation, p.111 San Francisco CA (2003).

73 A. De. Feo, S. Lee & D. Dornfeld, in *CMP-MIC Proc.*, Institute for Microelectronics Interconnection, p.540 Fremont CA (2006).

74 A. Prasad, E. E. Remsen, in *CMP-MIC Proc.*, Institute for Microelectronics Interconnection, p.554 Fremont CA (2006).

75 D. Ng, M. Kulkarni, G. Xu, P. Severs, R. Marvin, J. Xiao, and H. Liang, *Journal of ASTM International*, **2**(5), 1(2005).

76 H-J. Sue, M. E. Garcia, D. M. Pickelman, N. P. Cheremisinoff, *Elastomer Technology Handbook*. CRC Press, Boca Raton FL (1993).

77 H-J. Sue, K. T. Gam, N. Betaoui, A. Clearfield, M. Miyamoto, N. Miyatake, *Acta Mat.* **52**, 2239 (2004).

78 Z. Luo, Microscopic Imaging Center, Texas A&M University, College Station, TX.

79 P. Souza Santos, H. Souza Santos, S. P. Toledo, *Materials Research,* **3**(4), 104 (2000).

80 G. Paglia, PhD Thesis, Curtin University, Australia (2004).

81 B. Chen, D. Penwell, L. R. Benedetti, R. Jeanloz, and M. B. Kruger, *Physical Review* B **66** (144), 101 (2002).

82 F. B. Kaufman, D. B. Thompson, R. E. Broadie, M. A. Jaso, W. L. Guthrie, D. J. Perusons and M. B. Small, *Journal of the Electrochemical Society,* **138**, 3460 (1991).

83 H. Nishizawa, Y. Tateyama, T. Saitoh , *Thin Solid Films,* **455**, 491 (2004).

84 T. Du, D. Tamboli, V. Desai, *Microelectronic Engineering*, **69**, 1 (2003).

85 S. Seal, S.C. Kuiry, B. Heinmen, *Thin Solid Films*, **423**, 243 (2003).

86 T-H. Tsai, Y-F. Wu, S-C. Yen, *Microelectronic Engineering*, **243**, 22 (2004).

87 N-H. Kima, J-H. Limb, S-Y. Kimc, E-G Chang, *Materials Letters*, **57**, 4601 (2003).

88 T-H. Tsai, Y-F. Wu, S-C. Yen, *Microelectronic Engineering*, **242**, 79 (2004).

89 C. Yi-Hsiu, K. Jiun-Shian, H. Jui-Hsiung, H. Jui-Hsiung, Y. Shi-Chen, The study of copper etching in acid solution, http://ecsmeet.peerx-press.org/ms_files/ecsmeet/2005/01/02/00021320/00/21320_0_art_file_1_1104763117.pdf [May 2005].

90 J. M. Steigerwald, S. P. Murarka, R. J. Gutmann, D. J. Duquette, *Materials Chemistry and Physics*, **41**, 217 (1995).

91 K. L. Chavez and D. W. Hess, *Journal of the Electrochemical Society*, **148**(11), G640 (2001).

92 Ed. J. R. Davis, *Metals Handbook* 2nd Ed., ASM International, Materials Park, OH (1998).

93 E. Cano, J. M. Bastidas, J. L. Polo, N. Mora, *Journal of the Electrochemical Society*, **148** (11), B431 (2001).

94 R. Carpio, J. Farkas, R. Jairath, *Thin Solid Films*, **266**, 238 (1995).

95 J. Huo, R. Solanki, J. McAndrew, *Journal of Materials Engineering and Performance*, **13**(4), 413(2004).

96 D. Zeidler, Z. Stavreva, K. Drescher, *Microelectronic Engineering,* **33,** 259 (1997).

97 Y. Ein-Eli, E. Abelev, D. Starosvetsky, *Electrochimica Acta*, **49,** 1499 (2004).

98 T. Du, V. Desai, *Journal of Materials Science Letters*, **22,** 1623 (2003).

99 T. Du, D. Tamboli, V. Desai, *Microelectronic Engineering*, **1**, 69 (2003).

100 V. Brusic, in *Proceedings World Tribology Congress III,* Society for Tribological and Lubrication Engineering, p.139 Washington DC (2005).

101 S. Barnartt, *Electrochemical Techniques for Corrosion Engineering*, Ed. R. Baboian, NACE, Houston TX(1985).

102 M. Pourbaix, *Lectures on Electrochemical Corrosion*, NACE International, Houston TX(1956).

103 G. Helen Xu, H. Liang, *Journal of Electronic Materials*, **31**(4), 272 (2002).

104 H. Liang, *Tribology International* **38**, 235 (2005).

105 K. C. Yung, T. M. Yue, K. C. Chan, and K. F. Yeung, *IEEE Tran. on Electronics Packaging Manufacturing*, **26**(2), 106 (2003).

106 W. Kautek, M. G. M. Sahre, P. Zhaos, S. Mirwald, *Surface and Interface Analysis*, **25**, 548 (1997).

107 R. Guan, H. Hashimoto, T. Yoshida, *Acta. Cryst*., **B40**, 109 (1984).

108 R. Guan, H. Hashimoto, K. H. Kuo, *Acta. Cryst*., **B40**, 560 (1984).

109 E. Rabinowicz, *Friction and Wear of Materials,* 2nd Ed., John Wiley, New York (1995).

APPENDIX I

LIST OF COMPANIES PERFORMING CMP

ADVANCED MICRO DEVICES (AMD)
ANALOG DEVICES, INC.
ATMEL CORP.
BEIJING XUNCHUANG IC CO., LTD.
CYPRESS SEMICONDUCTOR
DALLAS SEMICONDUCTOR CORP.
FUJITSU, INC.
HEWLETT-PACKARD
HITACHI
HOLMATE SEMICONDUCTOR INC.
HUAXIA SEMICONDUCTOR MANUFACTURING CO., LTD.
HYUNDAI ELECTRONICS INDUSTRIES CO., LTD.
IBM MICROELECTRONICS
INFINEON TECHNOLOGIES AG
INTEGRATED DEVICE TECHNOLOGY (IDT)
INTEL
LSI LOGIC CORP.
LUCENT TECHNOLOGIES
MICRON TECHNOLOGY
MITSUBISHI ELECTRIC SEMICONDUCTOR GROUP
MAXIM INTEGRATED CIRCUITS
MOTOROLA
NATIONAL SEMICONDUCTOR CORP.
NANTONG FUJITSU MICROELECTRONICS CO., LTD.
NIPPON ELECTRIC CORP. (NEC)
PHILIPS SEMICONDUCTORS
RICOH CO., LTD.
SAMSUNG ELECTRONICS CO. LTD.
SEMICONDUCTOR MANUFACTURING INTERNATIONAL CORP. (SMIC)
ST MICROELECTRONICS N.V.
SHARP CORP.
SIEMENS AG
SONY SEMICONDUCTOR COMPANY OF AMERICA
TAIWAN SEMICONDUCTOR MANUFACTURING CO., LTD. (TSMC)
TEXAS INSTRUMENTS
TOSHIBA CORP.
VANGUARD INTERNATIONAL SEMICONDUCTOR CORP.
VLSI TECHNOLOGY
WINBOUND ELECTRONICS CORP.

VITA

Name: Milind Sudhakar Kulkarni

Address: Department of Mechanical Engineering
Engineering Physics Building, PO Box J10
Texas A&M University
College Station, TX 77843-3123

Email Address: milindatuaf@yahoo.com

Education: B.E., Metallurgical Engineering, University of Pune, 1988
M. Tech., Materials Technology, Indian Institute of Technology, Mumbai, 1990

Teaching Experience:

Fall 2005 Teaching Assistant, Department of Mechanical Engineering
Texas A&M University, College Station, TX.
Course: Corrosion Engineering (430).

Aug 1991- Dec 2003 Asst. Prof., Department of Mechanical Engineering
Maharashtra Institute of Technology, University of Pune.
Courses Taught: Materials Science I & II, Materials Selection, Physical Metallurgy, Engineering Materials, Corrosion, Testing and Protection, Materials Testing.

Professional Experience:

May 1992 - Dec 2003 Industrial Consultant Metallurgical Consultancy and Development Centre, Maharashtra Institute of Technology, Pune.
Testing, consultancy and failure analysis work.

Mar 1990 - July 1991 Trainee Engineer, Materials, Kirloskar Cummins Limited, Kothrud, Pune.
Procurement and development of steel forgings and steel raw material.